Inaugural dissertation

for

obtaining the doctoral degree

of the

Combined Faculty of Mathematics, Engineering and Natural Sciences

of the

Ruprecht - Karls - University

Heidelberg

Presented by

M.Res. (Biomedical Sciences) Denise Grieshober

Born in: Karlsruhe, Germany

Oral examination: 18.07.2023

The role of the N-fragment of Angiopoietin-like 4 during malignant melanoma metastasis formation

Referees:

Prof. Dr. Viktor Umansky

Prof. Dr. Hellmut Augustin

Die vorliegende Arbeit wurde in der Abteilung „Vaskuläre Onkologie und Metastasierung“ am Deutschen Krebsforschungszentrum (DKFZ) in Heidelberg zwischen Februar 2019 und Februar 2023 durchgeführt.

Acknowledgments

The more than four years of PhD have been an exciting journey and I would like to thank everyone who made the completion of this thesis possible. I am extremely thankful for the colleagues, friends and family who supported me towards my aim.

First, I would like to thank **Prof. Dr. Hellmut Augustin** for his guidance and constant support during my time in the Division of Vascular Oncology and Metastasis. Thank you Hellmut for giving me the opportunity to work on this exciting project and for all science- and career-related discussions. I am convinced that the professional and personal skills that I acquired while working in your lab will help me in my future endeavors.

I would like to express my gratitude to **Prof. Dr. Moritz Felcht** for his mentorship and constant guidance during my PhD thesis. Thank you for giving me the opportunity to discuss my latest results in our Friday meetings and for giving me both constructive feedback and encouragement. Further, I would like to thank **Corinne Hübers** for your scientific support and for being good team mates.

I express my sincere gratitude to **Prof. Dr. Viktor Umansky** for giving me the opportunity to accomplish my doctoral thesis at the Combined Faculty of Natural Sciences and Mathematics of the Ruperto Carola University of Heidelberg and the German Cancer Research Center. Thank you for being part of my Thesis Advisory Committee together with **Prof. Dr. Karibaan Hodivala Dilke** and for giving me constructive feedback over the past years. In addition, I would like to thank **Prof. Dr. Ingrid Lohmann** and **PD Dr. Karin Müller-Decker** for taking part in my Defense Committee as Examiners and Chair.

I am also thankful to the **RTG2099** for the financial support and for providing a collaborative research environment. Further, I would like to thank the "**Helmholtz International Graduate School for Cancer Research**" for the opportunity to work in a highly international institution. Moreover, I would like to thank the FACS, light microscopy core facilities and laboratory animal core facilities for the technical support and expertise.

Thank you to **Ashik Ahmed Abdul Pari** for being a good team mate and friend. I really appreciate your constant moral and scientific support and your constructive feedback. Thank you Ashik for all the inspiring scientific and non-scientific discussions and for taking your time to read and correct my thesis. Thank you also to **Benjamin Schieb** and **Claudine Fricke** for your support in this project.

I am very glad that I got the opportunity to work in the A190 team. Through scientific discussions, technical support or suggestions everyone has contributed to this project. Beyond all the scientific input, I highly appreciate all the lab dinners, birthday parties, girls trip to Hamburg, lab retreats and much more. Thank you to everyone who accompanied me during this journey: Anja G, Anja R, Ashik,

Biplap, Catalina, Dimitri, Divya, Donato, Evangelia, Guanxiong, Jingjing, Katharina, Ki Hong, Laura, Mahak, Michi, Miki, Moritz, Nico, Niklas, Paula, Robert, Stephanie G, Stephanie P, Till, Xiaowen, Yiwen.

I would like to express my profound gratitude to Barbara, Carleen, Clara, Eva, Luisa, Maria, Marius, Monika, Petra and Sandra for supporting me and answering all my technical and bureaucratic questions.

I would like to thank Steffi and Anja for all the science- and non-science-related discussions. I know that I can always count on you and I am extremely happy that we became such good friends during our time in the lab.

Thank you to my friends outside the lab who have always supported me: Thanks to Chrissi, Nina, Aki, Chris, Lea, Melli for a long friendship and that you are always there for me. I am thankful for our weekend trips, parties, brunches and skype calls, which always kept me going through the hard times of my PhD.

Vor allem danke ich meiner Familie, ohne die ich nicht die wäre, die ich bin. Danke Mama, Papa und Julian für Eure bedingungslose Unterstützung. Danke, dass Ihr immer zu mir haltet und, dass ihr mir immer ermöglicht habt, mich auf mein Studium zu konzentrieren. Alles, was ich erreicht habe, habe ich Euch zu verdanken. **Danke!**

Table of contents

List of figures

List of tables

Summary

Melanoma belongs to the most aggressive forms of skin cancer. While the primary tumor can generally be controlled, most patients develop metastasis upon tumor resection. Multiple reports show that the primary tumor secretes certain factors that limit metastatic outgrowth by restricting angiogenesis. Angiopoietin-like 4 (ANGPTL4) represents one of these primary tumor-derived factors as its expression enhances with malignancy. However, the published literature on ANGPTL4 function during angiogenesis and metastasis is highly controversial. While some studies describe ANGPTL4 as a stimulator of metastasis, other studies show that ANGPTL4 can also restrict tumor growth and secondary colonization.

Given the conflicting literature, our lab has previously overexpressed the two cleavage fragments of ANGPTL4, namely nANGPTL4 and cANGPTL4, in tumor cells. The results indicated that overexpression of cANGPTL4 in tumor cells enhances metastasis, whereas nANGPTL4 overexpression reduces metastatic dissemination. However, the mechanism of nANGPTL4 action as well as its therapeutic and clinical potential, remain elusive. Therefore, the present thesis was aimed at mechanistically understanding how nANGPTL4 limits metastatic outgrowth and corroborate the clinical relevance of cleavage fragments of ANGPTL4 in tumor patients. Further, the study aimed to design and evaluate the efficacy of nANGPTL4 treatment in clinically relevant mouse models. Assessing the levels of ANGPTL4 cleavage fragments in primary tumors and serum samples of melanoma and lung cancer patients depicted that nANGPTL4 and cANGPTL4 were differentially distributed in primary tumor and serum samples. While cANGPTL4 was shown to be localized in the primary tumor, nANGPTL4 was highly expressed in the systemic circulation. Additionally, longitudinal studies of melanoma patient sera revealed that the expression of nANGPTL4 negatively correlated with disease progression whereas increasing nANGPTL4 levels in the serum correlated with higher overall survival in melanoma patients. In line, pre-clinical analyses showed that systemic administration of nANGPTL4 reduced metastasis formation and increased the overall survival of mice in both experimental and spontaneous metastasis models. *In vitro* studies negated a direct effect of nANGPTL4 on cancer cell behavior. Mechanistically, global gene expression profiling of endothelial cells from the metastatic site unveiled that nANGPTL4 specifically downregulated Wnt signaling and thereby reduced vascularity at the metastatic site. Correspondingly, *in vitro* spheroid sprouting assays and *in vivo* cornea pocket assays revealed that nANGPTL4 inhibited sprouting angiogenesis. This effect depends on the interaction of nANGPTL4 and its downstream receptor SDC4.

As nANGPTL4 is a potent inhibitor of LPL, high levels of nANGPTL4 were previously shown to upregulate plasma triglyceride levels, thereby increasing the risk of developing cardiovascular disease. Recent

studies have shown that a missense mutation in nANGPTL4 (E40K) strongly correlates with lower TG levels. As increased triglyceride levels may represent a significant side effect of nANGPTL4 treatment, the second part of this study was aimed at analyzing whether the E40K mutated nANGPTL4 affected tumor development and metastasis. Primary tumor experiments revealed that overexpression of E40K mutated nANGPTL4 did not affect primary tumor growth and the vasculature. In addition, overexpression of E40K mutated nANGPTL4 in the primary tumor and systemic administration of E40K mutated nANGPTL4 had no effect on metastasis and survival in pre-clinical mouse models.

In conclusion, this study identified nANGPTL4 as an endogenous primary tumor-derived inhibitor of metastasis and substantiated the therapeutic efficacy of nANGPTL4 treatment. Further, the data unveil that oligomerization of nANPGTL4 is required to sustain its anti-metastatic activity. Moreover, the results show that serum nANGPTL4 levels can be a biomarker to determine disease progression in cancer patients.

Zusammenfassung

Das Melanom gehört zu den aggressivsten Formen von Hautkrebs. Während der Primärtumor in der Regel kontrolliert werden kann, entwickeln die meisten Patienten nach der Resektion des Tumors Metastasen. Aus mehreren Berichten geht hervor, dass der Primärtumor bestimmte Faktoren absondert, die das Wachstum von Metastasen begrenzen, indem sie die Angiogenese einschränken. Angiopoietin-like 4 (ANGPTL4) stellt einen dieser vom Primärtumor stammenden Faktoren dar, da seine Expression mit der Malignität zunimmt. Die veröffentlichte Literatur über die Funktion von ANGPTL4 während der Angiogenese und Metastasierung ist jedoch höchst widersprüchlich. Während einige Studien ANGPTL4 als Stimulator der Metastasierung beschreiben, zeigen andere Studien, dass ANGPTL4 das Tumorwachstum und die sekundäre Kolonisierung einschränken kann.

Angesichts der widersprüchlichen Literatur hat unser Labor zuvor die beiden Spaltfragmente von ANGPTL4, namens nANGPTL4 und cANGPTL4, in Tumorzellen überexprimiert. Die Ergebnisse zeigten, dass die Überexpression von cANGPTL4 in Tumorzellen die Metastasierung fördert, während die Überexpression von nANGPTL4 die Metastasenausbreitung verringert. Der Mechanismus der nANGPTL4-Wirkung sowie sein therapeutisches und klinisches Potenzial sind jedoch bisher nicht geklärt. Ziel der vorliegenden Arbeit war es daher, mechanistisch zu verstehen, wie nANGPTL4 das metastatische Wachstum einschränkt, und die klinische Relevanz von ANGPTL4-Spaltfragmenten bei Tumorpatienten zu untersuchen. Darüber hinaus zielte die Studie darauf ab, die Wirksamkeit der nANGPTL4-Behandlung in klinisch relevanten Mausmodellen zu entwickeln und zu bewerten. Die Untersuchung der ANGPTL4-Spaltfragmente in Primärtumor- und Serumproben von Melanom- und Lungenkrebspatienten zeigte, dass nANGPTL4 und cANGPTL4 in Primärtumor- und Serumproben unterschiedlich verteilt waren. Während cANGPTL4 nachweislich lokal im Primärtumor detektierbar war, wurde nANGPTL4 in der systemischen Zirkulation stark exprimiert. Darüber hinaus ergaben Längsschnittstudien von Melanom-Patientenseren, dass die Expression von nANGPTL4 negativ mit dem Fortschreiten der Krankheit korreliert und dass steigende nANGPTL4-Konzentrationen im Serum mit einer höheren Gesamtüberlebensrate bei Melanompatienten korrelieren. Im Einklang damit zeigten präklinische Analysen, dass die systemische Verabreichung von nANGPTL4 die Metastasenbildung reduziert und das Gesamtüberleben von Mäusen sowohl in experimentellen als auch in spontanen Metastasenmodellen erhöht. *In vitro* Studien zeigten keine direkte Wirkung von nANGPTL4 auf das Verhalten von Krebszellen. Die Erstellung eines globalen Genexpressionsprofils von Endothelzellen aus dem Metastasenherd ergab, dass nANGPTL4 spezifisch die Wnt-Signalübertragung herunterreguliert und dadurch die Vaskularität am Metastasenherd verringert. Dementsprechend zeigten *in vitro* Sphäroid Assays und *in vivo* Cornea Pocket Assays, dass nANGPTL4 die Angiogenese

hemmt und dieser Effekt von der Interaktion von nANGPTL4 und seinem nachgeschalteten Rezeptor SDC4 abhängt.

Da nANGPTL4 ein potenter Inhibitor von LPL ist, wurde zuvor gezeigt, dass hohe nANGPTL4 Konzentrationen die Triglyceridspiegel im Plasma erhöhen und damit das Risiko für Herz-Kreislauf-Erkrankungen steigern. Neuere Studien haben gezeigt, dass eine Missense-Mutation in nANGPTL4 (E40K) stark mit niedrigeren TG-Werten korreliert. Da erhöhte Triglyceridspiegel eine erhebliche Nebenwirkung der nANGPTL4-Behandlung darstellen könnten, sollte im zweiten Teil dieser Studie untersucht werden, ob das E40K-mutierte nANGPTL4 die Tumorentwicklung und Metastasierung beeinflusst. Primärtumorexperimente zeigten, dass die Überexpression von E40K-mutiertem nANGPTL4 keinen Einfluss auf das Wachstum und die Gefäße des Primärtumors hat. Darüber hinaus hatten die Überexpression von E40K-mutiertem nANGPTL4 im Primärtumor und die systemische Verabreichung von E40K-mutiertem nANGPTL4 keine Auswirkungen auf die Metastasierung und das Überleben in präklinischen Mausmodellen.

Zusammenfassend lässt sich sagen, dass diese Studie nANGPTL4 als endogenen, vom Primärtumor stammenden Inhibitor der Metastasierung identifiziert und die therapeutische Effizienz der nANGPTL4-Behandlung belegt hat. Darüber hinaus zeigen die Daten, dass die Oligomerisierung von nANPGTL4 erforderlich ist, um seine anti-metastatische Aktivität aufrechtzuerhalten. Außerdem zeigen die Ergebnisse, dass der Serumspiegel von nANGPTL4 ein Biomarker zur Bestimmung des Krankheitsverlaufs bei Krebspatienten sein kann.

1. Introduction

1.1. Cancer

Cancer is a multistep succession of events in which progressive genetic and epigenetic alterations lead to the transition of normal cells into malignant cells. As these cells transform into neoplastic growth states, they acquire a set of functional capabilities. As such, tumor cells sustain proliferative signaling, evade growth suppressors, escape cell death, enable replicative immortality, induce angiogenesis, enhance invasion and metastasis, reprogram their cellular metabolism and prevent destruction by the immune system (*1*). The different types of cancer are commonly named for the organs or tissues where the cancer forms. From a histological standpoint, the types of cancers can be grouped into 5 major categories. The most common type of cancers are carcinomas. They account for 80% to 90% of all cancer cases. They are of epithelial origin and refer to cancers of the internal or external lining of the body. Sarcomas originate from supportive and connective tissues such as bones, cartilage, muscle and fat. Myelomas arise from plasma cells of the bone marrow. Leukemias are cancers of cells of the bone marrow and develop through an overproduction of immature white blood cells. Lastly, lymphomas develop in the glands or nodes of the lymphatic system (*2*).

Cancer represents a major public health problem as it is the primary cause of death in high income countries (*3*). The overall burden and incidence of cancer is rapidly growing. This is mainly due to an aging population and a higher exposure to main risk factors for cancer development such as pollution, alcohol consumption, smoking and an unhealthy diet. Based on the GLOBOCAN 2020 study, an estimate 19.3 million new cancer cases and 10.0 million cancer death occurred in 2020. Overall, female breast cancer (11.7%) and lung cancer (11.4%) represent the most commonly diagnosed cancer types (*4*). Today, the mechanistic understanding of cancer is increasing and large-scale screening approaches are performed to identify cancer patients at an earlier stage. At these earlier stages, many epithelial tumors can be treated by resection. However, at later stages of tumor development metastasis might occur after primary tumor removal. In the end, metastasis development represents the primary cause of cancer-related mortality (*5*).

1.2. Melanoma

Melanoma belongs to the most aggressive forms of skin cancer. Although only 3% of detected skin cancers are melanoma, it accounts for 65% of skin cancer-related deaths (*6*). The worldwide incidence of melanoma is increasing at a rapid rate compared to any other cancer type (Fig. 1). In the cohort of 20-40 year old patients, melanoma is already the most common cancer in Germany (*7*). This is mainly due to an increased ultraviolet (UV) light exposure as the thickness of the ozone layer is constantly decreasing (*8, 9*). Mechanistically, UV light induces specific mutations in the cellular genome and

thereby represents the main environmental risk factor for melanoma development. Therefore, 94% of melanoma occur in sun exposed areas of the skin (*10*). In addition, there are host risk factors for melanoma such as increased number and size of nevi, genetic susceptibility and a family history (*9*).

Melanoma arises from genetic mutations in melanocytes, which are neural crest-derived cells in the basal epidermis. In response to UV-induced deoxyribonucleic acid (DNA) damage, melanocyte-stimulating hormone (MSH) is produced by keratinocytes in the skin. Subsequently, MSH binds to the melanocortin receptor 1 (MC1R) on melanocytes, which triggers them to produce and release melanin. The secreted melanin protects the skin from further UV-induced DNA alterations (*11*). Melanoma is classified into four subtypes based on the tissue of origin: cutaneous melanoma (most frequent type) arises on non-glabrous skin, (2) acral melanoma originates in the glabrous skin of the palms, (3) uveal melanoma develops from melanocytes in the uveal tract of the eye, (4) mucosal melanoma (rarest type) arises from melanocytes in the mucosal lining of internal tissues (*12*).

Melanoma carries the highest mutational frequency across human cancer types (*13*). Its mutational landscape is dominated by the UV mutational signature and therefore carries many C>T or CC>TT transitions. Genes, like the cell cycle regulator cyclin-dependent kinase inhibitor 2A (CDKN2A), the oncogene Rac family small GTPase 1 (RAC1) and the tumor suppressor phosphoprotein phosphatase 6 (PPP6C) have been reported to frequently contain UV induced mutations in melanoma (*14*). Yet, the most common somatic mutation found in melanoma is the v-raf murine sarcoma viral oncogene homolog B1 (BRAF) V600E mutation, which is not a UV fingerprint mutation (*15*) and occurs in 35-50% of melanomas. BRAF encodes for RAF proteins, which are part of the mitogen-activated protein kinases (MAPK) pathway. The MAPK pathway is known to regulate cellular proliferation and survival. As the V600E mutation leads to an over activation of BRAF, it increases the oncogenic signaling through the MAPK pathway. Despite BRAF mutations, other proteins of the MAPK pathway can also be mutated. As such, 30% of melanoma patients carry mutations in NRAS and 14% of patients have a mutation in neurofibromin 1 (NF1) (*16*).

The main treatment for melanoma is surgical resection of the primary tumor (*17*). To improve overall survival, adjuvant therapies, such as immunotherapy and targeted therapy are commonly administered to late stage melanoma patients (*18*). In patients with mutations in the MAPK pathway, targeted therapy was shown to be efficient. The therapeutic combination of BRAF and mitogen-activated protein kinase (MEK) inhibitors has become a standard of care in patients with metastatic melanoma carrying BRAF mutations. In patients without BRAF mutations, immunotherapy is widely applied. This primarily includes a combination of the anti- cytotoxic T-lymphocyte-associated protein 4 (CTLA4) agent ipilimumab and the anti- programmed death 1 (PD-1) agents nivolumab or pembrolizumab (*19*). As an additional therapy for melanoma the talimogene laherparepvec (T-VEC)

has been approved in 2015 based on results from the randomized phase III open-label OPTiM (*20*). T-VEC is a herpes simples virus, type 1 (HSV-1) which preferentially replicates in tumor cells and produces granulocyte-macrophage colony-stimulating factor (GM-CSF), thereby enhancing the anti-tumor immune response (*21*).

Despite the dramatic increase in melanoma incidence, the death rates of patients remained constant in the last years (Fig. 1). This is mainly due to the advancement in therapeutic options. However, many patients still develop resistance mechanisms to current melanoma therapies (*19*). Therefore, there is an urgent need to identify novel therapeutic agents for treating patients with metastatic melanoma.

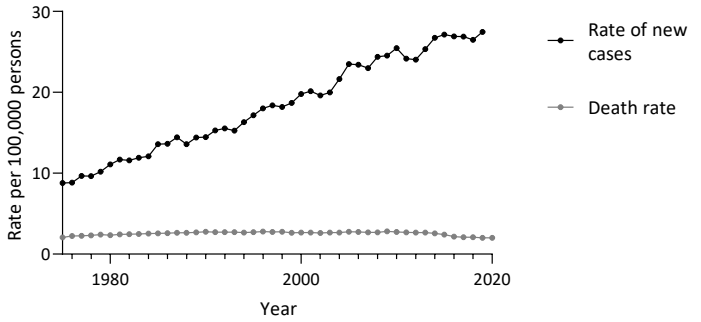

Figure 1: Trends in melanoma cases and death rates.
The graph represents the rate of new melanoma cases and death rate per year among 100,000 Americans. The data were retrieved from the Surveillance, Epidemiology and End Results registry (SEER 12).

1.3. Tumor microenvironment

During the past decades, the focus of cancer research has shifted from the cancer cell itself to the tumor microenvironment (TME), which contributes to tumor progression. The TME consists of stromal cells such as fibroblasts, endothelial cells, pericytes, leukocytes and extracellular matrix. Tumor cells secrete certain signaling molecules and metabolites to build the microenvironment. Subsequently, the tumor microenvironment actively participates in tumor progression (*22*). Specifically, the recruitment of endothelial cells (ECs) and neovascularization of the tumor is essential to nurture the tumor with nutrients and remove metabolic waste. Due to the diffusion limit of oxygen and nutrients, tumors need to develop their own vascular system to grow beyond 1 mm in diameter. Within this process, EC progenitor cells are recruited and differentiate into mature vascular ECs when stimulated by local tumor-derived factors. The process by which ECs form new blood vessels from existing ones is called angiogenesis (*23*). Besides forming vessels to provide nutrients to tumor cells, ECs in the tumor

microenvironment distribute angiocrine factors, which are EC-derived paracrine growth factors, thereby affecting tumor growth (*24*).

1.3.1. The cardiovascular system

The cardiovascular system maintains cellular homeostasis through a complex network of arteries, capillaries and veins. It moves blood through the circulatory system absorbing essential nutrients and removing cellular waste products. Blood vessels consists of a layer of ECs mounted on a basement membrane. Below the basement membrane, connective tissue and elastic lamina enable flexibility and stability of the EC layer (*25*). Perivascular cells, also referred to as pericytes, are mural cells which are embedded within the vascular basement membrane. They are highly elongated and branched cells that extend around the vessel and are physically connected to ECs by cell junctions. Therefore, pericytes decrease vessel permeability (*26*).

Within the cardiovascular system, oxygenated blood is returned from the lungs and ejected into an extensive network of arteries via the heart. The arterial system transitions into the venous system via capillaries. More specifically, capillaries are categorized into three types: continuous, fenestrated and discontinuous type (*25*). Continuous capillaries are most commonly found in the human body. They permit the diffusion of water, small solutes and lipid-soluble molecules into the adjacent tissue. However, larger molecules require specific transporters in order to pass though the EC layer. Fenestrated capillaries have intracellular pores with a diaphragm penetrating the endothelial lining. These pores allow the transport of larger molecules up to the size of small peptides and increase the transport speed. Fenestrated capillaries are found in endocrine organs and the absorptive areas in the intestinal tract. Lastly, ECs are separated by gaps in sinusoidal capillaries. This type of capillary possesses an irregular shape and inconsistent coverage by basal lamina. Therefore, water and large molecules such as plasma proteins can be exchanged freely. Sinusoidal capillaries can be found in the liver, spleen and bone marrow as well as several endocrine organs. Even though recent advances in single-cell technologies allowed a more detailed analysis of the capillary heterogeneity, further research has to be conducted to fully understand the molecular differences and differentiation processes in organ specific vascular beds (*27*).

1.3.2. Sprouting angiogenesis

In adults, ECs mostly maintain a quiescent state and barely proliferate under homeostatic conditions, with the exception of the menstrual cycle and pregnancy (*28, 29*). However, they can rapidly form new vessels from preexisting ones in response to growth factors. This process is referred as angiogenesis.

Remodeling of the vascular network is initiated according to the respective demands and can be activated through conditions such as nutrient deprivation and hypoxia (*28*).

Sprouting angiogenesis is initiated by pro-angiogenic growth factors, which are especially present in areas of low oxygen and nutrient levels (*28*). Pro-angiogenic growth factors activate ECs, which secrete matrix metalloproteinases (MMPs) to degrade the basal membrane. This feature allows motile ECs, named tip ECs, to migrate toward the angiogenic signal (*30*). Tip ECs are highly migratory and proliferate minimally. They extend their filopodia to guide the sprout in the direction of the hypoxic area. These tip cells are closely followed by stalk cells, which are highly proliferative in nature and assist in sprout elongation. Once two tip cells from independent sprouts meet, they merge to build a new vessel. Subsequently, perfusion of the vessel promotes vessel maturation by recruiting pericytes, which stabilize the newly built vessel. Upon establishment of the vessel, ECs re-acquire their quiescent state and become highly connected by forming junctional molecules, which further strengthen the vessel (*28*).

Tight regulation of angiogenesis is required in healthy tissue and disruption of this balance can result in various diseases due to too much or too little angiogenesis. Angiogenesis can also become a fundamental step in the transition of a tumor to a malignant state (*31*). As the limited diffusion rate of oxygen into tissues (100-150 µm) restricts tumor growth, initiation of angiogenesis is essential for the tumor to grow beyond a certain size (*32*). In the absence of vascular support, tumors may become necrotic. In addition to its role in the primary tumor, angiogenesis is also required for the metastatic process in order to travel to distant organs. At the metastatic site, cancer cells need to attract blood vessels in order to grow at the new location (*31*).

1.3.2.1. Endothelial cell signaling pathways during sprouting angiogenesis

The angiogenic response is tightly coordinated by proangiogenic growth factors, which are released by hypoxic cells. The most important molecule in this process is vascular endothelial growth factor (VEGF), which signals through VEGF receptors (VEGFRs) on vascular ECs (*33*). Hypoxia is the major regulator of VEGF expression via induction of hypoxia inducible factor (HIF). The VEGF ligand family consists of VEGFA-F and the placental growth factor (PlGF) (*34*). Among these proteins, VEGF-C and VEGF-D are primarily implicated in regulating lymphangiogenesis (*35*) and VEGF-A is considered the most potent isoform in regulating sprouting angiogenesis. The different VEGF family members bind to unique receptors: VEGF-B and PlGF bind to VEGFR1, whereas VEGF-C and VEGF-D bind to VEGFR3, which is implicated in lymphangiogenesis. Despite binding to VEGFRs, VEGF and PlGF can also bind to neuropilin 1 (NRP-1), increasing the binding affinity to VEGFR2. Similary, NRP-2 can interact with VEGFR3. VEGFR1 and VEGFR2 are mainly expressed on ECs and VEGF-A binds to both VEGFR1 and VEGFR2. Despite the

fact that VEGFR1 possesses a higher affinity towards VEGFA, its weak tyrosine kinase activity reduces its signal transduction. Therefore, the lower-affinity VEGFR2 is the main signaling receptor for VEGF (*36*).

VEGF-A is considered the most potent isoform in regulating sprouting angiogenesis, which primarily acts on VEGFR2 to enhance EC migration and proliferation. VEGFR2 activation initiates signaling events in ECs, which promote tip cell and filopodia formation (*37*). VEGF signaling is essential for EC homeostasis and can be dysregulated in pathologic angiogenesis. As such, the homozygous and heterozygous deletion of VEGF is embryonically lethal in mice (*38*). Ligand binding to VEGFR2 induces its dimerization, which further leads to trans-phosphorylation of the tyrosine residues on the receptors intracellular domain. Activation of VEGFR2 turns on intracellular signaling pathways which are essential for EC biology. Firstly, VEGF induces extracellular signal-regulated kinase (ERK) signaling, which regulates EC proliferation and migration. To induce ERK signaling, Phospholipase Cγ (PLCγ) is activated, which causes the generation of inositol 1,4,5-trisphosphate (IP3) and diacylglycerol (DAG). IP3 activates Ca2+ release from the endoplasmatic reticulum which then regulates the RAF1–MEK–ERK1/2 cascade (*39*). In addition, VEGF can activate VEGFR2-SRC-AKT signaling. Activation of SRC proto-oncogene, non-receptor tyrosine kinase (SRC) at cell-cell junctions affects vessel permeability (*40*). AKT-mediates the activation of endothelial nitric oxide synthase (eNOS), which induces NO signaling in the adjacent smooth muscle cells and promotes vasodilation (*41*).

Besides VEGFA-VEGFR2 signaling, Notch signaling also plays an essential role in forming the vascular system as it regulates the specification of tip and stalk cells during angiogenic sprouting. In response to VEGF, delta-like canonical Notch ligand 4 (Dll4) is induced in tip cells and activates Notch in adjacent stalk cells (*42*). This process, also referred to as lateral inhibition, regulates the ratio between tip cells and stalk cells in response to angiogenic factors and restricts excessive tip cell formation (*43*). Deletion of Dll4 induces hyper-capillary sprouting and branching due to excessive tip cell formation and EC proliferation. Therefore, Dll4-Notch signaling is essential for regulating sprouting downstream of VEGF (*42*). Upon generation of perfused vessels, mural cells are recruited by platelet-derived growth factor B (PDGF-B), which supports vessel stabilization (*33*).

The Angiopoietin/Tie signaling is one of the most prominent circuits affecting vessel maturation. Upon recruitment to the vessel, mural cells produce Angiopoietin 1 (Ang1), which promotes vascular quiescence by binding to its receptor Tie2 on ECs (*44*). While the Ang1-Tie2 signaling axis maintains EC quiescence, the contextual agonist Ang2 can destabilize already established vessels to promote sprouting angiogenesis (*44, 45*).

1.3.2.2. The role of canonical Wnt signaling in sprouting angiogenesis

Wnt proteins represent a family of 19 secreted glycoproteins in humans. They transduce their cellular signals by binding to several cell surface receptors. Among them, Frizzled (Fzd) and lipoprotein receptor-related proteins 5 or 6 (LRP5/6) are the most important receptors (*46*). The canonical Wnt signaling pathway targets β-catenin. Without Wnt ligands, β-catenin is phosphorylated by Casein kinase1 (CK1) at Thr41 and by glycogen synthase kinase-3β (GSK3β) at Ser33 and Ser37. Phosphorylation of β-catenin leads to its ubiquitination and proteasomal degradation. Upon binding of Wnt to Fzd, LRP5/6 is recruited, resulting in the activation of Dishevelled (Dvl), which prevents phosphorylation of β-catenin. Subsequently, β-catenin translocates to the nucleus, where it binds to a variety of transcription factors and induces the transcription of genes involved in proliferation, Wnt signal transduction and vascular growth (*47*). A widely expressed Wnt transcriptional target is Axin2. Axin2 acts as a negative feedback loop to limit Wnt signaling as it is a crucial component of the complex that targets β-catenin for degradation in the absence of Wnt (*48*).

Wnt signaling is reported to affect sprouting angiogenesis in physiological and pathological conditions. It was reported in colon cancer that Wnt/β-catenin signaling upregulates VEGF transcriptionally. Concordantly, constitutive activation of β-catenin results in VEGF overexpression (*49*). In addition, β-catenin is also involved in the transcriptional regulation of MMPs, which are key drivers in angiogenesis (*47*). The essential role of Wnt signaling in vascular development is further strengthened by gain and loss of function studies of Wnt signaling mutants. For example, deletion of Wnt7b in mice leads to defects in vascular development in the lung and subsequent respiratory failure (*50*). Deletion of the Fzd-5 receptor is embryonically lethal in mice, due to defects in placental angiogenesis (*51*). In contrast, the overactivation of the Wnt pathway leads to the hyperproliferation of ECs. In the mouse brain, overexpression of Wnt1 increases the proliferation of the brain microvascular ECs (*52*). In pathological neovascularization during tumor growth or myocardial infarction, β-catenin translocation to the nucleus is increased in ECs. Thus, Wnt signaling plays a vital role in actively growing vessels (*53*).

1.3.3. Other forms of tumor vascularization

Besides sprouting angiogenesis, vessel growth can be driven by a nonsprouting angiogenic process, called intussusceptive angiogenesis. During intussusceptive angiogenesis, preexisting vessels are longitudinally split into new vessels. Within this process, a transluminal bridge is formed and intracellular junctions within this bridge are restructured to centrally puncture the endothelial lining. This leads to the formation of a small hole, called pillar. Subsequently, myofibroblasts and pericytes are recruited to the pillar core. The covered pillar core increases in size and fuses with the adjacent pillar to divide one vessel into two vessels (*28*). This process is fast and efficient as it does not require

immediate proliferation or migration (*31*). Intussusceptive angiogenesis is regulated by several factors, including PDGF-B, angiopoietins, erythropoietin and ephrins (*54*). As compared to sprouting angiogenesis, intussusceptive angiogenesis is less dependent on VEGF (*55*). Therefore, this process is resistant to anti-VEGF therapy. Earlier studies have shown that tumors can switch from sprouting angiogenesis to intussusceptive angiogenesis in response to anti-angiogenic treatment and thereby restore the tumor vasculature (*56*).

Vessel co-option is a non-angiogenic mechanism of tumor vascularization in which cancer cells use pre-existing blood vessels instead of inducing the formation of new blood vessels. During this process, cancer cells adhere and proliferated along the abluminal surface of vessels and thereby get incorporated into the host blood vascular network. Tumors thereby manipulate already pre-existing vessels to meet their metabolic demand. In several tumor types such as breast, colorectal, lung, glioblastoma and melanoma, vessel co-option was shown to be an effective mechanism against anti-angiogenic therapies (*57*). However, the molecular mechanism underlying this process and the main characteristics of co-opted vessels are still poorly understood (*58*).

An additional process of tumor vascularization is vascular mimicry, whereby cancer cells act like ECs and construct their blood conducting channel without ECs. For building these channels, cancer cells increase plasticity and undergo epithelial-to-mesenchymal transition, allowing them to adopt an EC-like phenotype. Subsequently, plastic cancer cells form a tubular network and connect to the existing microcirculation. Thereby, a mosaic EC/ non-EC vasculature is formed (*28*). Vascular mimicry was reported in melanoma, breast, ovarian, prostate, lung, liver cancer and glioblastoma. Especially tumors with resistance to angiogenesis inhibitors display high levels of vascular mimicry (*59*).

It was long hypothesized that solely mature ECs can initiate neovascularization. However, this notion was challenged through the discovery of angioblast-like circulating endothelial precursor cells (CEPs), which were shown to support revascularization of ischemic tissue (*60*). A recent study has shown that CEPs are required to revascularize a pre-injured vascular network but are dispensable for regenerating the vasculature in healthy conditions (*61*). Besides from vascular regeneration, an increasing body of evidence indicates that EPC are also involved during tumor neovascularization. Mechanistically, EPCs are recruited from the bone-marrow to the tumor vasculature by tumor-derived cytokines. Within the primary tumor, EPCs transdifferentiate into ECs and aid in tumor vascularization by secreting angiogenic molecules (*62*).

1.3.4. Anti-angiogenic therapy

As tumor growth highly depends on angiogenesis, Folkman hypothesized in 1971 that anti-angiogenic therapies would starve tumors and result in their regression (*63*). In the following decades, neutralizing monoclonal antibodies for VEGF were produced. Especially bevacizumab, a humanized murine recombinant antibody against VEGF, was assessed in human clinical trials after its approval by the US FDA in 2004 (*36*).

Clinical trials revealed that VEGF pathway inhibition alone fails to produce an enduring clinical response in most patients. After an initial benefit, the tumors begin to grow again (*64*). Existing clinical and pre-clinical data suggests that tumors adapt to anti-angiogenic therapies and acquire mechanisms to evade angiogenesis blockade. Experiments in a genetically engineered mouse model of pancreatic neuroendocrine (islet cell) cancer, Rip1–Tag2, suggests that tumor regrowth after VEGF receptor blockade might be due to the upregulation of other pro-angiogenic factors. Relapsing tumors showed an upregulation of fibroblast growth factor 1 or 2 (FGF1/2), ephrin A1, ephrin A2 and Ang1 (*65*). Concordantly, serum analysis from glioblastoma patients treated with a VEGFR inhibitor revealed higher levels of FGF2 in the serum of patients in the relapse phase as compared to the levels in the response phase (*66*). An alternative mechanism for evading therapy resistance is via recruitment of endothelial progenitor cells to necrotic areas of tumors treated with VEGFR inhibitor. These cells can further facilitate the revascularization of the tumor (*67*). Moreover, a growing body of evidence suggests that ECs recruit pericytes to protect themselves from VEGFR blockade-induce death. In particular, pre-clinical data revealed that targeting both pericytes and ECs by combining VEGFR inhibition with platelet-derived growth factor receptor (PDGFR) inhibition increases the efficiency of anti-angiogenic therapy (*68*). The resistance mechanisms against VEGFR-blockade highlight the urgent need to identify new angiogenic molecules that affect the vasculature to target multiple signaling circuits and thereby prevent evading resistance mechanisms.

Due to the limited efficiency of angiogenesis inhibitors alone, they mainly were approved in combination with other drugs. Clinical trials in colorectal cancer non-squamous non-small cell lung carcinoma, renal cell carcinoma, glioblastoma multiforme, ovarian cancer, and cervical cancer confirmed the benefits of bevacizumab in combination with chemotherapy (*36*). However, it has been commonly observed that reduced vessels in the tumor will limit the delivery of the combination drug to the tumor. Therefore, the concept of vessel normalization gained importance, in which the abnormal vasculature is stabilized and remodeled. By increasing vessel normalization, immune cell infiltration and drug efficiency can be enhanced (*69*). Supporting this notion, treatment with low-dose anti-VEGFR2 antibody showed a significantly better effect than high dose therapy, due to a more favorable reprogramming of the tumor microenvironment (*70*). By normalizing blood vessels and

increasing the infiltration of immune cells, anti-VEGFR therapy can transform the tumor microenvironment from immunosuppressive to immune-supportive. Therefore, combining anti-angiogenic therapy with immunotherapy is a promising strategy for cancer treatment (*69*). A clinical trial in patients with hepatocellular carcinoma showed increased survival when patients were treated with the programed death ligand 1 (PD-L1) inhibitor atezolizumab and bevacizumab compared to treatment with the multi-kinase inhibitor sorafenib (*71*).

1.4. Metastasis

Metastasis is the final step in the metamorphosis of a tumor and accounts for the majority of cancer-related deaths. Metastasis is defined as the process in which cells disseminate from the primary tumor and form secondary tumors at distant sites (*72*). In order to form metastasis, tumor cells from the primary tumor have to undergo subsequent steps and failure to undergo one of these steps will significantly perturb metastasis formation (*73*).

In general, metastasis is a highly inefficient process as only a small percentage of cells released from the primary tumor successfully form distant nodules (*74*). However, if patients develop metastasis at the time of diagnosis, their 5-year survival rate is significantly lower. For example, the 5-year survival rate for women with breast cancer in the United States is 90% if the cancer is located only in the breast. If the cancer has spread to regional lymph nodes, the 5-year survival rate drops to 86% and if the cancer has spread to distant parts of the body, it is only 30% (*75*). A similar trend can be observed in patients with melanoma where the 5-year survival rate is 99% if the cancer is localized and drops to 71% with regional spread and 32% if the cancer has metastasized to distant tissues (*75*). Despite multiple discoveries in the last decade, metastasis is still the number one cause of cancer-related deaths. This highlights that there is an urgent need to further in-depth decipher the steps of the metastatic cascade and identify rate-limiting steps that will aid in developing novel therapies in the near future.

1.4.1. The metastatic cascade

Metastasis was defined as a “hallmark of cancer” by Hanahan and Weinberg. The multistep process of metastasis can be described as a sequence of steps, often called the invasion-metastasis cascade. Cancer cells from the primary tumor must succeed in multiple changes in order to form metastasis (Fig. 2). Initially, cancer cells have to invade locally through the adjacent tissue and intravasate into nearby blood or lymphatic vessels. After traveling through the vessels, the cancer cells have to escape from the vessel lumina into distant tissues, which is referred to as extravasation. After the formation

of micrometastasis, the distant tumor has to grow into macroscopic metastasis. This step is termed colonization [16].

In order to go through these steps, a founder cell has to gain multiple capabilities. During the invasion step, tumor cells from the primary tumor disrupt the basement membrane and penetrate the underlying stroma. In order to undergo invasion, tumor cells alter cell-cell and cell-matrix adhesion and re-organize the extracellular matrix (ECM) and cellular motility (*76*). Invasive tumor cells frequently change their cell shape to a more motile mesenchymal phenotype, known as epithelial-mesenchymal transition (EMT). Cancer EMT is characterized by the loss of E-cadherin from the adherens junctions. This results in dissociation of the cell and reduces cell-cell adhesion to increase the cancer cells's ability to migrate (*77*). In order to remodel the ECM, tumor cells produce proteolytic enzymes such as MMP which contribute to matrix degradation and thereby facilitate tumor cell invasion (*78*).

Following the invasion, tumor cells intravasate into nearby blood or lymphatic vessels. A partial degradation of the ECM and basement membrane is required to intravasate into the vessel. Subsequently, tumor cells squeeze between neighboring ECs and extend their filopodia into the vessel lumen. The process of invasion is facilitated in the tumor vasculature as it possesses a higher permeability (*76*). Tumor intravasation can be further enhanced by intracellular signaling mechanisms such as TGFB signaling, which increases EMT induction in cancer cells. In addition, other cells such as macrophages, fibroblasts and neutrophils, can play a role in enhancing tumor cell intravasation (*79*).

Upon entry into the circulation, tumor cells in the vasculature, referred to as CTCs, are under continuous exposure to environmental stressors such as oxidative stress, shear force and the immune system. Therefore, only a few cells remain alive in the circulation. In normal conditions, cells undergo programmed cell death upon detachment from the ECM, which is referred to as anoikis. In order to survive in the circulation, tumor cells have to develop mechanisms to become anoikis resistant (*80*). Activating transforming growth factor-β (TGF-β) signaling in cancer cells increases anoikis resistance by an ERK-mediated inhibition of E-cadherin (*81*). In addition, CTCs upregulate HIF-1α, which protects CTCs from anoikis by promoting metabolic reprogramming due to an increase in cellular glucose uptake (*82*). In order to enhance their survival in the circulation, CTCs often form clusters, which contain multiple cancer cells, immune cells and stromal cells. CTC clusters are more likely to survive the circulation than single cells as they suppress leukocyte activation (*72*). In addition, high flow velocity and shear stress inside the vessels can cause mechanical stress and CTC death. Platelets within the circulation were reported to form aggregates around CTCs and CTC clusters and thereby provide a shield from shear stress (*83*).

The metastatic potential of CTCs depends on their ability to extravasate into the surrounding tissue. When tumor cells arrest in small capillaries, they can either directly migrate through the vessel wall or

proliferate within the blood vessel and then extravasate (*84*). In order to extravasate, active adhesion between tumor cells and the endothelium is required. A wide range of ligands such as selectins, cadherins, integrins and CD44, are involved in the adhesion process. Upon adhesion to the endothelium, tumor cells modulate the endothelial barrier and eventually undergo transendothelial migration to the underlying tissue (*85*). Tumor cells can directly promote their extravasation by secreting certain factors which promote the extravasation process. For example, the extravasation of breast cancer cells is promoted by the expression of epidermal growth factor (EGF) receptor ligands and MMP1/ MMP2 (*86*). As the host microenvironment plays an important role in extravasation, this process is often organ-specific. For example, organotropism can be observed in breast cancer which most frequently metastasizes to the bone (*87*).

Colonization at secondary sites requires favorable conditions in the metastatic niche, such as sufficient oxygenation and nutrients. Initially, micrometastasis can grow in the absence of angiogenesis. However, due to the diffusion limit of oxygen and nutrients, the development of new vessels is necessary for tumors to grow beyond 1 mm in size. Colonization does not require immediate cell division. Disseminated tumor cells (DTCs) can remain dormant for months to years post-seeding. This process can be mediated by immune mechanisms or insufficient blood supply (*76*). Metastasis can further metastasize when tumor cells from the metastatic nodule undergo the same sequence of steps (*88*).

There are two hypotheses describing metastatic progression. According to the linear model, cancer cells undergo genetic and epigenetic alterations and acquire the capabilities for successful metastasis formation within the primary tumor. The parallel model predicts that less advanced DTCs are distributed and selected independently to the primary tumor at distant sites, which might occur in a cell type-dependent manner [17]. Finally, gaining a better understanding on the dynamics of metastasis and the molecules involved in the different steps of the metastatic cascade is essential for providing better treatment regiments to target metastasis.

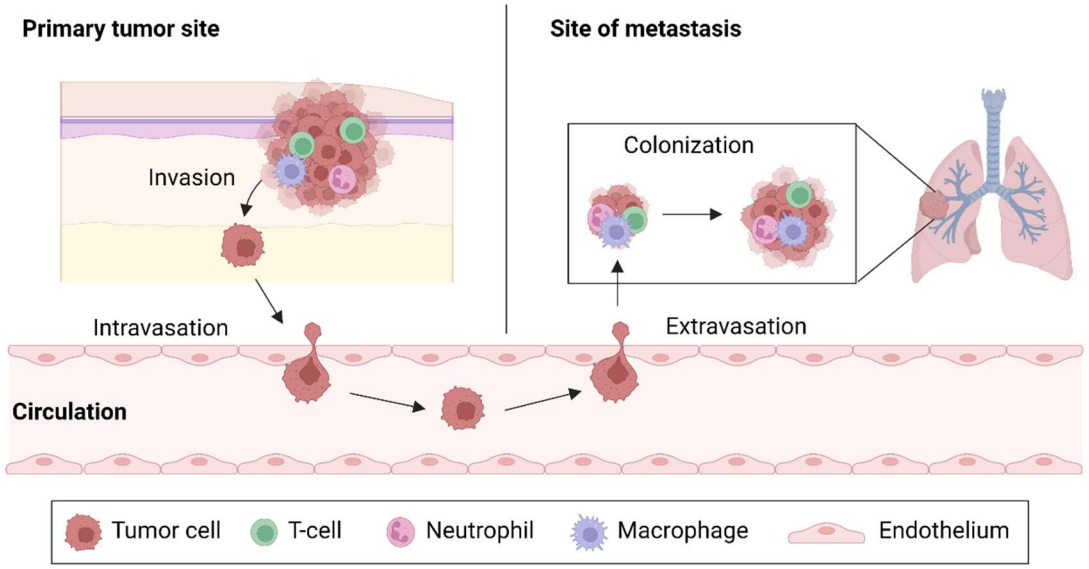

Figure 2: Steps of the metastatic cascade.
The figure illustrates the main steps of the metastatic cascade. Initially, tumor cells from the primary tumor locally invade the surrounding tissue. Subsequently, invaded tumor cells intravasate into a nearby blood or lymphatic vessel. The so-called CTCs have to survive in the circulation for a defined period of time until they extravasate through the EC barrier and eventually reach the metastatic site. During colonization, micrometastasis grows into overt macrometastasis. This figure was generated with BioRender.com.

1.5. The metastatic niche

Metastatic cancer cells encounter great resistance upon entering distant organs. However, signaling cues from the local microenvironment support colonization of metastatic cells. This microenvironment, which favors colonization, is referred to as metastatic niche (*89*). At the metastatic niche, immune cells, fibroblasts, stromal cells and ECs reside in the tissue parenchyma and secrete chemokines, growth factors, matrix-degrading enzymes and adhesion molecules which promote the outgrowth of the metastatic lesion (*90*).

Several characteristics of the metastatic niche promote the colonization of tumor cells. The assembly of a functional vasculature is essential to allow expansion of micrometastasis to macrometastasis by activating the angiogenic switch (*90*). During this event, the balance of pro- and anti-angiogenic factors tilts towards a pro-angiogenic outcome, thereby vascularizing DTC and promoting their proliferation (*91*). In addition, an immunosuppressive microenvironment is established by upregulating regulatory, immunosuppressive cells such as myeloid-derived suppressor cells (MDSCs), macrophages and regulatory T-cells (Tregs). Thereby, DTCs can overcome immunological elimination. Metastatic outgrowth is further promoted by chronic inflammation in the metastatic niche (*92*).

1.5.1. The effect of primary tumor-derived factors on the metastatic niche

Primary tumor and metastasis form an interacting network, whereby primary tumor-derived factors can effect metastatic outgrowth by altering the metastatic niche (Fig. 3). A few reports show that the primary tumor can promote metastatic outgrowth. Pro-angiogenic platelets were shown to accumulate in the metastatic niche and secrete a multitude of cytokines, such as VEGF, TGF-β1, PDGF-B and PlGF (*93*). Thereby, they promote vessel formation. In addition, growth differentiation factor 15 (GDF15) expressing, cancer-associated fibroblasts in the prostate tumor microenvironment were shown to promote the dissociation of tumor cells. Moreover, growth differentiation factor 15 (GDR15)-expressing fibroblasts were shown to systemically effect the outgrowth of distant tumor cells at the metastatic site (*94*).

In contrast, there are multiple publications reporting the secretion of primary tumor-derived factors, which limit the outgrowth of metastasis. This phenomenon, which is commonly referred to as concomitant tumor resistance (CTR) was first reported in 1906 (*95*) and was since then studied in mouse models of melanoma (*96, 97*), breast cancer (*98, 99*), lung cancer (*100, 101*), lymphoma and fibrosarcoma (*102, 103*). The current hypothesis is that the primary tumor affects both the host's immune system and releases systemically-acting anti-angiogenic cytokines, thereby effecting the metastatic niche (*104*). In a B16F10 melanoma model, the primary tumor was shown to change the immune landscape and thereby reduce metastasis formation of intravenously injected tumor cells (*96*). Further, the colonization of DTCs was shown to be inhibited in an EMT6 mammary carcinoma model due to the activation of CD8 T-cells (*98*).

The angiogenesis-based hypothesis of CTR was raised by Folkman *et al.* in 1994 who discovered the primary tumor-derived factor Angiostatin. Angiostatin inhibits EC proliferation and acts as an inhibitor of angiogenesis. Upon surgical removal of the primary tumor, distant metastasis rapidly colonizes the lung due to the lack of Angiostatin (*100*). Subsequently, Endostatin was identified as an additional anti-angiogenic factor, secreted by the primary tumor, which inhibits metastasis. Mechanistically, Endostatin inhibits cyclin D1 and thereby induces EC apoptosis. In addition, Endostatin binds to integrin α5β1 and suppresses angiogenesis by affecting the EC cytoskeleton (*105*).

The pre-clinical findings of CTR supports the clinical observation that metastasis mainly occurs after the primary tumor has been removed. For example, in patients with bladder cancer, a fast metastatic progression is observed upon radical cystectomy. This effect was shown to be due to the lack of Endostatin and Angiostatin, which are highly expressed in human bladder cancer (*106*). Concordantly, in patients with colorectal cancer, a reduced vascular density is observed in the liver upon primary tumor removal (*107*). Overall, these clinical observations validate the preclinical findings that the primary tumor actively limits growth of metastasis by secreting anti-angiogenic cytokines.

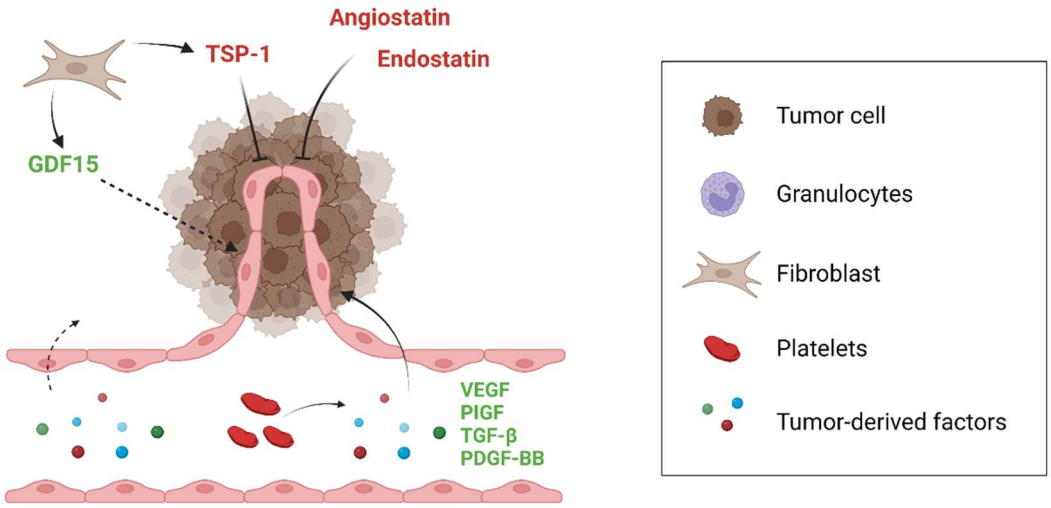

Figure 3: Effect of primary tumor-derived factors on the metastatic niche.
Tumor-educated platelets secrete VEGF, PlGF, TGF-β and PDF-BB, which induces EC sprouting and promotes tumor colonization. In addition, cancer associated fibroblasts from the primary tumor secrete GDF15 and TSP-1, which enhance or reduce angiogenesis at the metastatic site, respectively. Angiostatin and Endostatin are secreted by the primary tumor and directly act on ECs to reduce angiogenesis. Tumor-derived factors stimulating cancer cell dissemination or colonization are highlighted in green and tumor-derived factors suppressing these processes are represented in red. This figure was created with BioRender.com.

1.6. ANGPTL4 signaling

Angiopoietin-like 4 (ANGPTL4) belongs to a family of 8 structurally similar Angiopoietin-likes (ANGPTL1-8). The ANGPTL proteins share a common amino-terminal coiled-coil domain, a linker region and a carboxy-terminal fibrinogen-like domain. However, ANGPTL8 is structurally different from the other molecules of the ANGPTL family, as it has no fibrinogen-like domain. Due to the structural differences compared to the related angiopoietins, the ANGPTL proteins can not bind to the angiopoietin receptors tyrosine kinase with immunoglobulin-like and EGF-like domain 1 and 2 (Tie1/2) (*108*).

In 2000, ANGPTL4 was simultaneously discovered by three research groups as a hepatic protein (*109*), which is induced upon fasting (*110*) and plays a role during pre-adipocyte differentiation (*111*). Due to its expression in adipose tissue and liver, ANGPTL4 was thereafter characterized as an adipokine. ANGPTL4 expression is regulated by peroxisome proliferator-activated receptors (PPARs) in hepatocytes and adipose tissue and its expression is upregulated during fasting. Therefore, ANGPTL4 is also called fasting-induced adipose factor (Fiaf). In addition, ANGPTL4 is upregulated during hypoxia in a HIF-1 dependent manner (*112*). Since its discovery, intensive studies have been performed on

ANGPTL4, which characterized ANGPTL4 as a multifunctional protein involved in a variety of physiological and pathological conditions (*113*).

1.6.1. Structural basis of ANGPTL4 signaling

ANGPTL4 is a 50 kDa, 406-amino-acid glycoprotein consisting of an n-terminal signal sequence, which is followed by a α-helical region predicted to form a coiled-coil. The protein contains a linker region and a globular fibrinogen-like domain on its c-terminal side. Upon secretion, ANGPTL4 is cleaved at the linker region by proprotein convertases, releasing an n-terminal fragment (nANGPTL4) and a c-terminal fragment (cANGPTL4) (*114*). The cleavage of ANGPTL4 is tissue specific. For example, the human liver mainly contains the ANGPTL4 cleavage products, while adipose tissue contains the full-length form (flANGPTL4). Several proprotein convertases were shown to be involved in ANGPTL4 cleavage. Proprotein convertase subtilisin/kexin type3 (PCSK3), furin and proprotein convertase 5/6 (PC5/6) can cleave ANGPTL4 at its $R^{161}RKR^{164}$ linker region. Post-transcriptionally, nANGPTL4 is glycosylated and sialylated. In addition, it forms intermolecular disulfide bonds, which are responsible for the oligomerization of nANGTPL4 in dimeric or tetrameric structures (*113*).

ANGPTL4 and its cleavage fragments were reported to bind to different receptor signaling systems. nANGPTL4 is known chiefly to bind and inhibit lipoprotein lipase (LPL), which is the enzyme responsible for the hydrolysis of TGs from very low-density lipoproteins and chylomicrons. Mechanistically, the n-terminal region of ANGPTL4 binds LPL with high affinity and converts the catalytically active dimers into inactive LPL monomers, thereby irreversibly inactivating the enzyme (*114*). Besides LPL, nANGPTL4 was recently shown to bind to the heparan-sulfate proteoglycan syndecan-4 (SDC4) in HepG2 hepatocellular carcinoma cells, which triggers the internalization and degradation of the SDC4 receptor (*115*). cANGPTL4 is reported to bind to extracellular matrix proteins. As such, cANGPTL4 modulates wound healing by binding to integrins β1 and β5 (*116*) as well as fibronectin and vitronectin on keratinocytes (*117*). In ECs, ANGPTL4 binds to integrin α5β1, weakening cell-cell contact and leading to vascular disruption (*118*). Despite extracellular matrix proteins, cANGPTL4 was recently reported to bind to the transmembrane glycoprotein neuropilin in the context of diabetic macular edema (DME) to increase the permeability of retinal vasculature (*119*). As nANGPTL4 and cANGPTL4 bind to distinct receptors, they activate different signaling mechanisms, thereby contributing to the multifunctional role of ANGPTL4.

1.6.2. Multifunctional roles of ANGPTL4

ANGPTL4 is a multifunctional protein, which is involved in a variety of processes such as the regulation of energy metabolism, inflammation, kidney disease, wound repair, tumorigenesis vascular permeability and angiogenesis (*113*).

ANGPTL4 regulates energy metabolism on multiple layers. Hypothalamic ANGPTL4 expression can mediate anorexic effects by inhibiting hypothalamic AMP-activated protein kinase (AMPK) activity. As such, ANGPTL4 knockout (ko) mice were shown to display increased body weight and food intake and a diminished anorexic response (*120*). Further, ANGPTL4 links the gut microbiota to fat metabolism as various probiotic bacteria upregulate circulating ANGPTL4 levels, which leads to reduced fat storage and changes in serum triglyceride (TG) levels due to the inhibition of LPL (*121*). One of the most studied functions of ANGPTL4 is its effect on lipid metabolism. As ANGPTL4 inhibits LPL, it inhibits the clearance of TGs to free fatty acids (*122*). The effect of ANGPTL4 on lipid metabolism is described in detail in section 1.3.2.2. In addition to lipid metabolism, ANGPTL4 also effects glucose homeostasis. Adenoviral overexpression of ANGPTL4 reduced plasma glucose and improved glucose tolerance. In diabetic mice, ANGPTL4 alleviated glucose intolerance and hyperinsulinemia. Mechanistically, ANGPTL4 lowers plasma glucose by decreasing hepatic glucose output (*123*). In contrast, ANGPTL4 ko mice, fed on a diet rich in unsaturated fatty acids and cholesterol, display improved glucose tolerance and elevated insulin levels (*124*). The reason for the discrepancy in the literature is unclear. However, it is assumed that the diet plays a role in the ANGPTL4 mediated effects on glucose homeostasis. As such, ANGPTL4 overexpressing mice fed on a chow diet are only marginally glucose tolerant and become highly glucose intolerant on a high-fat diet (*125*).

As lipid uptake is typically associated with immune stimulation, ANGPTL4 regulates inflammation in an LPL-dependent manner (*126*). Specifically, ANGPTL4 expression is induced in macrophages by fatty acids and thereby leads to inhibition of TG hydrolysis. In mice lacking ANGPTL4, fatty acids induce the activation of macrophages, foam cell formation, and an uncontrolled cascade of fat-induced inflammation is initiated (*126*). In addition, mesenchymal stem cell-derived ANGPTL4 can blunt the polarization of macrophages towards the proinflammatory phenotype. Therefore, ANGPTL4 therapy was suggested to facilitate macrophage polarization and to induce cardiac repair after infarction (*127*). In addition, ANGPTL4 was characterized as an acute phase protein, whose expression is stimulated during the acute phase response, such as upon LPS stimulation. By inhibiting LPL, ANGPTL4 contributes to hypertriglyceridemia, often observed during the acute phase response (*128*). Overall, ANGPTL4 is essential for regulating the maintenance of a healthy state and to prevent uncontrolled inflammation.

Multiple studies reported the role of ANGPTL4 in kidney disease. In patients with nephrotic syndrome, it was shown that ANGPTL4 is overexpressed in the glomerulus, the filtering unit of the kidney. In line

with these findings, podocyte-specific overexpression of ANGPTL4 in rats resulted in many characteristic symptoms of kidney disease, such as proteinuria and the loss of the glomerular basement membrane (*125*). In contrast, ANGPTL4 was recently found to ameliorate hyperlipidemia-induced renal injury by downregulating α-actinin-4 (ACTN4) (*129*). Overall, the effect of ANGPTL4 on kidney disease seems to be sialylation-dependent. Upregulation of the unsialylated form, which is secreted by podocytes, induces the manifestations of nephrotic syndrome. By contrast, a sialylated form of ANGPTL4, secreted from skeletal muscle, heart and adipose tissue reduced proteinuria (*130*).

In wound healing, ANGPTL4 is expressed by keratinocytes to coordinate cell-matrix communication. ANGPTL4 interacts with vitronectin and fibronectin, thus promoting re-epithelization of the wound (*117*). In addition, ANGPTL4 interacts with integrins β1 and β5 on keratinocytes to activate the FAK-Src-PAK1 signaling pathway and thereby enhance cell migration. Concordantly, ANGPTL4-deficient mice exhibit delayed wound re-epithelialization and impaired keratinocyte migration (*116*).

As wound healing shares many similarities with the process of tumor development and invasion, many molecules involved in re-epithelization also play a role in tumorigenesis. Consistent with this notion, ANGPTL4 has been shown to be upregulated in many tumor types. Tumor-derived ANGPTL4 interacts with integrin β1 and β5 and thereby elevates the intracellular O_2-:H_2O_2 ratio. As a consequence, tumor cells transmit a pro-survival signal and become anoikis resistant. Notably, pre-clinical studies showed that treatment with a monoclonal antibody against cANGPTL4 significantly reduced melanoma primary tumor growth, whereas treatment with nANGPTL4 blocking antibody did not affect tumor growth (*131*). In hepatoma cells, ANGPTL4 has been found to contribute to anoikis resistance as ANGPTL4 knockdown enhances apoptosis and makes tumor cells more susceptible to drug treatment. This further strengthens the role of ANGPTL4 in promoting anoikis resistance in tumor cells (*112*).

1.6.2.1. Role of ANGPTL4 in angiogenesis and metastasis

Despite its direct role on cancer cells, ANGPTL4 effects tumorigenesis by effecting angiogenesis and metastasis. However, the reported literature is highly controversial, with some studies reporting an anti-angiogenic (*132-134*) and anti-metastatic effect of ANGPTL4 (*135, 136*) and others reporting the opposite (*118, 137-139*).

Many studies describe angiogenesis-promoting characteristics of ANGPTL4. In the tumor setting, ANGPTL4 is induced in a HIF1-dependent manner in ECs in necrotic areas surrounding hypoxic regions of renal cell carcinoma to induce angiogenesis (*140*). Similarly, inhibition of ANGPTL4 reduced the angiogenic potential of uveal melanoma in an orthotropic mouse transplant model (*137*). In obese mice, the expression of adipocyte-derived ANGPTL4 was shown to be upregulated and to drive breast cancer progression by increasing tumor angiogenesis. Concordantly, ANGPTL4-deficiency reduces

obesity-induced angiogenesis and tumor growth (*141*). An angiogenesis promoting-role of PPAR-induced ANGPTL4 was shown in mammary carcinoma. Mechanistically, ANGPTL4 promotes vascular EC migration, which further enhanced angiogenesis and primary tumor growth (*142*). In addition, ANGPTL4 is upregulated in Kaposi's sarcoma and promotes angiogenesis and vessel permeability by upregulating GTPases, such as Ras homolog family member A (RhoA) in tumor ECs (*143*). Despite enhancing angiogenesis in the tumor setting, ANGPTL4 has been reported to enhance angiogenesis in other pathologies, such as ischemia and eye disease. In patient tissues, ANGPTL4 is upregulated in critical leg ischemia, which is characterized by a decrease in blood supply. Within this pathology, ANGPTL4 contributes to enhancing angiogenesis (*140*). In the context of age-related macular degeneration, ANGPTL4 actively promotes the growth of abnormal leaky blood vessels in the eye, which promotes irreversible vision loss. Therefore, targeting both ANGPTL4 and Vegf in patients with macular degeneration is more effective in treating this blinding disease than targeting VEGF alone (*144*). In a second eye disease, diabetic macular edema, ANGPTL4 was also shown to act synergistically with VEGF to destabilize the retinal barrier. Mechanistically, cANGPTL4 binds to neuropilins on ECs, which leads to an activation of the RhoA signaling pathway. Overall, proangiogenic roles of ANGPTL4 have been reported in the setting of tumor angiogenesis, ischemia and eye diseases.

ANGPTL4 has been reported to enhance metastasis by promoting different steps within the metastatic cascade. Invasion of tumor cells from the primary tumor into adjacent tissue was shown to be promoted by ANGPTL4 in oesophageal squamous cell carcinoma and osteosarcoma (*138, 145*). In colorectal cancer cells, overexpression of ANGPTL4 enhances cell migration and invasion via upregulation of bone morphogenetic protein 7 (BMP7) (*146*). Concordantly, siRNA-mediated knockdown of ANGPTL4 promotes invasion abilities of gastric cancer cell lines (*147*). In addition, ANGPTL4 was shown to enhance the survival of tumor cells in the circulation and promote metastasis. In patients with gastric cancer, ANGPTL4 is induced by hypoxia and increases resistance to anoikis, thereby enhancing tumor cell survival in the circulation and ultimately, promoting metastasis (*139*). A significant body of literature reported that ANGPTL4 promotes tumor cell extravasation by disruption of the EC barrier. cANGPTL4 interacts with integrin α5β1, VE cadherin and claudin-5, leading to endothelial disruption and inducing vascular leakiness, thereby facilitating lung metastasis (*118*). Similarly, TGFβ from the breast cancer tumor microenvironment induces ANGPTL4 in cancer cells, which disrupts lung vascular EC-cell junction and thereby increases metastasis (*148, 149*).

Although many reports portray pro-metastatic and pro-angiogenic functions of ANGPTL4, anti-angiogenic and anti-metastatic roles have been described in several publications. Anti-angiogenic functions have been reported in a mouse model of hind limb ischemia. In response to hypoxia, ANGPTL4 accumulates in the vessels, decreasing the motility of ECs and reducing sprouting (*132*). In the context of retina development, ANGPTL4 ko mice show an increased vascular density and ANGPTL4

was shown to play a critical role in hypoxia-induced angiogenesis (*150*). Additionally, tumor-derived ANGPTL4 reduces angiogenesis by suppressing ERK signaling (*136*). Apart from affecting angiogenesis, ANGPTL4 has been reported to inhibit vascular permeability. In the heart, ANGPTL4 acts vasculoprotective and ANGPTL4 ko mice show disrupted adherens junctions leading to increased vascular permeability (*133*). A similar phenotype was observed in the context of metastasis: When ANGPTL4 is overexpressed systemically in mice via *in vivo* DNA electro transfer, cancer cells metastasize less as compared to control mice. Mechanistically, ANGPTL4 induces reorganization of the actin cytoskeleton by inhibiting actin stress fiber formation (*135*). In addition, adenovirus-mediated overexpression of ANGPTL4 inhibits invasiveness and metastasis by suppressing tumor angiogenesis in liver tumors (*151*).

Overall, the reported role of ANGPTL4 on angiogenesis and metastasis is highly controversial and further studies will be needed to clarify the contextually of ANGPTL4's pro- and anti-metastatic functions.

1.6.2.2. Role of ANGPTL4 in lipid metabolism

Lipids are mainly carried through the bloodstream in the form of lipoproteins. Especially, TGs are carried in chylomicrons and very-low-density lipoproteins. TGs are hydrolyzed to free fatty acids by the enzyme LPL in the capillary bed. Mechanistically, LPL is transported from cells of production, which are mostly adipocytes and cardiomyocytes, to the capillary surface, where it is anchored by binding to the glycosylphosphatidylinositol anchored high density lipoprotein binding protein 1 (GPIHBP1). The binding of LPL to GPIHBP1 is essential for LPL activity (*122*). In the blood, chylomicrons and very-low-density lipoproteins interact with LPL, which catalyzes their hydrolysis. The resulting free fatty acids are taken up by adipocytes and cardiomyocytes, where they are either stored or oxidized. In order to regulate fatty acid uptake to the needs of the respective tissue, LPL is subjected to multiple regulatory influences. Dysregulation of these mechanisms can lead to lipid overload in metabolic disorders such as cardiovascular diseases (*152*).

ANGPTL4 is a potent LPL activity inhibitor, therefore playing a vital role in lipid metabolism. ANGPTL4 expression in adipocytes, heart and liver is induced during fasting by PPARs. After its secretion and cleavage, nANGPTL4 specifically bind to LPL in the capillary lumen and inhibits the hydrolysis of TG to free fatty acids (Fig. 4). Conversely, reduced fatty acid levels reduce PPAR activity, whereby a feedback loop is formed which tightly regulates TG hydrolysis (*152*). The inhibitory mechanism of ANGPTL4 is still controversial, as several alternate mechanisms have been suggested in the literature. Initially, ANGPTL4 was reported to inhibit LPL activity by preventing LPL dimerization and converting the active dimeric state into an inactive monomeric state (*153*). However, an additional mechanism suggested

that ANGPTL4 binds to LPL and dissociated its complex with GPIHBP1. Thereby, ANGPTL4 inactivates LPL irreversibly by promoting the unfolding of its hydrolase domain (*154*). A recent report states that ANGPTL4 binds to the lipid domain of LPL and prevents catalysis of the substates at the active site near the lid domain (*155*). Besides directly inhibiting LPL activity at endothelial surfaces, ANGPTL4 prevents TG clearance by promoting intracellular degradation of LPL in adipocytes (*156*). Overall, ANGPTL4 can inhibit LPL activity by effecting both LPL stability and activity.

Given its ability to inhibit LPL, ANGPTL4 plays an important role in lipid metabolism and manipulation of ANGPTL4 levels affects circulating TG levels. Indeed, overexpression and injection of recombinant ANGPTL4 significantly increased plasma TG levels and decreased LPL activity in mice (*157*). Conversely, studies in ANGPTL4 deficient mice revealed increased plasma LPL activity and decreased plasma TG clearance (*158*). In humans, ANGPTL4 serum levels positively correlate with body mass and TG levels (*159*).

As elevated plasma TG levels are associated with an increased risk of developing cardiovascular disease, the role of ANGPTL4 on cardiovascular pathologies has been extensively studied. In humans, plasma ANGPTL4 levels have been reported to correlate positively with future cardiovascular events and the development of coronary artery disease (CAD) (*160*). This result aligns with animal studies, as genetic depletion or antibodies against ANGPTL4 reduces circulating TG and leads to the formation of smaller atherosclerotic lesions in mice (*161*).

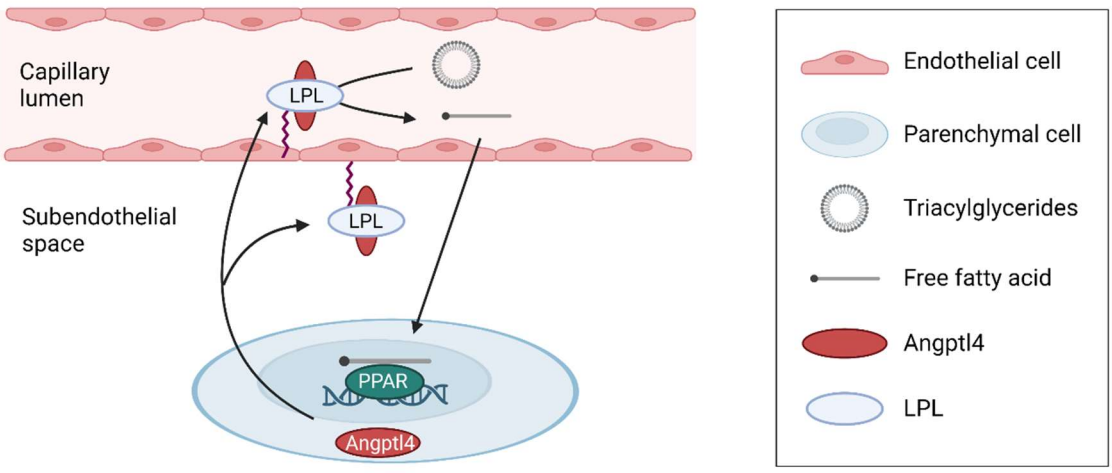

Figure 4: Mechanism of Lipoprotein lipase (LPL) inhibition by ANGPTL4.
Upon starvation, ANGPTL4 expression is induced by PPAR transcription factors in parenchymal cells. Subsequently, ANGPTL4 is transported into the capillary lumen, where it binds to GPIHBP1-anchored LPL. By inhibiting LPL, ANGPTL4 inhibits the conversion from TGs to free fatty acids. Reduced fatty acid levels reduce PPAR activity, forming a feedback loop that tightly regulates TG hydrolysis. Adapted according to (*152*). This figure was created with BioRender.com.

1.6.3. The role of the E40K mutation in ANGPTL4

Human genetic studies of coding variants of ANGPTL4 found the E40K missense variant in 3% of European Americans. Carriers of the E40K mutation had significantly lower plasma TG levels than patients without the mutation (*162*). Patients carrying the E40K mutation have a single base pair substitution, which changes the CAG codon into the AAG codon, leading to an exchange of the amino acid number 40 from glutamic acid (E) to lysine (K) (*163*). The discovery of the E40K mutation and its correlation with lipid levels led to further research on the effect of this mutation on ANGPTL4 structure and processing. The results indicate that after secretion, the E40K mutation interferes with nANGPTL4 and flANGPTL4 oligomerization. As oligomerization of ANGPTL4 is essential for its inhibitory activity on LPL, the E40K mutation renders ANGPTL4 unfunctional with respect to its regulatory role in lipid metabolism (*114*).

The ANGPTL4 E40K variant was shown to be beneficial in several pathologies. As such, besides having lower levels of TG, carriers of the E40K mutation are significantly less likely to develop coronary artery disease (*163*). Among participants with obesity, the E40K variant protects against dyslipidemia and improves the lipid profile, resembling a more metabolically healthy phenotype (*164*). In addition, ANGPTL4 improves glucose homeostasis, lowers fasting glucose and enhances insulin sensitivity, and is therefore correlated with reduced risk of developing type 2 diabetes. However, the mechanism linking the loss of ANGPTL4 function to improved insulin sensitivity is not entirely understood (*165*).

1.7. SDC4 signaling

The cell surface proteoglycan SDC4 regulates multiple cellular processes such as cell adhesion, proliferation, migration, mechanotransduction and endocytosis. SDC4 contains an extracellular domain to which glycosaminoglycans, linear chains of polysaccharides, are covalently linked. This domain mediates the extracellular actions of SDC4. The membrane-spanning region consists of a single-pass domain and the intracellular domain defines the signaling pathways that are initiated by SDC4. Therefore, SDC4 has the ability to form a connection between the ECM and intracellular signaling cascades, thereby affecting growth and differentiation in several tissues (*166*).

SDC4 interacts with multiple growth factors, chemokines and morphogens with its extracellular domain. Due to its extracellular heparan sulfate chains, SDC4 binds to heparin-binding growth factors, including FGFs, VEGFs and PDGFs. Thereby, SDC4 can organize their distribution in the extracellular space (*167*). In addition, SDC4 mediates the direct contact of cells with ECM proteins, such as fibronectin. The extracellular attachment sites can develop into focal adhesions, which are specialized membrane regions with increased tensile strength. Within this process, SDC4 binding to fibronectin is

necessary to activate focal adhesion kinase (FAK), which regulates focal adhesions. Besides its role in focal adhesion formation, SDC4 is a sensor of extracellular stress and transmits mechanical force into signaling events, such as MAPK activation (*166*).

The variety of signaling events of SDC4 is mainly due to its diverse intracellular binding partners. SDC4 maintains low RhoG and Rac1 activity. However, binding of growth factors or fibronectin triggers SDC4-mediated activation of PKCα thus increasing RhoG and Rac1 activity. Consequently, these events affect cell polarity, actin polymerization and cell migration. SDC4-dependent activation of PKCα also has a crucial role regulating the mammalian target of rapamycin (mTOR) complex 2 (mTORC2), which in turn controls the activation of AKT serine/threonine kinase. Due to its AKT-activating function, SDC4 affects proliferation, angiogenesis and cell survival (*166*). In embryonic development, ANGPTL4 was shown to bind to SDC4, which forms a complex with the Wnt co-receptor LRP6. Upon binding of ANGPTL4, the complex is internalized via clathrin-mediated endocytosis and degraded in lysosomes. Eventually, Wnt/β-catenin signaling is downregulated due to LRP6 degradation (*115*).

Several reports have shown that SDC4 alters EC signaling, thereby affecting pathological angiogenesis. Wound vascularization was impaired in SDC4 ko mice compared to wild-type littermates (*168*). In mouse models of myocardial infarction and hind limb ischemia, SDC4 overexpression increases vessel density and blood perfusion, thus improving cardiac and muscle function (*169, 170*). A recent report has shown that post-natal retinal and tumor development is hindered in SDC4 ko mice. Mechanistically, SDC4 is upregulated in pathological angiogenesis on immature vessels and promotes VEGFA-induced VE-cadherin internalization. Therefore, targeting of SDC4 is an viable option as an antiangiogenic therapy (*171*).

2. Aim of the study

Angiopoietin-like 4 (ANGPTL4) has been characterized as a primary tumor-derived protein that acts as crucial regulator of cancer progression (*112, 172*). However, the published literature on ANGPTL4 functions during tumor progression is highly controversial. While the majority of studies describe ANGPTL4 as a pro-angiogenic and pro-tumorigenic molecule (*118, 137-139*), considerable literature exists that supports an anti-angiogenic (*132-134*) and anti-tumorigenic function of ANGPTL4 (*135, 136*). Upon secretion, ANGPTL4 has been shown to be proteolytically cleaved into two fragments, namely nANGPTL4 and cANGPTL4. Both fragments carry out unique functions, with nANGPTL4 being shown to act as an inhibitor of LPL and to reduce circulating TG levels (*122*), whereas the cANGPTL4 acts as a stimulator of angiogenesis by binding to integrin (*173*). The conflicting reports on ANGPTL4 functions in metastasis raised the hypothesis of proteolytic cleavage-dependent pro- and anti-tumorigenic functions of ANGPTL4. Our laboratory has previously demonstrated distinctly opposing functions of the ANGPTL4 cleavage fragments in preliminary experiments. When overexpressed by the tumor cells, cANGPTL4 promoted tumor growth and metastasis leading to reduced overall survival, whereas nANGPTL4 inhibited metastasis and enhanced overall survival in mouse models of melanoma and lung cancer. Mechanistically, cANGPTL4 enhanced angiogenesis by binding to integrins (*174*). However, the mechanism of nANGPTL4 action as well as its therapeutic and clinical implications remain elusive. Therefore, it was the aim of the first part of this PhD thesis (1) to identify the mechanism of nANGPTL4 anti-metastatic action, (2) to assess the therapeutic potential of nANGPTL4 by systemic administration of nANGPTL4 in pre-clinical mouse models of metastasis and (3) to correlate the amount and distribution of ANGPTL4 and its fragments with disease progression and survival in human samples.

As nANGPTL4 is a potent inhibitor of LPL (*122*), overexpression of recombinant ANGPTL4 significantly increases plasma TG levels and decreases LPL activity in mice (*157*), which is a potential side effect of nANGPTL4 treatment. A previous study revealed that carriers of the missense E40K variant of ANGPTL4 display lower TG levels (*163*). E40K mutation prevents oligomerization of ANGPTL4 thereby abolishing its ability to inhibit LPL activity (*114*). Therefore, in order to optimize the potential nANGPTL4-mediated anti-metastatic therapy, the second part of this PhD thesis was aimed at studying the effect of an E40K mutation of nANGPTL4 on tumor metastasis, angiogenesis and lipid metabolism.

3. Results

3.1. nANGPTL4 acts as a systemic inhibitor of angiogenesis and metastasis

3.1.1. nANGPTL4 has no effect on tumor cell proliferation and adhesion

Previous results from our lab have shown that overexpression of nANGPTL4 in tumor cells inhibits metastasis in a spontaneous metastasis lung cancer model (LLC) as well as in experimental melanoma metastasis models (B16F10) (*174*). Therefore, the first aim of this study was to determine the mechanism of nANGPTL4 anti-metastatic action. It has previously been reported that ANGPTL4 can affect tumor cell proliferation, which was mainly attributed to cANGPTL4 (*174*). However, no report exists on whether nANGPTL4 directly acts on tumor cells to affect tumor cell proliferation. To investigate whether tumor-cell derived nANGPTL4 could alter tumor cell proliferation in an autocrine manner, nANGPTL4 was lentivirally upregulated in B16F10 cells, and a FACS-based EdU assay was performed (Fig. 5A). Lentiviral upregulation of nANGPTL4 did not affect tumor cell proliferation of the B16F10 cell line (Fig. 5B). Similarly, lentiviral upregulation of nANGPTL4 in LLC (Fig. 5C) did not alter proliferation (Fig. 5D).

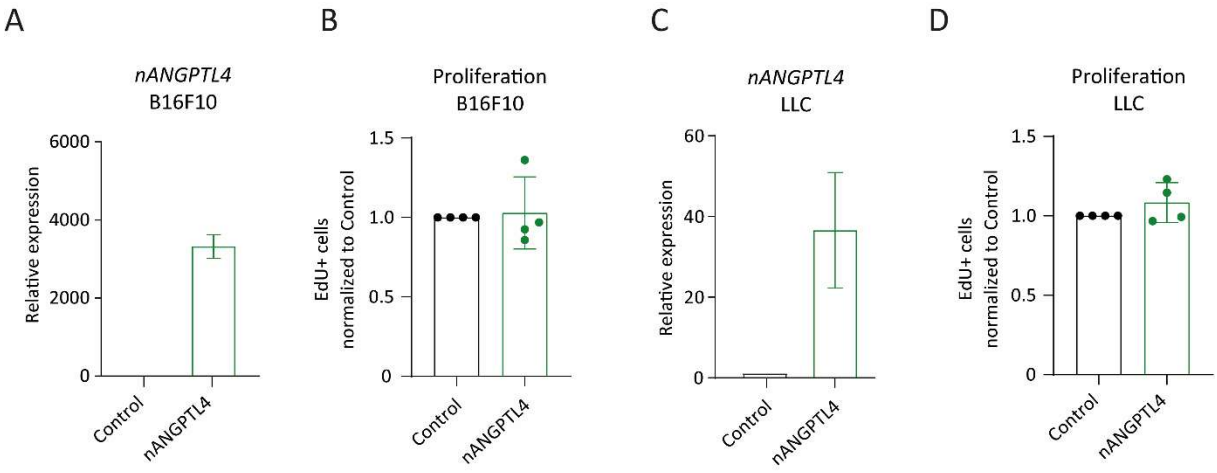

Figure 5: Autocrine nANGPTL4 has no direct effect on tumor cell proliferation.
(A) RNA levels of *nANGPTL4* in control and nANGPTL4 overexpressing B16F10 tumor cells were determined by qPCR (n=2). (B) Proliferation of control or nANGPTL4 overexpressing B16F10 tumor cells was determined by EdU flow cytometry assays (n=4; mean±SD). (C) RNA levels of *nANGPTL4* in control and nANGPTL4 overexpressing LLC tumor cells were determined by qPCR (n=3). (D) Proliferation of control or nANGPTL4 overexpressing LLC tumor cells was determined by EdU flow cytometry assay (n=4; mean±SD).

As autocrine nANGPTL4 had no effect on tumor cell proliferation, the next aim was to assess whether paracrine nANGPTL4 could affect tumor cells. Towards this end, recombinant murine nANGPTL4 was produced in insect cells. Therefore, the nANGPTL4 sequence, followed by a StrepIITag, was cloned into the pAceBac1-EGT plasmid (Fig. 6A). After the transfection and cultivation of Hi5 insect cells, the growth medium was collected and recombinant murine nANGPTL4 was purified from the culture medium with Streptavidin beads. The presence of nANGPTL4 was confirmed on an SDS-PAGE gel (Fig. 6B). To investigate the role of systemic nANGPTL4 treatment on tumor cell proliferation, a FACS-based EdU Assay was performed on B16F10 cells, which were treated with recombinant mouse nANGPTL4 for 16h (Fig. 6C). The experiment showed that nANGPTL4 administration did not affect tumor cell proliferation (Fig. 2D).

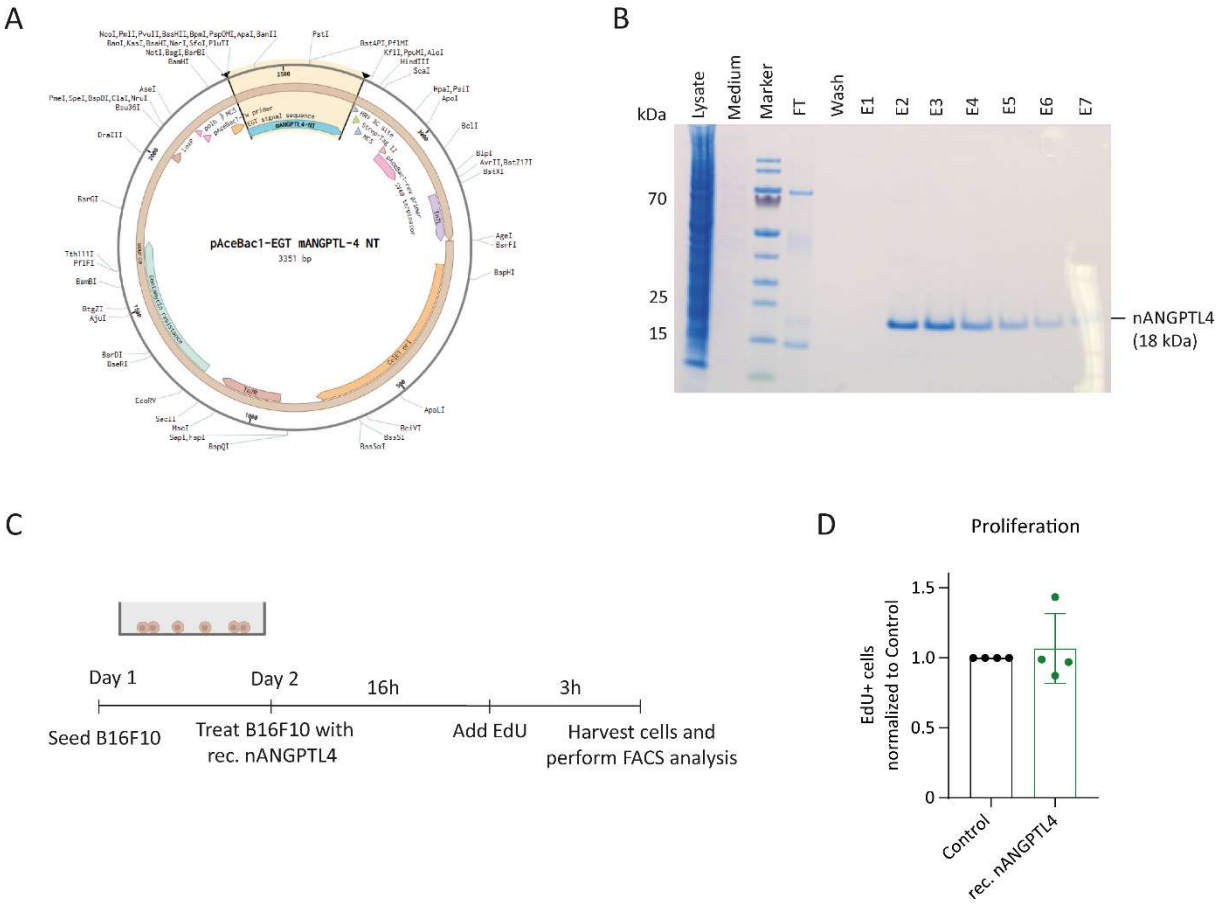

Figure 6: Recombinant nANGPTL4 has no effect on tumor cell proliferation.
(A) The mouse nANGPTL4 sequence was cloned into the pAceBac1-EGT vector. (B) SDS-PAGE gel of nANGPTL4 overexpressing insect cells lysate, the respective cell culture medium, flow-through (FT) from StrepTactinXT column, wash solution used in StrepTactinXT column and eluates (E1-E7) from StrepTactinXT column. Probes were separated on a gradient gel (4-12%) and colored with Coomassie blue. (C) Experimental scheme of B16F10 treatment with recombinant nANGPTL4 to analyze the effect on proliferation. (D) Quantitation of cellular proliferation of rec. nANGPTL4 or control (storage buffer) treated B16F10 tumor cells analyzed by EdU flow cytometry assay (n=4; mean±SD).

It is well-established that, despite tumor-cell intrinsic effects, the bidirectional interaction of tumor cells with their microenvironment is essential for tumor progression and metastasis (*175*). The absence of a direct effect of nANGPTL4 on tumor cell proliferation led me to hypothesize that nANGPTL4 might indirectly alter tumor cell behavior by affecting other cell types in the tumor microenvironment. As ANGPTL4 was previously shown to affect EC adhesion, migration and sprouting (*132*), the effect of nANGPTL4 on the EC tumor cell interaction was assessed. During metastasis, tumor cells interact with ECs by adhering to them. This allows the tumor cells to extravasate and to colonize new tissues (*176*). In order to investigate whether nANGPTL4 affects the capability of ECs to interact with tumor cells, an adhesion assay was performed. Within this assay, mLECs were treated with recombinant mouse nANGPTL4 for 16h followed by the seeding of GFP+ B16F10 tumor cells on the mLEC monolayer. After allowing the cells to adhere for 40 min, the percentage of GFP+ cells was analyzed (Fig. 7A). FACS analysis revealed that nANGPTL4 treatment of mLECs did not alter the adhesion of tumor cells (Fig. 7B).

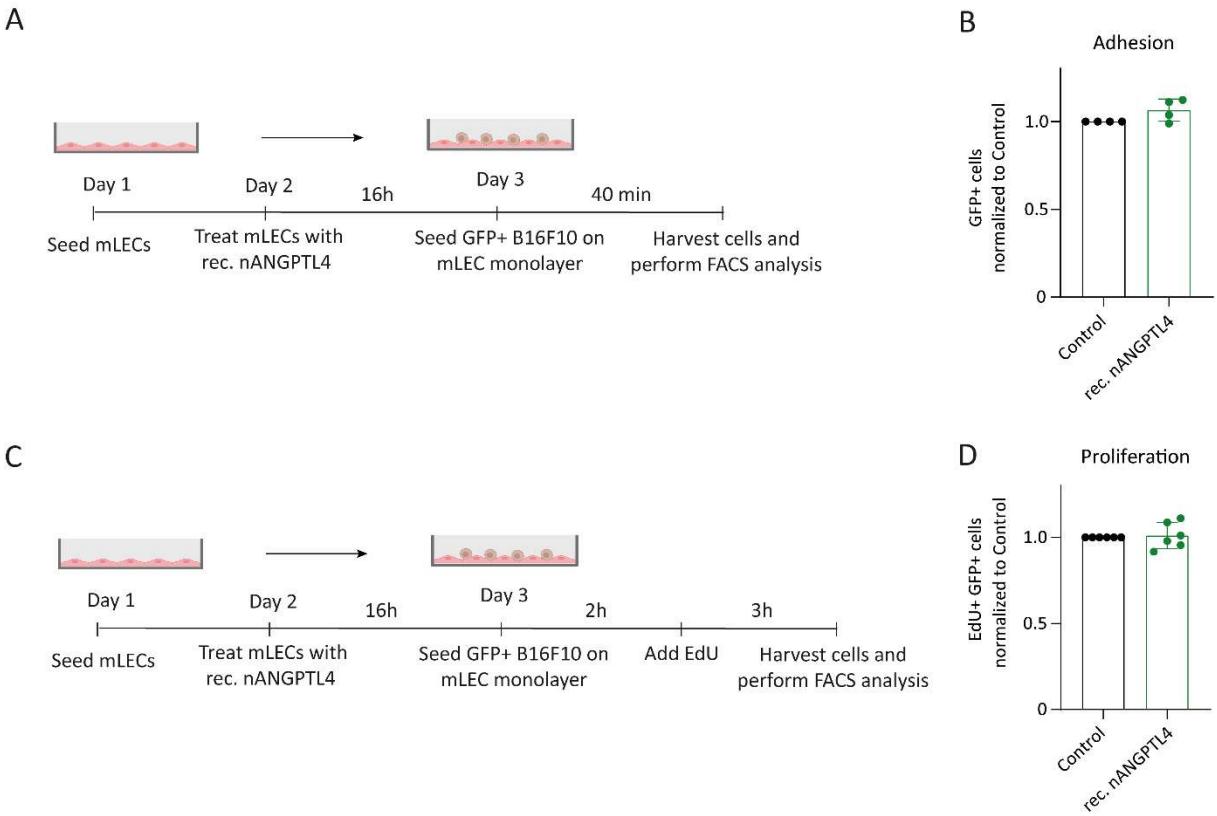

Figure 7: Treatment of endothelial cells with nANGPTL4 has no effect on tumor cell adhesion and proliferation.

Experimental scheme of the adhesion assay to evaluate the adhesion of B16F10 tumor cells to mLECs. (B) Quantification of the percentage of GFP+ cells adhering to the mLEC monolayer by EdU flow cytometry assay (n=4, mean±SD). (C) Experimental scheme of mLEC treatment with recombinant nANGPTL4 to analyze the effect on proliferation of B16F10 tumor cells. (D) Quantitation of cellular proliferation of B16F10, which were seeded on mLECs treated with rec. nANGPTL4 or control (storage buffer). Proliferation was assessed by EdU flow cytometry assay (n=6; mean±SD).

Besides affecting tumor cell adhesion, ECs can alter tumor cell proliferation. To assess whether nANGPTL4-treated ECs affect tumor cell proliferation, mouse lung ECs (mLECs) were treated with recombinant nANGPTL4 for 16h. This was followed by seeding GFP+ B16F10 tumor cells on the mLEC monolayer (Fig. 7C). FACS-based EdU Assay showed that treating mLECs with recombinant nNAGPTL4 did not change tumor cell proliferation (Fig. 7D). Overall, recombinant nANGPTL4 did not alter tumor cell proliferation and adhesion *in vitro*.

3.1.2. nANGPTL4 inhibits endothelial cell proliferation and sprouting angiogenesis

The formation and outgrowth of metastatic nodules are highly regulated by angiogenesis (*177*). Full-length ANGPTL4 was previously described to regulate EC proliferation and sprouting (*132, 136, 137*). However, the effect of nANGPTL4 on EC proliferation and sprouting has not been addressed so far. In order to investigate the effect of nANGPTL4 treatment on EC, an EdU assay was performed on human umbilical endothelial cells (HUVECs), which were treated with recombinant human nANGPTL4 or PBS. Treatment with recombinant nANGPTL4 reduced EC proliferation *in vitro* (Fig. 8A). As EC proliferation is essential for the growth of a vascular network, an EC sprouting assay was performed *in vitro* to assess the effect of nANGPTL4 on sprouting angiogenesis. PBS and two different concentrations of VEGF were used to determine the effect of nANGPTL4 on quiescent and minimally and highly activated EC spheroids. The experiment revealed that nANGPTL4 reduced sprouting of HUVEC spheroids both in combination with a low (1 ng) and with a high (10 ng) amount of VEGF (Fig. 8B, C). To further substantiate these findings *in vivo*, a cornea pocket assay was performed in which pellets with recombinant nANGPTL4, either alone or in combination with VEGF, were implanted into the cornea. Consistent with the *in vitro* findings, nANGPTL4 reduced VEGF-induced vascularization (Fig. 8D, E). Taken together, recombinant nANGPTL4 reduces EC proliferation and sprouting angiogenesis in both in *vitro* and *in vivo* angiogenesis assays.

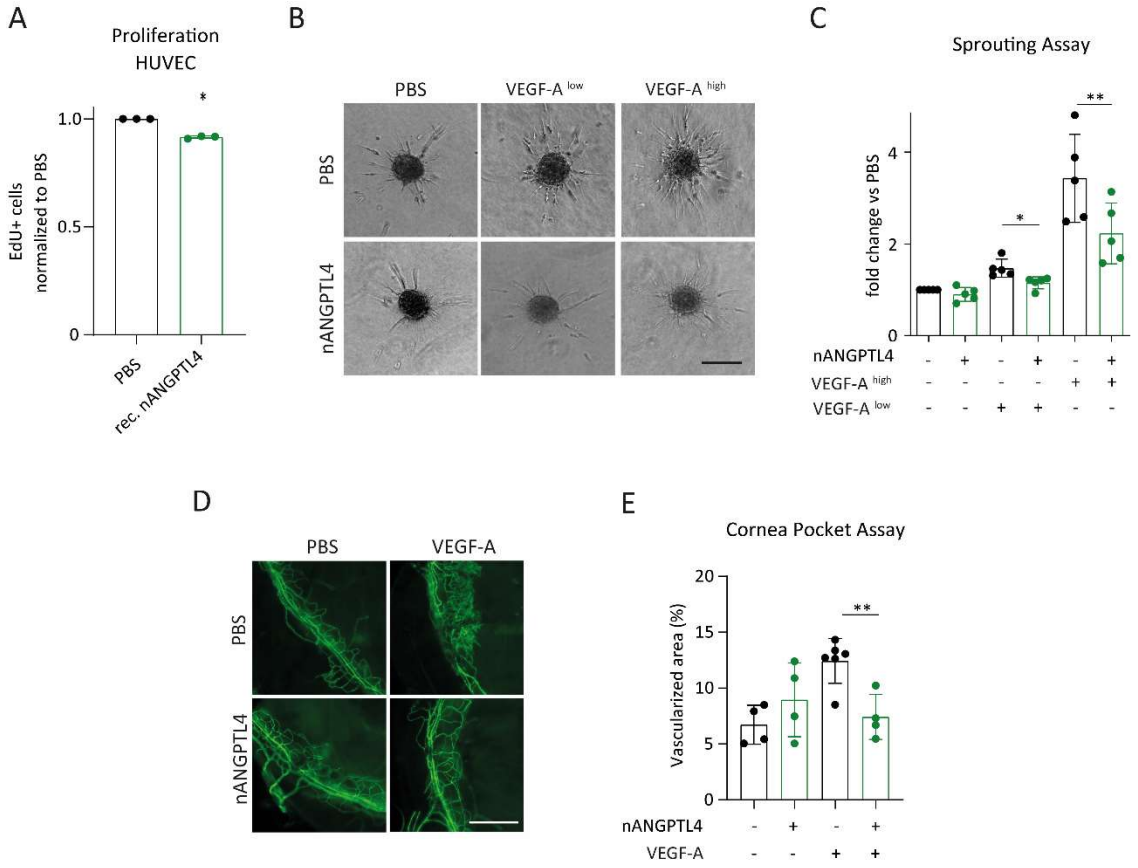

Figure 8: nANGPTL4 reduces endothelial cell proliferation and sprouting.
(A) Quantitation of cellular proliferation of HUVECs, which were treated with rec. nANGPTL4 or PBS. Proliferation was assessed by EdU flow cytometry assay (n=3; mean±SD). *, p<0.05, two-tailed paired Student's t-test. (B) Representative pictures of HUVEC spheroids. Spheroids were stimulated with the respective recombinant proteins. Scale bar: 200 µm. (C) Quantification of the cumulative sprout length of HUVEC spheroids. Spheroids were stimulated with the respective recombinant proteins (n=5, mean±SD). *, p<0.05; **, p<0.01, two-tailed paired Student's t-test. (D) Representative IF pictures of the corneas isolated from wildtype mice. Corneas were stimulated with either PBS or the indicated recombinant proteins. Staining for the EC marker CD31 (green) was performed. Scale bar: 500µm. (E) The vascularized corneal area was quantified in cornea pocket assays (n=4-6; mean±SD). **, p<0.01, unpaired Student's t-test.

3.1.3. nANGPTL4 reduces endothelial cell sprouting in an SDC4-dependent manner

The current literature suggests that ANGPTL4 can bind to integrins, thereby modulating keratinocyte migration and vascular junction integrity (*116, 118*). To investigate whether the nANGPTL4-mediated effect on sprouting angiogenesis is integrin-dependent, a sprouting assay was performed in the presence of integrin-blocking antibodies. However, the addition of integrin-blocking antibodies could not alter the nANGPTL4-mediated anti-angiogenic effect (Fig. 9A, B). This suggested that the effect of nANGPTL4 on sprouting was due to a different signaling receptor system.

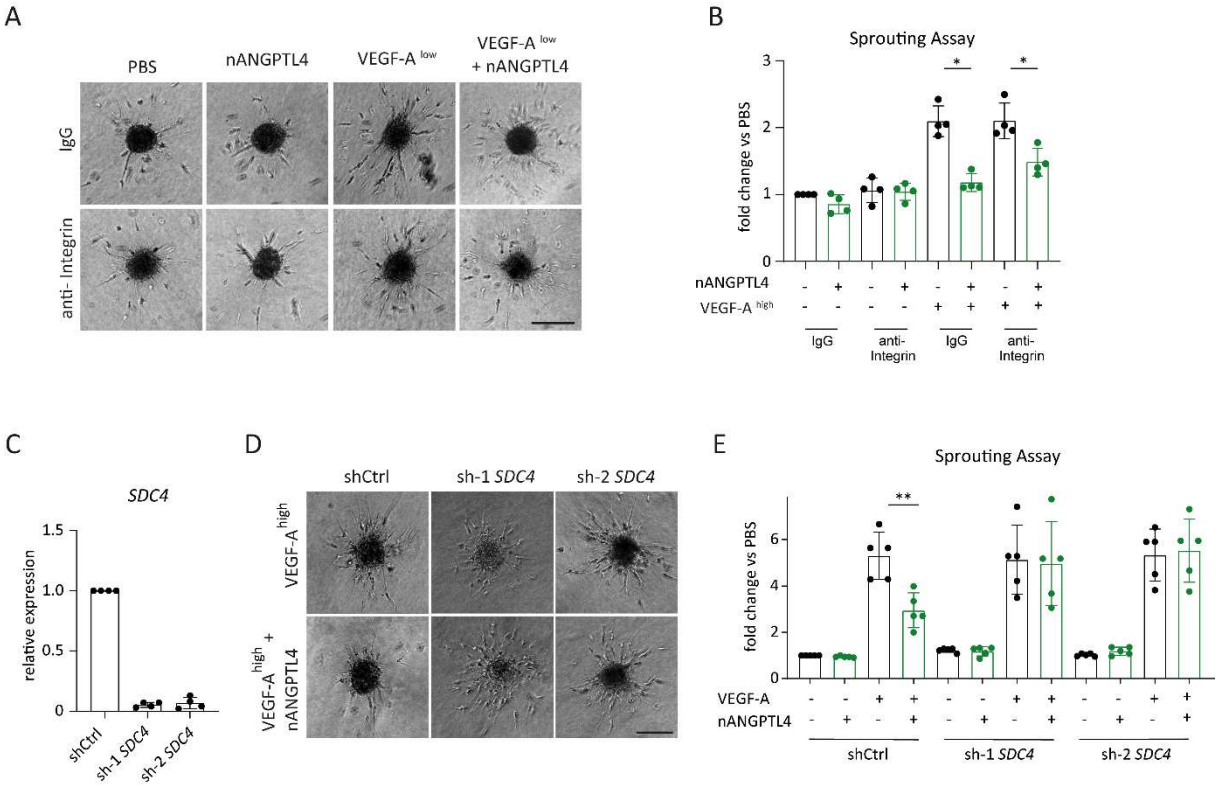

Figure 9: nANGPTL4 reduces sprouting in an integrin-independent and SDC4-dependent manner.
(A) Representative images of HUVEC spheroids pretreated with IgG or integrin blocking antibodies and stimulated with the depicted recombinant proteins. Scale bar: 200 µm. (B) Quantification of the cumulative sprout length of HUVEC spheroids pretreated with IgG or integrin blocking antibodies and stimulated with the depicted cytokines (n=4, mean±SD). *, p<0.05; **, two-tailed paired Student's t-test. (C) *SDC4* expression was quantified in shCtrl, sh-1 *SDC4* and sh-2 *SDC4* HUVEC cell lines (n=3, mean±SD). (D) Representative pictures of HUVEC spheroids stimulated with the depicted cytokines. Scale bar: 200 µm. (E) Quantification of the cumulative sprout length of HUVEC spheroids stimulated with the depicted recombinant proteins (n=5, mean±SD). **, two-tailed paired Student's t-test

nANGPTL4 was recently described to bind to the heparan sulfate proteoglycan syndecan-4 (SDC4) (*115*). Furthermore, loss-of-function studies in SDC4-deficient mice have identified SDC4 as a regulator of angiogenesis (*178*). Consequently, I hypothesized that the nANGPTL4-mediated effect on EC sprouting might be SDC4-dependent. Therefore, shRNA-mediated knockdown of SDC4 was performed in HUVEC cells. An effective silencing was achieved with two different shRNAs (sh-1 and sh-2, Fig. 9C). To characterize the effect of SDC4 depletion on the nANGPTL4-mediated anti-angiogenic effect; the sprouting assay was performed with shCtrl, sh-1 SDC4 and sh-2 SDC4 HUVEC cell lines. Indeed, nANGPTL4 reduced VEGF-induced sprouting angiogenesis in EC transduced with control shRNA. In contrast, silencing of SDC4 in HUVECs completely ablated the anti-angiogenic effect of nANGPTL4 (Fig. 9D, E), suggesting the anti-angiogenic effect of nANGPTL4 was SDC4-dependent.

3.1.4. nANGPTL4 reduces Wnt signaling *in vitro*

It was previously revealed that binding of nANGPTL4 to SDC4 downregulates Wnt-signaling by enhancing the lysosomal degradation of lipoprotein receptor-related protein 6 (*115*). Wnt signaling is a major driver for vessel formation and maturation (*179*). In order to investigate whether nANGPTL4 regulates Wnt signaling in ECs, HUVECs were treated with recombinant nANGPTL4. Treatment with nANGPTL4 resulted in transcriptional downregulation of *AXIN2* (Fig. 10A). Concordantly, addition of nANGPTL4 blocked Wnt3a-mediated upregulation of *AXIN2* in HUVECs (Fig. 10B). In addition, RT-qPCR of livers from global *ANGPTL4*-deficient mice showed that deletion of *ANGPTL4* resulted in *Axin2* upregulation (Fig. 10C, D).

Overall, the results suggest that nANGPTL4 reduces EC sprouting *in vitro* by downregulating Wnt signaling in a SDC4-dependent manner.

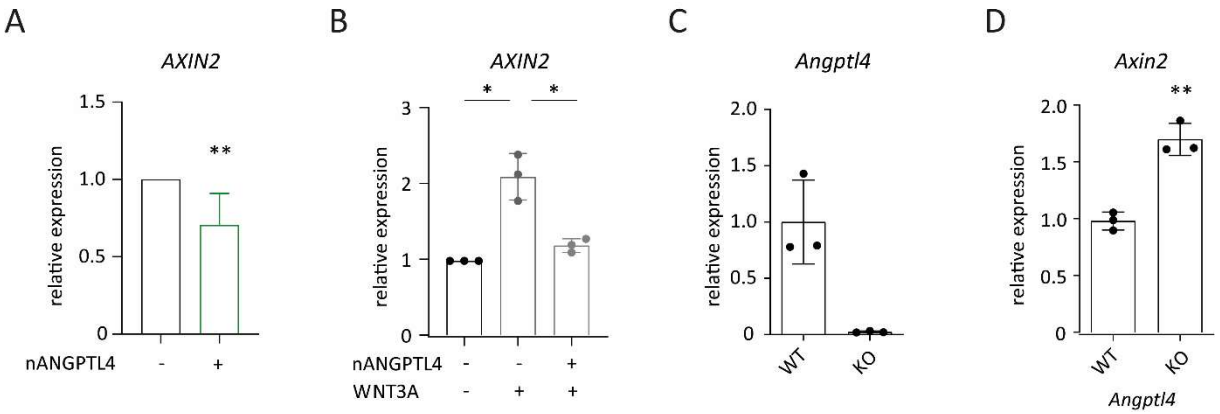

Figure 10: Wnt signaling is altered in nANGPTL4 treated HUVECs and ANGPTL4 ko mice.
(A) *AXIN2* expression was quantified by RT-qPCR in HUVECs upon treatment with recombinant nANGPTL4 (n=7; mean ± SD). **, p<0.01, two-tailed paired Student's t-test. (B) *AXIN2* expression was quantified by RT-qPCR in HUVEC treated with the depicted recombinant proteins (n=3; mean ± SD). *, p<0.05, two-tailed paired Student's t-test. (C) *ANGPTL4* expression was determined in whole liver lysates of wildtype (WT) and ANGPTL4-knockout (KO) mice (n=3, mean±SD). (D) Quantitation of *Axin2* expression in whole liver lysates of wildtype (WT) and ANGPTL4-deficient (KO) mice (n=3, mean±SD). **, p<0.01, unpaired Student's t-test.

3.1.5. Therapeutic administration of recombinant nANGPTL4 inhibits metastasis

As metastatic colonization and outgrowth rely on angiogenesis, anti-angiogenic drugs can potentially be used to reduce metastasis formation. Considering the anti-angiogenic effect of nANGPTL4, the therapeutic potential of nANGPTL4 was assessed in the experimental B16F10 metastasis model. Therefore, the B16F10 melanoma cell line was injected intravenously (i.v.). The mice were killed on day 14 after tumor cell injection and the number of lung metastases was counted. Recombinant nANGPTL4 (7ug/shot) or PBS was injected once prior to tumor cell injection. Afterwards, mice were intravenously injected with either PBS or recombinant nANGPTL4 twice per week for a period of 14

days (Fig. 11A). Quantifying the number of metastases in the lung revealed that nANGPTL4 strongly reduced metastasis formation (Fig. 11B, C). In order to confirm that the observed phenotype was primarily due to the functional nANGPTL4 protein, an experimental metastasis experiment was performed with heat-inactivated recombinant nANGPTL4. Treatment regimens identified in the previous experiments were applied where denatured nANGPTL4 or PBS were injected once before tumor cell injection and four times after tumor cell injection (Fig. 11D). Heat-inactivation of the nANGPTL4 recombinant protein resulted in the loss of its anti-metastatic properties (Fig. 11E, F), which confirms that the effect is genuinely due to the functional nANGPTL4. As an additional experimental metastasis model, the MT-RET melanoma cell line was injected i.v. and the nANGPTL4 treatment regime was applied (Fig. 11G). The results indicate that recombinant nANGPTL4 reduces metastasis in the MT-RET model (Fig. 11H, I). Thus, recombinant nANGPTL4 impairs metastatic outgrowth in two distinct experimental metastasis models.

Considering the metastasis reducing effect of nANGPTL4, different injection schemes were tested to investigate whether nANGPTL4 injections can be reduced and to dissect which step of the metastatic cascade is mostly affected by nANGPTL4 in the B16F10 model. Therefore, different therapeutic regimes were employed with recombinant nANGPTL4 to target extravasation, early and late colonization (Fig. 12). Pre-treatment with nANGPTL4 (7ug, i.v.) before tumor cell injection was insufficient to reduce metastasis (Fig. 12A-C). In a second and third model, recombinant nANGPTL4 was exclusively injected during the phases of early (Fig. 12D-F) or late metastasis (Fig. 12G-I). These injection schemes did not affect the number of lung metastases. In addition, 4 shots of recombinant nANGPTL4 were given during both the early and late phases of metastasis, but this was not sufficient to induce an effect on metastatic colonization in the lung (Fig. 12J-L). Overall, nANGPTL4 treatment during individual phases of metastasis did not alter the metastatic outgrowth of tumor cells.

Overall, the results suggest that a constant supply of nANGPTL4 is required during the metastatic process to suppress metastasis.

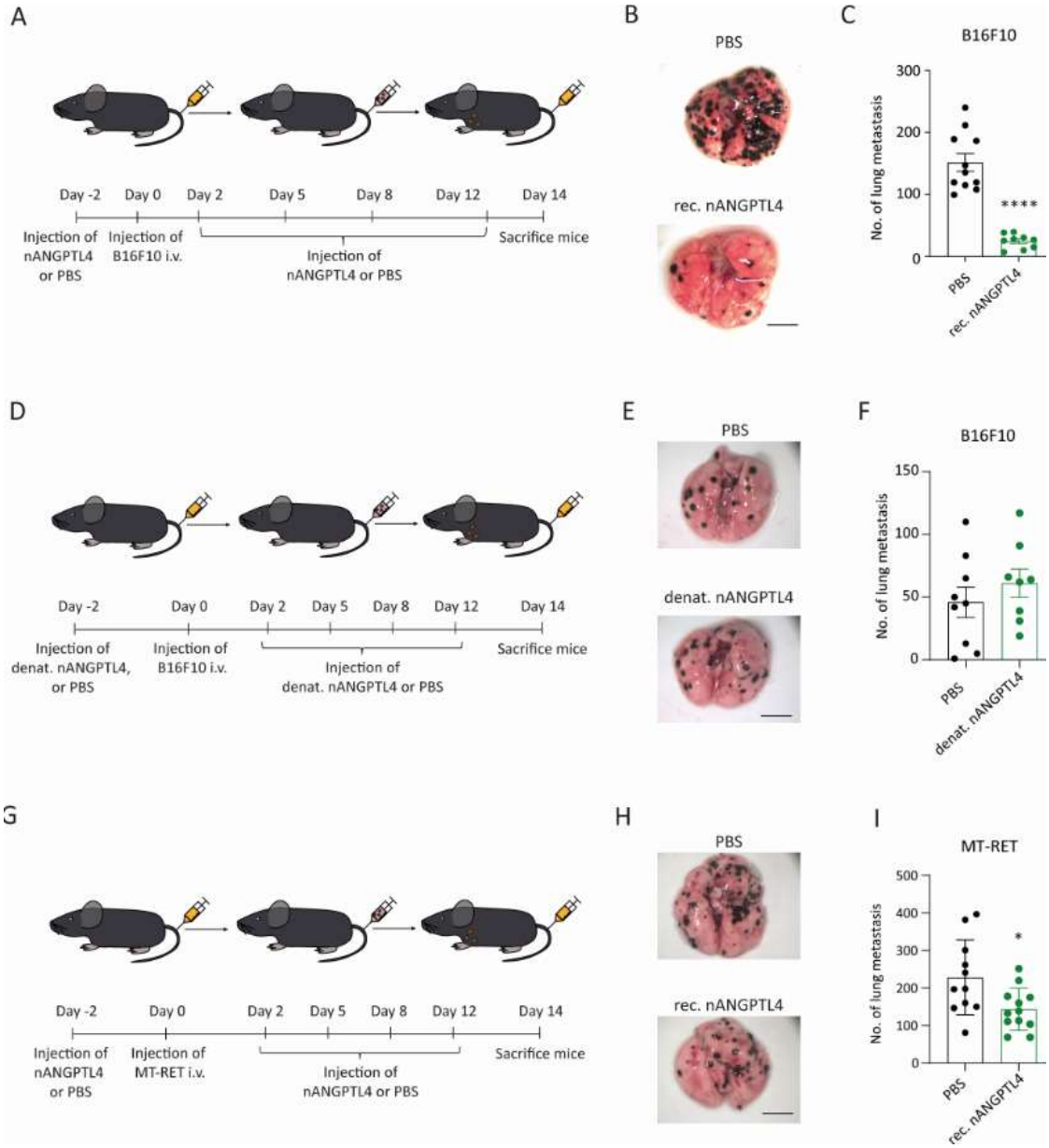

Figure 11: Constant therapeutic administration of recombinant nANGPTL4 reduces metastasis in the B16F10 and MT-RET model.

(A) Experimental scheme of recombinant nANGPTL4 administration in the B16F10 experimental metastasis model. (B) Representative images of lung metastatic foci. Scale bar: 2mm. (C) Quantification of lung metastases. (n=9-10; mean±SEM). ****, p<0.0001, Mann-Whitney U test. (D) Experimental scheme of denatured nANGPTL4 administration in the B16F10 experimental metastasis model. (E) Representative images of lung metastatic foci. Scale bar: 2mm. (F). (n=8-9; mean±SEM). (G) Experimental scheme of the MT-RET experimental metastasis model to evaluate the effect of recombinant nANGPTL4. (H) Representative pictures of metastatic lungs from mice which were injected with PBS or nANGPTL4. Scale bar: 2mm. (I) Quantification of lung metastases (n=11; mean±SD). *, p≤0.05, Mann-Whitney U test.

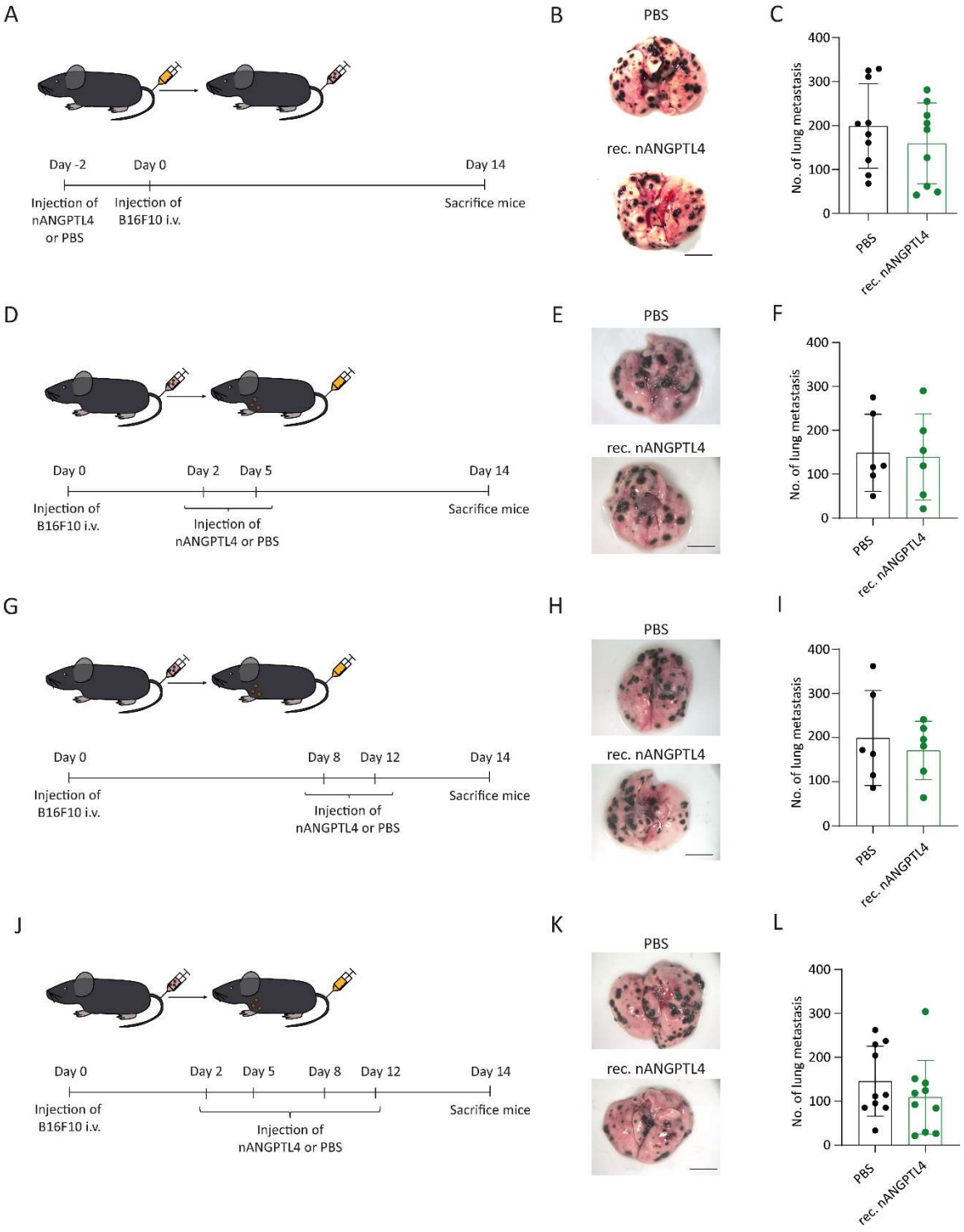

Figure 12: Short-term treatment with recombinant nANGPTL4 has no effect on metastasis.
Mice were injected with either recombinant nANGPTL4 (7 µg/shot) or PBS in the experimental metastasis model as depicted in the schemes. Representative images of lung metastatic foci and graphs representing the quantitation of metastatic foci. (A-C) Protein was given once before the tumor cell injection. n = 9-10. (D-F) Protein was given on Day 2 and 5 after the tumor cell injection. n = 6. (G-I) Protein was given on day 8 and 12 after the tumor cell injection. n = 6. (J-L) After tumor cell injection, protein was given on Day 2, 5, 8 and 12. Scale bar: 2mm. n=10; mean±SD.

3.1.6. Systemic overexpression of nANGPTL4 via AAV inhibits metastasis

Previous experiments have shown that a constant supply of nANGPTL4 is required to efficiently reduce metastasis. However, undertaking long-term metastasis experiments with recurring intravenous injections of recombinant protein is logistically and financially challenging in clinically relevant mouse models. Therefore, I opted for AAV-mediated systemic upregulation of nANGPTL4 for long-term experiments. To stably and systemically overexpress nANGPTL4 in mice, AAV expression vectors were designed which overexpress either GFP (control, Fig. 13A) or nANGPTL4 followed by a V5 tag, a P2A cleavage site and GFP (Fig. 13B). First, it was determined whether AAV-mediated upregulation of nANGPTL4 recapitulated the phenotypes observed with nANGPTL4 recombinant protein in the B16F10 experimental metastasis model. Towards this end, 10^{11} control or nANGPTL4-overexpressing viral particles were intravenously administered, followed by an intravenous injection of the melanoma cell-line B16F10 10 days later (Fig. 13C). Mice were sacrificed two weeks after tumor cell injection. The overexpression of nANGPTL4 was confirmed in the serum via Western blot (Fig. 13D). AAV-mediated overexpression of nANGPTL4 led to a significantly reduced number of lung metastases (Fig. 13E, F).

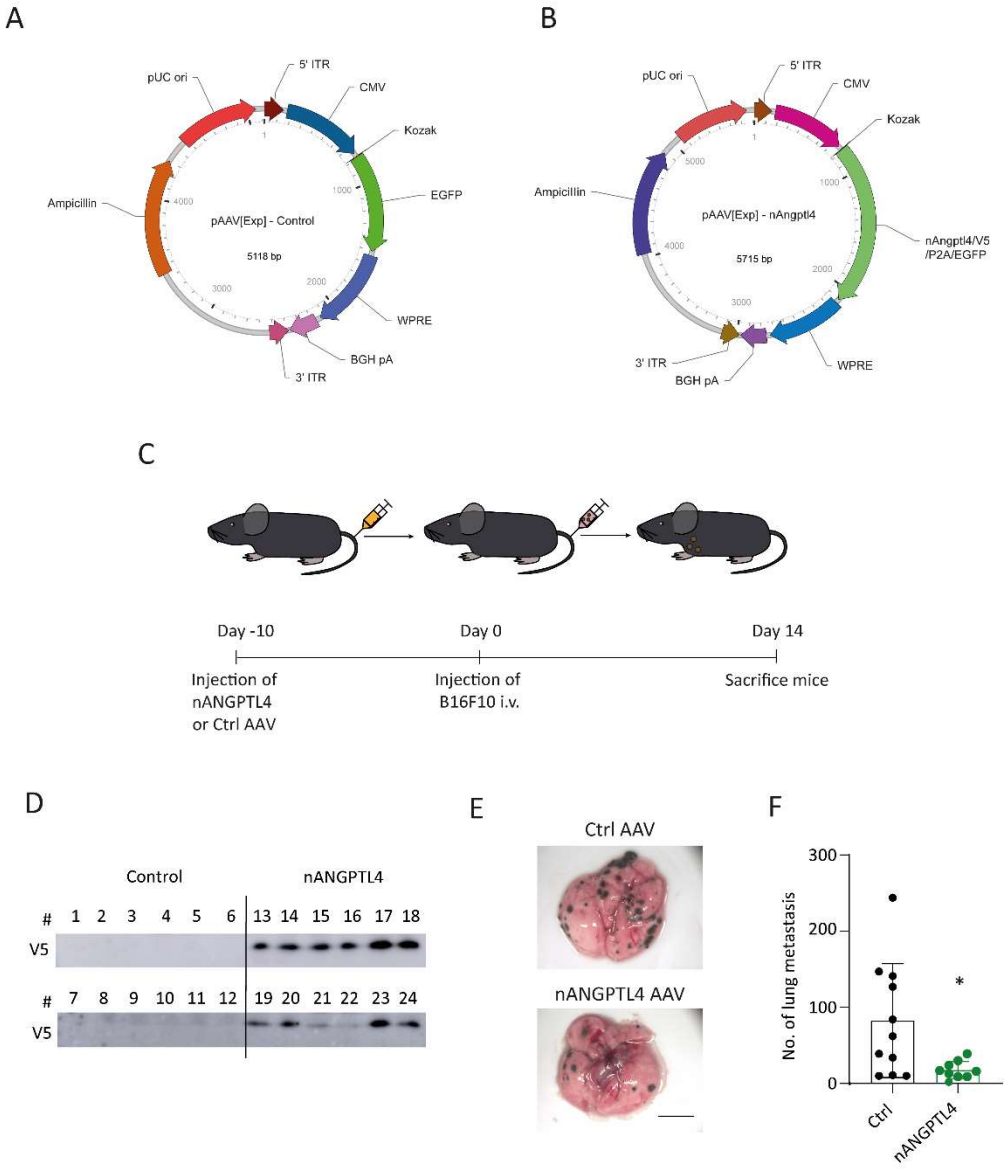

Figure 13: Therapeutic administration of nANGPTL4-AAV reduces metastasis in the B16F10 model.
(A) AAV expression vector for Control AAV. (B) AAV expression vector for nANGPTL4 overexpressing AAV. (C) Experimental scheme of nANGPTL4 AAV administration in the B16F10 metastasis model. (D) Western blot against V5-tagged nANGPTL4. Sera were taken at the endpoint of the B16F10 experimental metastasis model. (E) Representative images of metastasized lungs of Ctrl or nANGPTL4 AAV injected mice. Scale bar: 2mm. (F) Quantification of lung metastases (n=9-11; mean±SD). *, $p<0.05$, Mann-Whitney U test.

The experimental metastasis model represents an incomplete metastasis assay, reflecting the later steps of the metastatic cascade. On the contrary, spontaneous metastasis models recapitulate the entire metastatic cascade, in which tumor cells disseminate from the primary tumor to distant sites and form overt metastasis (*180*). In order to assess the effect of nANGPTL4 in a spontaneous metastasis model, an LLC post-surgical metastasis experiment was performed. In this model, the primary tumor is surgically resected, making metastatic growth rate-limiting for the survival of mice. Control or nANGPTL4-overexpressing AAVs were injected during LLC primary tumor growth, which did not affect

primary tumor growth kinetics (Fig. 14A, B). Subsequently, primary tumors were resected at approximately similar tumor volumes (Fig. 14C). After primary tumor removal, mice developed metastases in lungs and livers. The mice were sacrificed when they reached defined endpoint criteria. At the end of the experiment, the overexpression of nANGPTL4 in the serum was confirmed via Western blot (Fig. 14D). The experiment revealed that mice injected with nANGPTL4-expressing AAV had a significantly higher survival rate compared to control AAV injected mice (Fig. 14E).

Taken together, these experiments show that therapeutic administration of nANGPTL4 may be viable strategy in high-risk cancer patients.

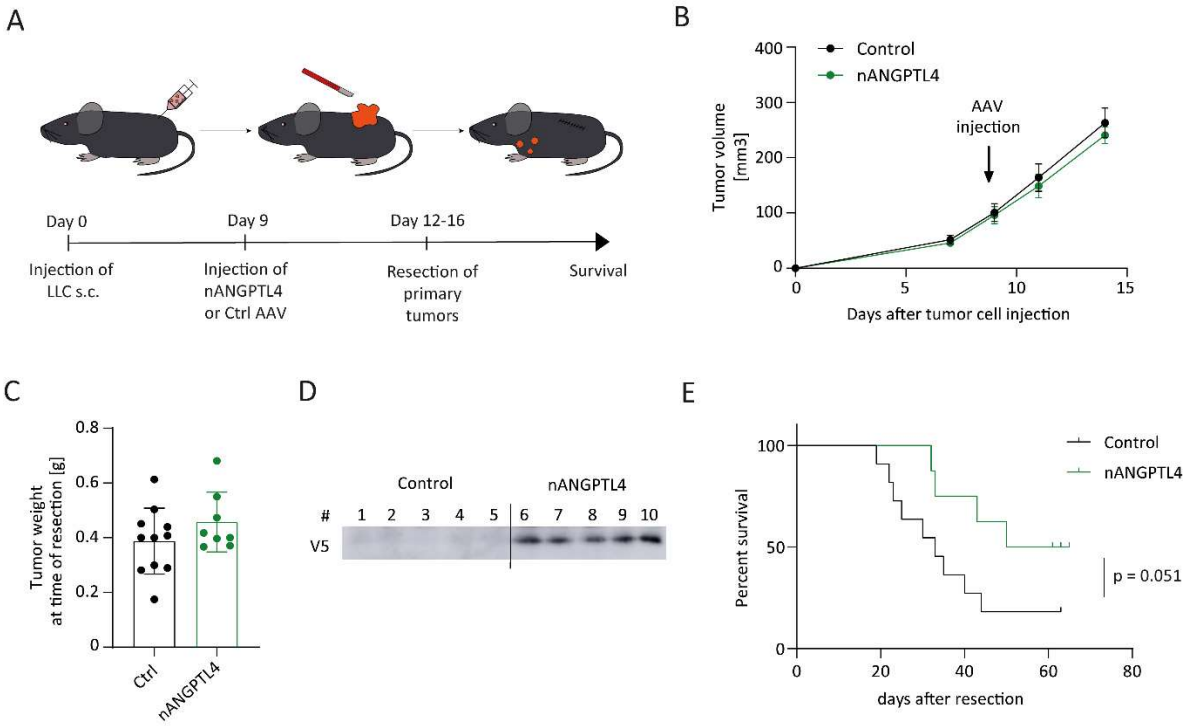

Figure 14: Therapeutic administration of nANGPTL4 AAV enhances survival in the LLC post-surgical metastasis model.

Experimental scheme AAV administration in the LLC post-surgical metastasis model. (B) Growth curve of LLC primary tumors in Ctrl or nANGPTL4 injected mice (n=8-11; mean±SEM). (C) Primary tumor weights at the time of resection (n=8-11). (D) Western blot against V5-tagged nANGPTL4. Sera were taken at the endpoint of the LLC post-surgical metastasis model. (E) Survival curve of Ctrl and nANGPTL4 AAV injected mice in the LLC post-surgical metastasis experiment. Mice were killed when they reached the defined endpoint criteria (n=8-11). Log-rank (Mantel-Cox) test.

3.1.7. nANGPTL4 reduces Wnt signaling at the metastatic site

The current data suggests that nANGPTL4 acts on SDC4 on ECs to reduce sprouting angiogenesis *in vitro*. To decipher the downstream molecular mechanism of nANGPTL4 on EC *in vivo*, genome-wide RNAseq of lung endothelial cells was performed. To stably and systemically overexpress nANGPTL4 in mice, AAVs were injected intravenously, lung endothelial cells were isolated and subjected to RNAseq

analysis (Fig 15A). Gene set enrichment analysis (GSEA) revealed that pathways affecting angiogenesis and Wnt signaling were downregulated upon nANGPTL4 treatment (Fig. 15B, C). These results from lung ECs validated the previous findings that nANGPTL4 reduced sprouting angiogenesis in the *in vitro* sprouting assay and *in vivo* cornea pocket assay (Fig. 8).

As previous experiments from our lab have shown that nANGPTL4 reduces metastasis but has no effect on the primary tumor vasculature, I hypothesized that this may be due to the distinct expression pattern of SDC4 in different vascular beds. To test this hypothesis, ECs were sorted from LLC primary tumors and lungs and the expression of SDC4 in ECs was analyzed. Indeed, SDC4 expression was shown to be higher in mouse lung EC isolated from metastatic lungs as compared with primary tumor-derived EC (Fig. 16A), indicating that nANGPTL4 has a higher likelihood of engaging its downstream receptor at the metastatic site.

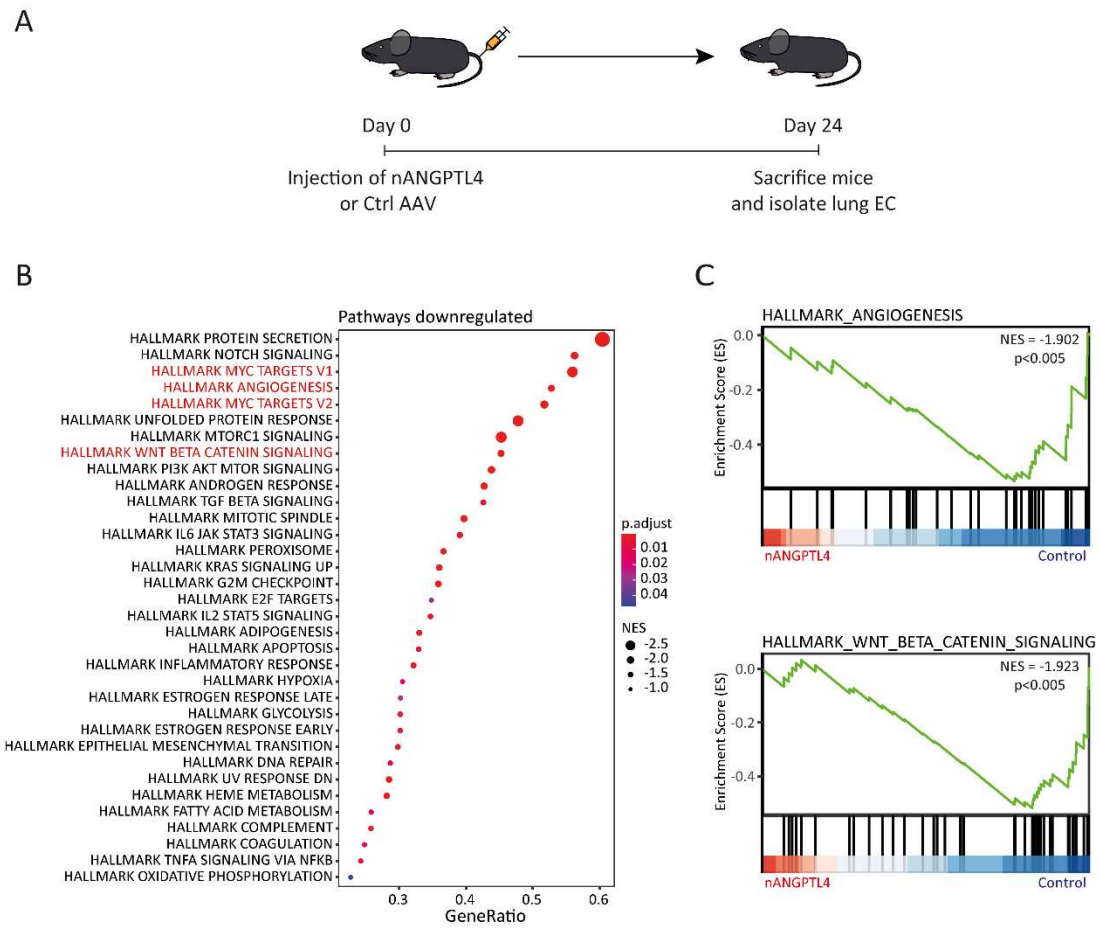

Figure 15: nANGPTL4 downregulates angiogenesis and Wnt signaling in metastatic lung ECs.
(A) Experimental scheme of the RNAseq experiment. Ctrl or nANGPTL4 were upregulated via AAV. (B) Gene set enrichment analysis (GSEA) of pathways downregulated upon nANGPTL4 treatment. Normalized enrichment score (NES). (C) The respected regulated hallmark pathways in nANGPTL4 treated lung ECs are shown as GSEA.

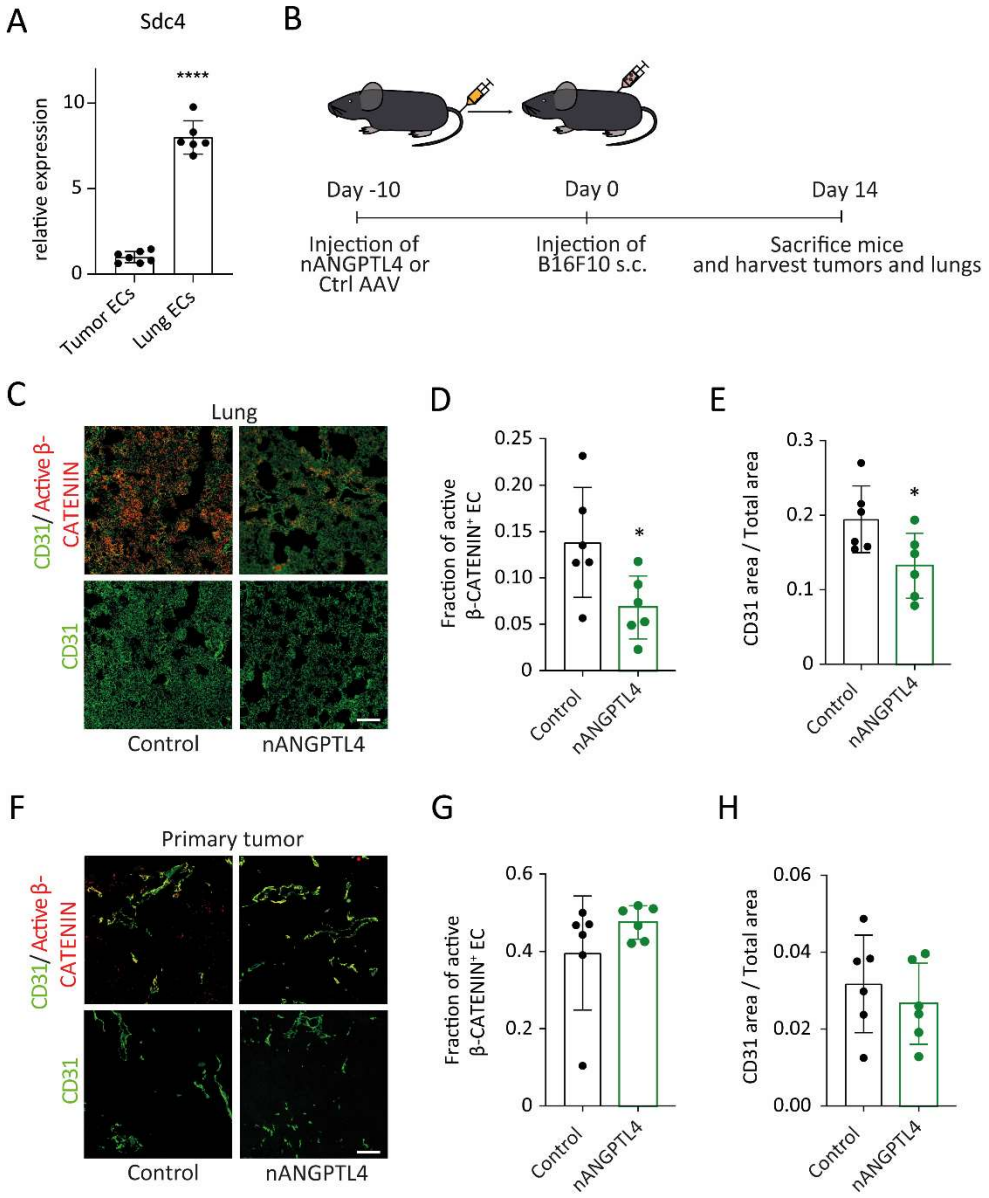

Figure 16: nANGPTL4 engages its downstream signaling at the metastatic site.
(A) Quantification of *SDC4* expression in sorted EC from LLC primary tumors and healthy lungs by RT-qPCR. (n=6-7; mean±SD). **** p<0.0001, unpaired Student's t-test. (B) Schematic representation of the LLC primary tumor experiment in mice treated with Ctrl or nANGPTL4 overexpressing AAV. (C) Representative immunofluorescent stainings of lung sections with CD31 (green) and active β-catenin (red). Scale bar: 100µm. Quantification of active β-catenin positive ECs (D) and CD31 (E) in lungs of mice treated with Ctrl or nANGPTL4 AAV. (n=6; mean±SD). *, p<0.05, Mann-Whitney U test. (F) Representative immunofluorescent stainings of B16F10 primary tumor sections with CD31 (green) and active β-catenin (red). Scale bar: 100µm. Quantification of active β-catenin positive ECs (G) and CD31 (H) in tumors of mice treated with Ctrl or nANGPTL4 AAV. (n=6; mean±SD).

To confirm the RNAseq findings and to compare the differential signaling of nANGPTL4 on the metastatic site and the primary tumor, a B16F10 primary tumor experiment was performed in which mice were injected with Ctrl or nANGPTL4 overexpressing AAV (Fig. 16B). Pre-metastatic lungs and B16F10 primary tumors were isolated 2 weeks after tumor cell injection and the primary tumor and the lung vasculature was analyzed. Levels of the vascular marker CD31 and the activated form of β-

catenin, a master transcription factor of Wnt signaling, were analyzed via immunofluorescence in the primary tumor and metastatic site. Mice treated with nANGPTL4 AAV showed an effective inhibition of Wnt signaling and CD31 expression at the metastatic site in nANGPTL4 treated mice (Fig. 16C-E). However, Wnt signaling and CD31 levels remained unchanged at the primary tumor site (Fig. 16F-H), suggesting that these changes depend on a high endothelial SDC4 expression. Overall, the data reveal that nANGPTL4 exerts its anti-metastatic functions in the lung by downregulating Wnt signaling and reducing vascularity at the metastatic site.

3.1.8. The anti-metastatic effect of nANGPTL4 is independent of tumor cell-derived SDC4

Considering that the effect of nANGPTL4 was shown to be dependent on endothelial cell-derived SDC4, the possible contribution of tumor-cell-derived SDC4 on the metastasis phenotype was evaluated. Although the lack of functional alterations in tumor cells after nANGPTL4 overexpression (Fig. 5) suggested that nANGPTL4 did not act in an autocrine manner on tumor cells, I still wanted to exclude the possible role of tumor cell-derived SDC4 in this context. Comparative analyses of different tumor cell lines used in this study showed that LLC had the highest expression of SDC4 amongst the tested cell lines (Fig. 17A). To precisely determine the function of tumor cell-expressed SDC4, SDC4 expression was depleted in control and nANGPTL4 overexpressing LLC tumor cells and an *in vivo* experimental metastasis assays were performed (Fig. 17B-D). The experiment revealed that loss of SDC4 expression in tumor cells did not affect the anti-metastatic activity of nANGPTL4, negating a functional role of tumor cell-expressing SDC4 in metastasis (Fig. 17E, F).

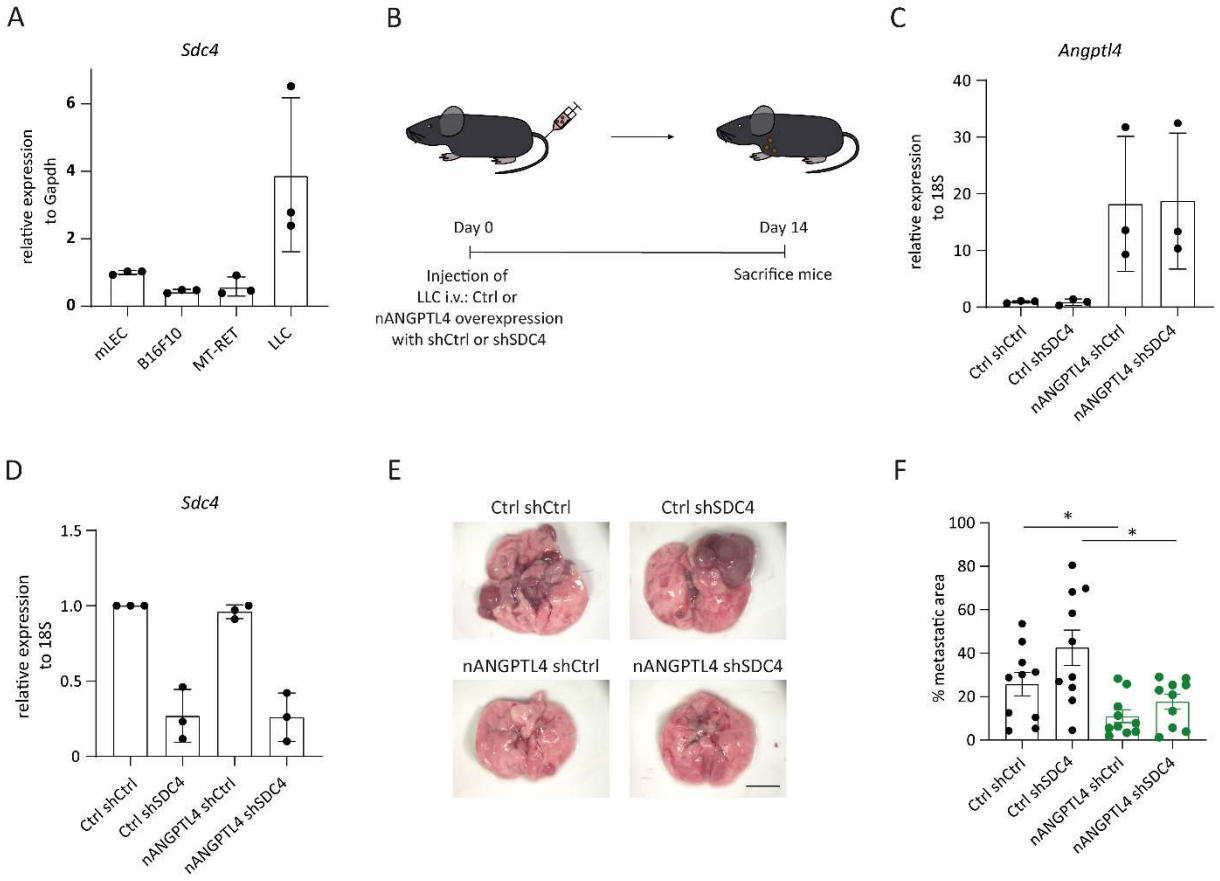

Figure 17: The anti-metastatic effect of nANGPTL4 is independent of tumor cell-derived SDC4.
(A) Quantification of the *Sdc4* expression in different murine cell lines via qPCR (n=3; mean±SD). (B) Schematic representation of the LLC tail-vein injection model. (C) Quantitation of ANGPTL4 expression via qPCR. (D) Quantitation of *Sdc4* expression via qPCR (n=3; mean±SD). (E) Representative images of lungs at day 14 after tumor cell injection. Scale bar: 2mm. (F) Quantification of the metastatic area in lungs was performed with Fiji (n=10; mean±SEM). *, p<0.05, Mann-Whitney U test.

3.1.9. nANGPTL4 predominates in the systemic circulation of cancer patients

ANGPTL4 is cleaved at its RRKR site by protein convertases, which generates the n-terminal and c-terminal fragments (Fig. 18A). By performing several pre-clinical mouse experiments, it could be shown that nANGPTL4 reduces metastasis (Fig. 11-14). However, previous data from the lab have shown that cANGPTL4 overexpression in tumor cells induced metastasis (*174*). As opposing effects of the ANGPTL4 cleavage fragments were observed, I hypothesized that the distribution of ANGPTL4 and its cleavage fragments might be an important modulator of ANGPTL4 function during tumor progression in patients. In order to analyze cANGPTL4 and nANGPTL4 in patient samples, two antibodies were chosen, which bind to the n-terminal and the c-terminal site of ANGPTL4, respectively (Fig. 18A). The specificity of the antibodies was confirmed by Western blotting, which showed that the c-specific antibody bound to recombinant flANGPTL4 and cANGPTL4, whereas the n-specific antibody bound to recombinant flANGPTL4 and nANGPTL4 (Fig. 18B).

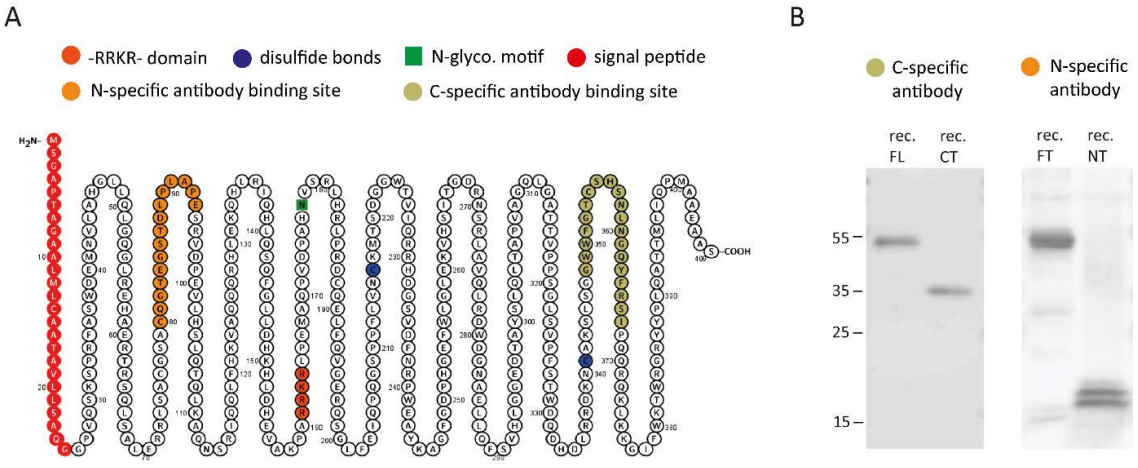

Figure 18: Validation of the cANGPTL4 and nANGPTL4-specific antibodies.
(A) Schematic representation of the protein sequence of ANGPTL4. Visualization was performed with the Protter software. The binding sites of the cANGPTL4 and nANGPTL4-specific antibodies are shown in green and orange, respectively. (B) Western blotting with the cANGPTL4 and nANGPTL4-specific antibodies and the respective recombinant proteins (FL = fl ANGPTL4, CT = cANGPTL4, NT = nANGPTL4).

To investigate the distribution of ANGPTL4 and its cleavage fragments in melanoma patients, indexed tumor tissues and serum samples were collected and analyzed with antibodies against specific epitopes in the c- and n-domains (Fig. 19A-E). Western blot analysis of matched melanoma tissue and serum samples detected flANGPTL4 as well as different amounts of cANGPTL4 and nANGPTL4 in all tumor tissues. While cANGPTL4 was present in the tumor tissues (Fig. 19A), it was not detectable in the patient sera (Fig. 19C). Western blot analysis of matched patient tumors and sera with the nANGPTL4-specific antibody revealed two different forms of nANGPTL4 with a size difference of approximately 3-4 kDa (Fig. 19B, D), corresponding to previous studies reporting two different forms (NT1 and NT2) of nANGPTL4 originating from post-translational modifications (*181*). Quantitative analysis revealed that the serum contained significantly higher levels of nANGPTL4 than flANGPTL4 (Fig. 19D).

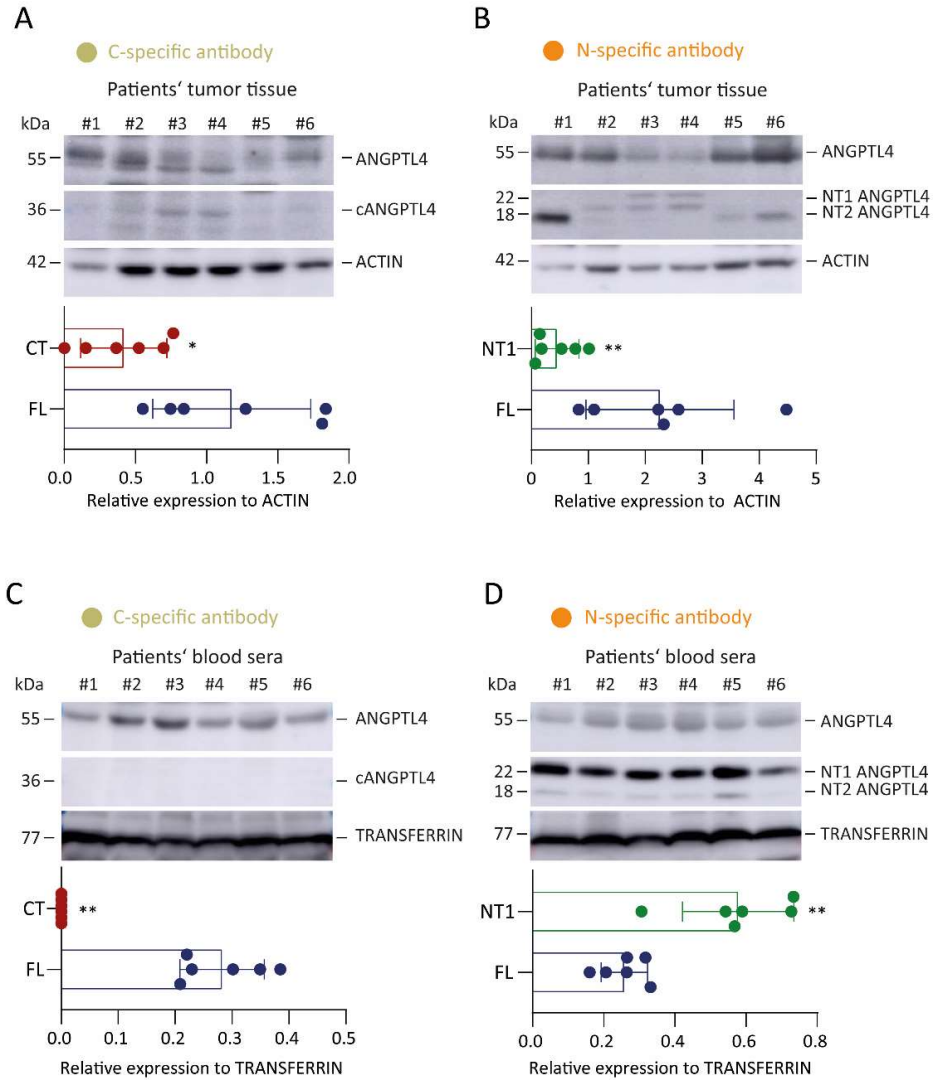

Figure 19: ANGPTL4 and its fragments are differentially distributed in melanoma patient's primary tumors and sera.

(A) Western blot analysis of melanoma tumor lysates with a cANGPTL4-specific antibody. Protein levels were normalized to ACTIN. (B) Western blot analysis of melanoma tumor lysates with a nANGPTL4-specific antibody. Protein levels were normalized to ACTIN. (C) Western blot analysis of melanoma serum samples with a cANGPTL4-specific antibody. Protein levels were normalized to TRANSFERRIN. (D) Western blot analysis of melanoma serum samples with a nANGPTL4-specific antibody. Protein levels were normalized to TRANSFERRIN (n=6; mean±SD). *, $p<0.05$; **, $p<0.01$, Mann-Whitney U test.

In order to substantiate these findings, an analysis of nANGPTL4 and cANGPTL4 levels was also performed in matching sera and tumor samples from lung cancer patients (Fig. 20). In line with the previous findings, primary lung tumors contained flANGPTL4 as well as both cleavage fragments (Fig. 20A, B). The serum of lung cancer patients contained no detectable cANGPTL4 but high levels of nANGPTL4 (Fig. 20C, D).

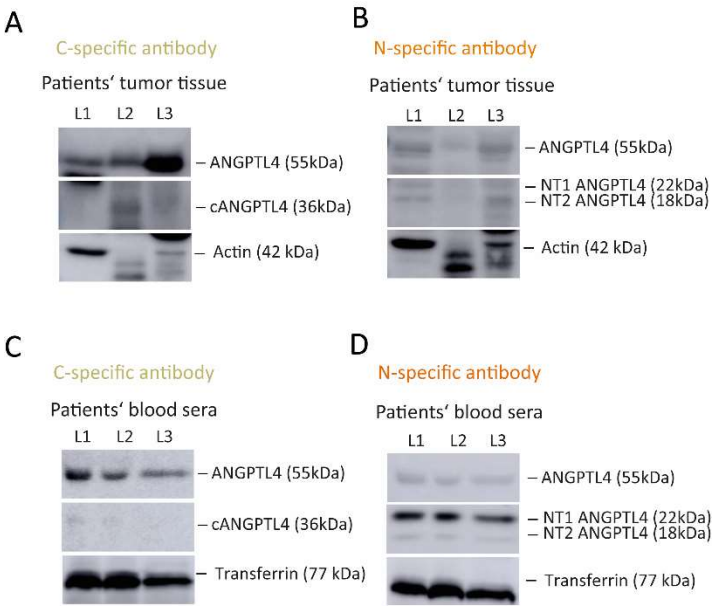

Figure 20: ANGPTL4 and its fragments are differentially distributed in primary tumors and sera of lung cancer patients.

(A) Western blot analysis of tumor lysates from lung cancer patients with a cANGPTL4-specific antibody. Protein levels were normalized to ACTIN. (C) Western blot analysis of tumor lysates from lung cancer patients with a nANGPTL4-specific antibody. Protein levels were normalized to ACTIN. (D) Western blot analysis of lung cancer serum samples with a cANGPTL4-specific antibody. Protein levels were normalized to TRANSFERRIN. (E) Western blot analysis of lung cancer serum samples with a nANGPTL4-specific antibody. Protein levels were normalized to TRANSFERRIN (n=3).

Taken together, a differential distribution of nANGPTL4 and cANGPTL4 in melanoma and lung cancer patient serum and tumor tissue was identified. While cANGPTL4 stays locally in the tumor tissue, high nANGPTL4 are found in the systemic circulation

3.1.10. nANGPTL4 levels correlate inversely with disease progression in melanoma patients

The high abundance of nANGPTL4 in the melanoma and lung cancer patient's sera and the survival-promoting effect of nANGPTL4 in pre-clinical mouse models led me to hypothesize that nANGPTL4 levels might correlate with disease progression in cancer patients. In order to address this question, a limited-size longitudinal analysis of 10 melanoma patient sera was performed. All patients had a primary melanoma tumor surgically resected and subsequently developed metastasis. Initially, the defined patient group had metastatic disease, which remained stable for a period of time, which was defined as stable disease (SD, time point A). Subsequently, the metastatic disease progressed, defined as progressive disease (PD, time point B), and the patients succumbed to metastatic growth (Fig. 21A).

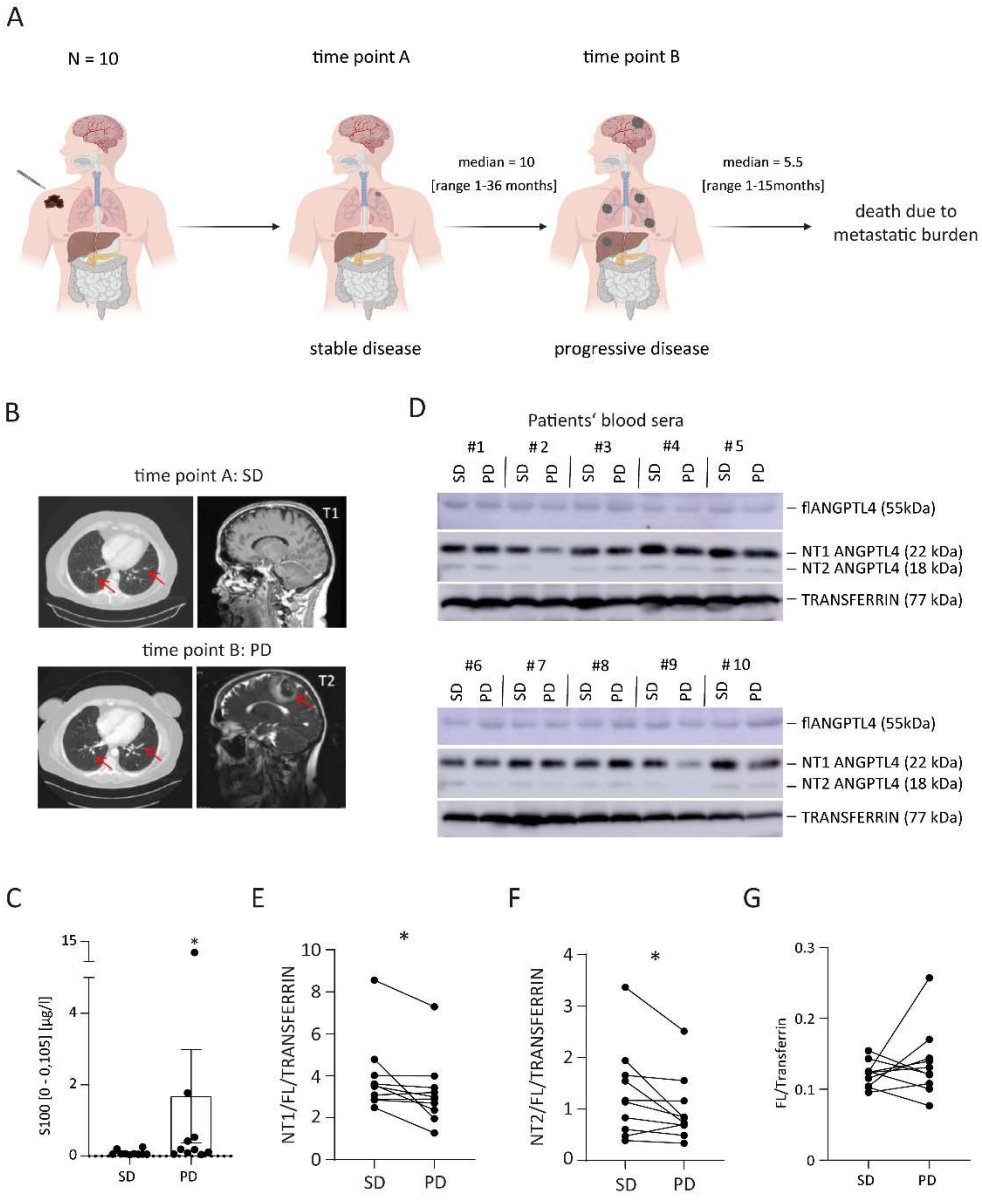

Figure 21: nANGPTL4 serum levels decline during metastatic disease progression in melanoma patients.

(A) Graphical scheme of the patient status at time point A (stable disease, SD) and time point B (progressive disease, PD). The primary tumor is depicted in brown and macro-metastases are depicted in black. The figure was created with biorender.com. (B) Representative MRI images of metastasized lungs and brains of patients with stable or progressive disease. Arrows highlight metastatic lesions, which are progressing from SD to PD. (C) Serum S100 levels of melanoma patients at stable and progressive disease (n=10), *, $p<0.05$, Mann-Whitney U test. (D) Western blots of melanoma patient sera at the stable and progressive disease timepoints with a nANGPTL4-specific antibody. Quantification of the NT1/FL/Transferrin ratio (E), NT2/FL/Transferrin ratio (F) and FL/Transferrin ratio (G) of melanoma patient's sera at stable or progressive disease was performed with Fiji (n=10). *, $p<0.05$, two-tailed paired Student's t-test.

Disease progression of patients was regularly determined in radiological examinations (Fig. 21B) and by monitoring serum S100 levels (Fig. 21C). Serum samples, which were collected during post-surgical visits, were subjected to Western blot analysis with the nANGPTL4-specific antibody (Fig. 21D).

Concordant with the previous observations, two different glycosylated forms of nANGPTL4 (NT1 and NT2), as well as flANGPTL4 were detected. Quantification of protein levels revealed that both glycosylated forms of nANGPTL4, which were analyzed as nANGPTL4/flANGPTL4/Transferrin levels) were decreasing as patients progressed from SD to PD (Fig. 21E, F). However, the flANGPTL4/Transferrin ratio stayed stable during disease progression (Fig. 21G).

To determine whether nANGPTL4 serum levels were associated with survival in melanoma patients, a longitudinal study on circulating nANGPTL4 levels was performed in a larger cohort of metastatic melanoma patients. Serum was taken from 32 melanoma patients during post-operative clinical visits. All patients developed metastatic disease after the initial surgical excision of the primary tumor (Fig. 22A). Western blot analysis showed that a decline of the NT/FL/Transferrin ratio during disease progression was associated with worse overall survival (Fig. 22B). Taken together, the data suggest that systemic nANGPTL4 in melanoma patients could contribute to delaying metastatic tumor progression.

Collectively, these experiments showed that therapeutic administration of nANGPTL4 in pre-clinical mouse experiments reduced metastasis by downregulating vascularity at the metastatic site via the SDC4-Wnt signaling pathway. In addition, nANGPTL4 was mainly present in the serum and serum nANGPTL4 levels negatively correlated with melanoma patient survival.

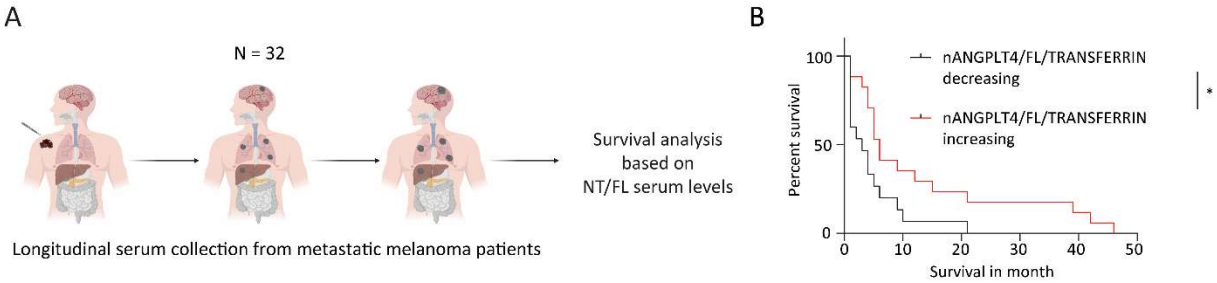

Figure 22: nANGPTL4 serum levels correlate with melanoma patient survival.
(A) Graphical representation of patient status during longitudinal serum collection from metastatic melanoma patients. The primary tumor is colored in brown and macro-metastases are highlighted in black. The figure was created with biorender.com. (G) Survival of patients with an increasing or decreasing nANGPTL4/FL/Transferrin ratio is shown in a Kaplan-Meyer plot. Survival is represented as months after withdrawal of the second serum sample (n=15-17). *, $p<0.05$, Log-rank (Mantel-Cox) test.

3.2. E40K mutated nANGPTL4 has no effect on tumor development and metastasis

3.2.1. Establishment of E40K mutated nANGPTL4 overexpressing cell lines

ANGPTL4 binds to LPL via its n-terminal site and inhibits LPL activity. Therefore, high levels of nANGPTL4 were previously shown to upregulate plasma TG levels and thereby increase the risk of developing cardiovascular disease (*182*). It was recently shown that the E40K mutation in nANGPTL4 strongly correlates with lower TG levels (*155*). Therefore, the second part of this study was aimed at analyzing whether the E40K mutated nANGPTL4 affected tumor development and metastasis. Towards this aim, a lentiviral nANGPTL4 E40K overexpression vector was generated. This vector overexpressed nANGPTL4 with a missense mutation from CAG to AAG, which encodes the amino acid lysine rather than glutamic acid (Fig. 23A). This tool was used to generate B16F10 cell lines that either contained an empty control vector or overexpressed nANGPTL4 or E40K mutated nANGPTL4 (Fig. 19B).

Figure 23: Generation of E40K mutated nANGPTL4 overexpressing cancer cell lines.
(A) Amino acid sequence (top) and protein sequence (botton) of E40K mutated nANGPTL4. The figure was generated with biorender.com. (B) Quantification of nANGPTL4 expression in Ctrl, nANGPTL4 and nANGPTL4 E40K overexpressing B16F10 by RT-qPCR. (n=3; mean±SD).

3.2.2. E40K mutated nANGPTL4 has no effect on the primary tumor

To examine whether E40K mutated nANGPTL4 has an effect on a B16F10 primary tumor, C57BL6/J mice were subcutaneously injected with Ctrl, nANGPTL4 and nANGPTL4 E40K overexpressing B16F10 cell lines (Fig. 24A). Tracing primary tumor growth revealed that tumor cell-derived nANGPTL4 and E40K mutated nANGPTL4 did not alter primary tumor growth characteristics (Fig. 24B). Primary tumors were collected at the same tumor weight (Fig. 24C) and serum was collected after the mice were exposed to 24h food-withdrawal. To validate whether the E40K mutation abolished the nANGPTL4-mediated effect on lipids, TG levels were measured in the serum. Serum analysis revealed that mice

with overexpression of nANGPTL4 in the primary tumor showed slightly increased TG levels in the circulation. However, mice overexpressing E40K mutated nANGPTL4 had similar TG levels as the control mice (Fig. 24D). In addition, BODIPY® staining was performed on B16F10 primary tumors to mark nonpolar lipids. Image analysis revealed an increase of lipids with nANGPTL4 upregulation, which was quenched when E40K mutated nANGPTL4 was overexpressed. (Fig.24E, F). Conclusively, the experiment indicates that E40K mutated nANGPTL4 has no effect on lipid metabolism.

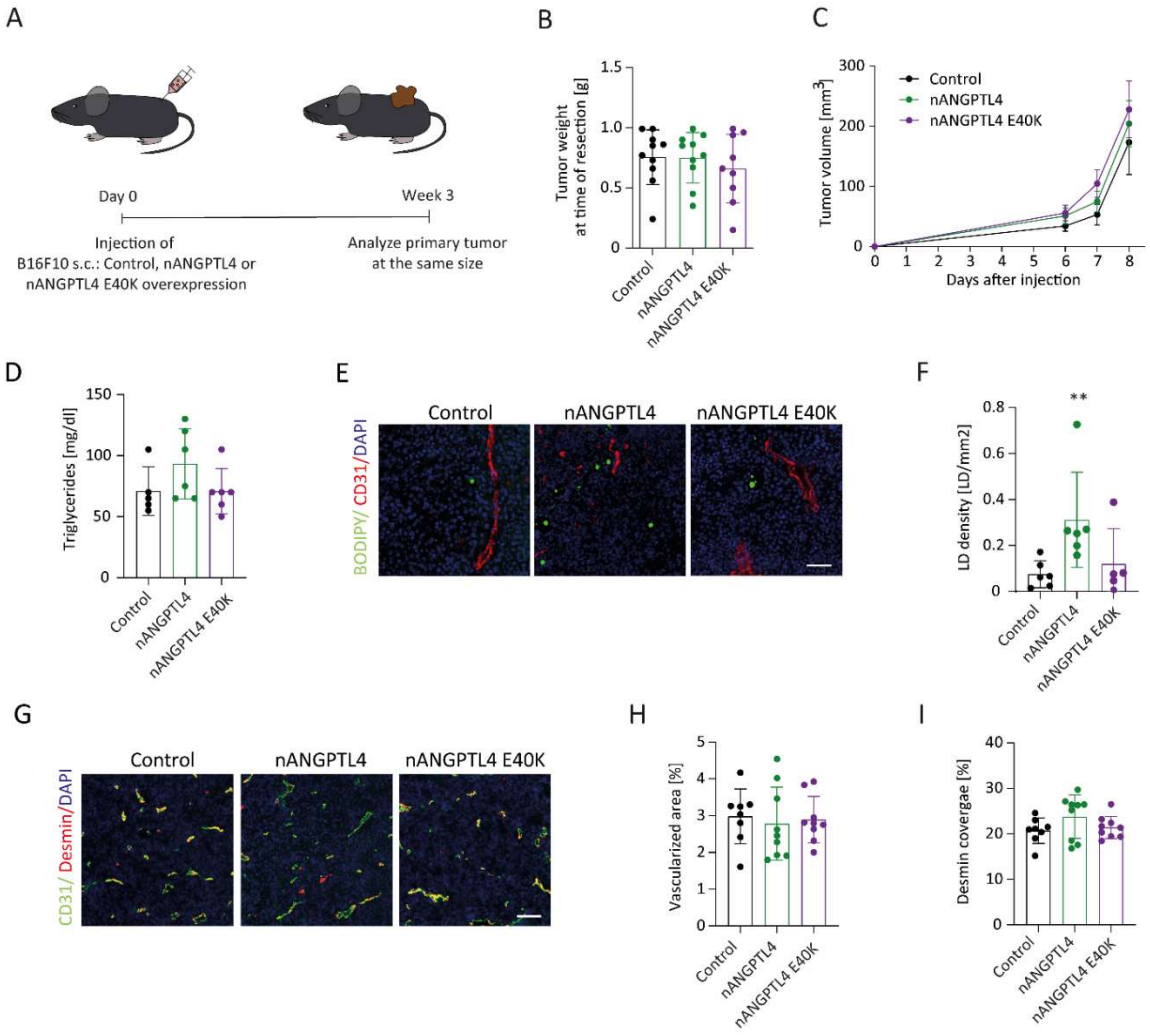

Figure 24: E40K mutated nANGPTL4 has no effect on B16F10 primary tumor growth and vasculature.

(A) Schematic representation of the B16F10 primary tumor experiment. (B) Growth kinetics of Ctrl, nANGPTL4 and nANGPTL4 E40K overexpressing B16F10 primary tumors (n=10). (C) Tumor weights at the time of primary tumor removal (n=9-10; mean±SD). (D) Serum TG levels of mice at the time of primary tumor removal (n=5-6; mean±SD). (E) Representative IF images of control, nANGPTL4 and nANGPTL4 E40K overexpressing B16F10 primary tumors. Sections were stained with CD31 (red), BODIPY (green) and DAPI (blue). Scale bar: 100 µm. (F) Quantification of lipid droplet (LD) density in B16F10 primary tumors (n=5-6; mean±SD). **, p<0.01, Mann-Whitney U test. (G) Representative IF images of control, nANGPTL4 and nANGPTL4 E40K overexpressing B16F10 primary tumors. Sections were stained with CD31 (green), desmin (red) and DAPI (blue). Scale bar: 100 µm. (H) Quantification of vessel density in B16F10 primary tumors (n=8-9; mean±SD). (I) Quantification of desmin coverage in B16F10 primary tumors (n=8-9; mean±SD).

Overexpression of primary tumor-derived nANGPTL4 was shown to have no effect on vessel density within the tumor (Fig. 13E, G). IF-based vascular analysis revealed that nANGPTL4 and E40K mutated nANGPTL4 had no effect on the B16F10 primary tumor vessel density (Fig. 24G, H) and pericyte coverage (Fig. 24I).

3.2.3. Overexpression of E40K mutated nANGPTL4 in the primary-tumor has no effect on metastasis

Previous data from our lab revealed that overexpression of nANGPTL4 in the primary tumor prolonged the survival of mice in the LLC post-surgical metastasis model (*174*). To investigate whether E40K mutated nANGPTL4 acted in the same fashion, two LLC cell lines were generated, which expressed empty control vector or overexpressed E40K mutated nANGPTL4 (Fig. 25A). Subsequently, an LLC post-surgical metastasis model was performed with LLC primary tumors containing a control vector or overexpressing E40K mutated nANGPTL4 (Fig. 25B). In this model, the primary tumors were surgically resected at the same size (Fig. 25C), making metastatic growth rate-limiting for the survival of the mice.

The vasculature of the resected LLC primary tumors was analyzed. In concordance with the previous results, IF analysis revealed that E40K mutated nANGPTL4 had no effect on the vascularized area and pericyte coverage (Fig. 25D-F). In addition, E40K mutated nANGPTL4 had no effect on the post-surgical survival of mice, indicating that the metastatic burden was not affected (Fig. 25G). Overall, overexpression of E40K mutated nANGPTL4 in the primary tumor has no effect on metastasis in the LLC resection model.

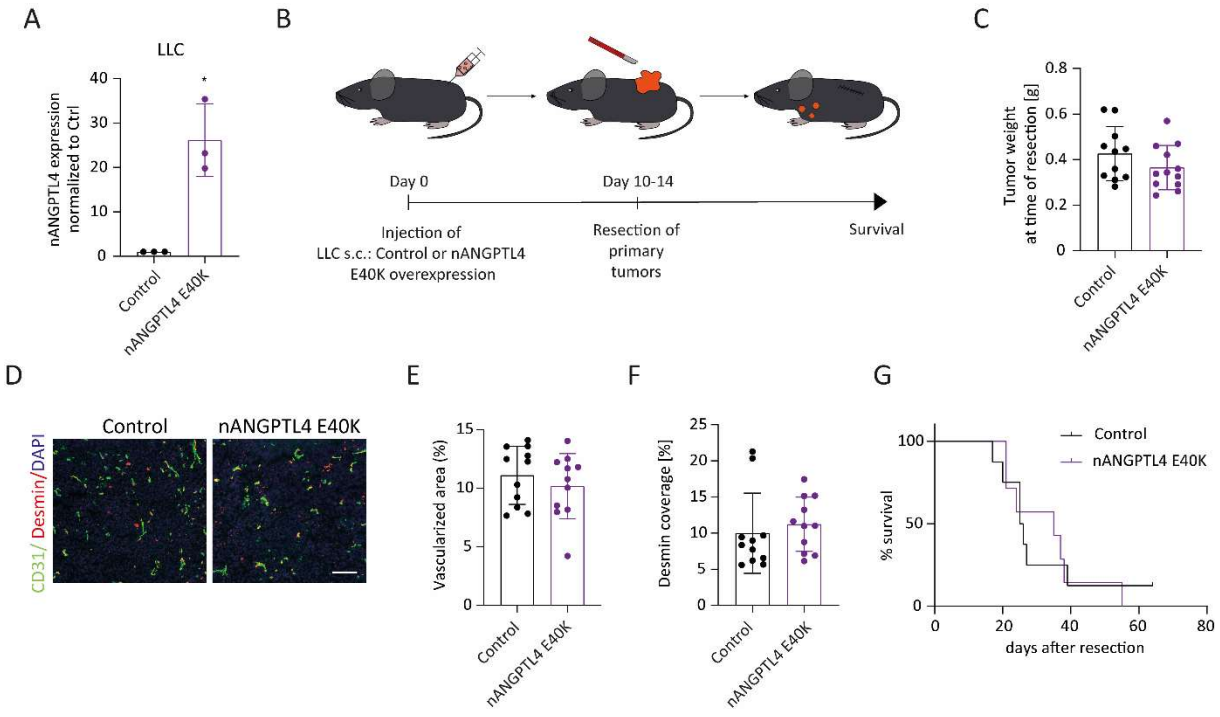

Figure 25: Overexpression of E40K mutated nANGPTL4 in the primary tumor has no effect on metastasis in the LLC post-surgical metastasis model.

(A) Quantification of nANGPTL4 expression in Ctrl and nANGPTL4 E40K overexpressing LLC by RT-qPCR. (n=3; mean±SD). * $p<0.05$, paired Student's t-test. (B) Schematic representation of the LLC post-surgical metastasis model with control or nANGPTL4 E40K overexpressing LLC cell lines. (C) Tumor weights at the time of primary tumor removal (n=11-12; mean±SD). (D) Representative IF images of control and nANGPTL4 E40K overexpressing LLC primary tumors. Sections were stained with CD31 (green), desmin (red) and DAPI (blue). Scale bar: 100 µm. (E) Quantification of vessel density in control and nANGPTL4 E40K overexpressing LLC primary tumors (n=11; mean±SD). (F) Quantification of desmin coverage in control and nANGPTL4 E40K overexpressing LLC primary tumors (n=11; mean±SD). (G) Survival curve of the LLC post-surgical metastasis experiment with control and nANGPTL4 E40K overexpressing LLC cell lines. Mice were killed when they reached the defined endpoint criteria (n=7-8). Log-rank (Mantel-Cox) test.

3.2.4. Systemic overexpression of E40K mutated nANGPTL4 has no effect on metastasis

Considering that tumor cell-derived E40K mutated nANGPTL4 had no effect on metastasis, the role of systemically administered E40K mutated nANGPTL4 was evaluated. Therefore, the B16F10 experimental metastasis model with AAV-mediated systemic upregulation of E40K mutated nANGPTL4 was performed. AAV expression vectors were designed which overexpressed either GFP (control, Fig. 26A) or nANGPTL4 E40K followed by a V5 tag, a P2A cleavage site and GFP (Fig. 26B). Towards this aim, control or E40K mutated nANGPTL4-overexpressing viral particles were administered, followed by an intravenous injection of the melanoma cell-line B16F10 10 days later (Fig. 26C). Mice were sacrificed two weeks after tumor cell injection and the overexpression of nANGPTL4 E40K was confirmed in the serum via Western blot (Fig. 26D). AAV-mediated overexpression of nANGPTL4 E40K had no effect on the number of lung metastases (Fig. 26E, F).

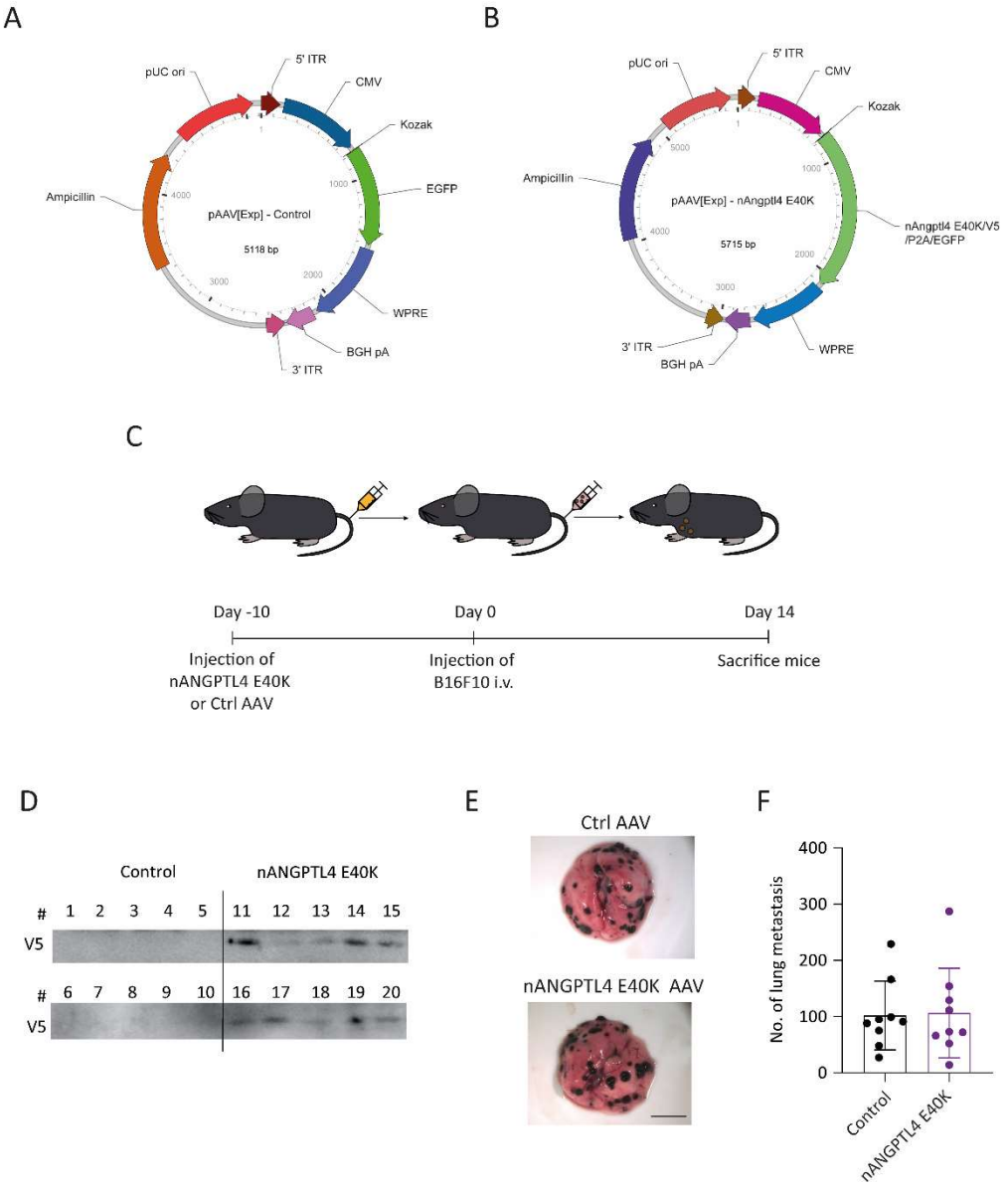

Figure 26: Systemic, AAV-mediated upregulation of E40K mutated nANGPTL4-has no effect on metastasis in the B16F10 model.

(A) AAV expression vector for Control AAV. (B) AAV expression vector for nANGPTL4 E40K overexpressing AAV. (C) Experimental scheme of nANGPTL4 E40K AAV administration in the B16F10 metastasis model. (D) Western blot against V5-tagged nANGPTL4 E40K. Sera were taken at the endpoint of the B16F10 experimental metastasis model. (E) Representative images of metastasized lungs of Ctrl or nANGPTL4 E40K AAV injected mice. Scale bar: 2mm. (F) Quantification of B16F10 lung metastatic foci in mice injected with control or nANGPTL4 E40K AAV (n=9; mean±SD).

In order to validate this finding in a spontaneous metastasis model, the LLC post-surgical metastasis model was performed with nANGPTL4 E40K AAV treatment. Therefore, control or E40K mutated nANGPTL4-overexpressing AAVs were injected during LLC primary tumor growth (Fig. 27A) and primary tumors were resected at approximately the same size (Fig. 27B) leading to the development of metastasis. When the mice were sacrificed at defined endpoint criteria, the overexpression of

nANGPTL4 E40K in the serum was confirmed via Western blot (Fig. 27C). In concordance with the results from the B16F10 model, E40K mutated nANGPTL4-overexpression had no effect on survival in the LLC resection model (Fig. 27D). Overall, the results indicate that an E40K mutation abolishes the ability of nANGPTL4 to inhibit metastasis and can thereby not be used as an alternative to the nANGPTL4 treatment.

Overall, these experiments showed that overexpression of E40K mutated nANGPTL4 has no effect on lipid metabolism. In addition, E40K mutated nANGPTL4 does not maintain the anti-metastatic phenotype of nANGPTL4 and thereby can not be used as an alternative treatment in cancer patients.

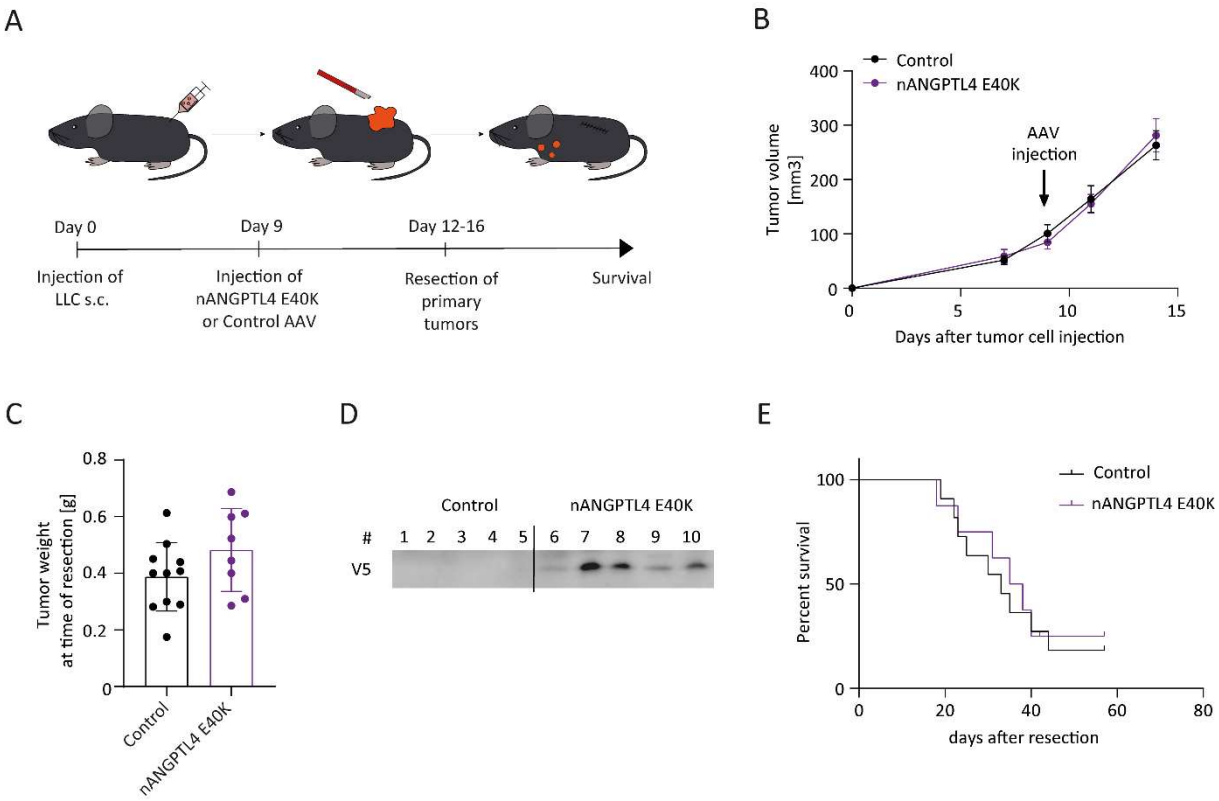

Figure 27: Systemic, AAV-mediated upregulation of E40K mutated nANGPTL4-has no effect on metastasis in the LLC model.

(A) Experimental scheme of control and nANGPTL4 E40K AAV administration in the LLC post-surgical metastasis model. (B) Growth curve of LLC primary tumors in Ctrl or nANGPTL4 E40K AAV injected mice (n=9-11; mean±SEM). (C) Primary tumor weights at the time of resection (n=8-10). (D) Western blot against V5-tagged nANGPTL4 E40K. Sera were taken at the endpoint of the LLC post-surgical metastasis model. (E) Survival curve of control and nANGPTL4 E40K AAV injected mice in the LLC post-surgical metastasis experiment. Mice were killed when they reached the defined endpoint criteria (n=8-11).

4. Discussion

4.1. nANGPTL4 acts as a systemic inhibitor of angiogenesis and metastasis

The published literature on ANGPTL4 function during angiogenesis and metastasis is highly controversial. While some studies describe ANGPTL4 as a stimulator of metastasis (*118, 137-139*), other studies report anti-metastatic functions of ANGPTL4 (*135, 136*). In light of the conflicting literature, our lab has previously overexpressed the two cleavage fragments of ANGPTL4, namely nANGPTL4 and cANGPTL4, in tumor cells to investigate whether pro-and anti-tumorigenic functions of ANGPTL4 are due to a differential effect of the cleavage fragments. Indeed, cANGPTL4 was shown to enhance metastasis while nANGPTL4 reduced metastasis when overexpressed by the tumor cells (*174*). However, the mechanism of nANGPTL4 action as well as its therapeutic and clinical potential, remain elusive. Therefore, the present study was aimed at studying the role of nANGPTL4 during malignant melanoma metastasis formation. Employing a wide array of clinical and pre-clinical analyses, the first part of this PhD thesis demonstrates that (1) nANGPTL4 perturbs Wnt signaling and angiogenesis at the metastatic site, (2) therapeutic administration of nANGPTL4 decreases metastasis, (3) serum nANGPTL4 correlates with disease progression and survival in melanoma patients.

4.1.1. nANGPTL4 perturbs Wnt signaling and angiogenesis at the metastatic site

Several endogenous angiogenesis inhibitors have been discovered and clinical trials were initiated for a few (*183, 184*). However, many of these inhibitors could not be translationally exploited and have reached limited success due to the development of resistance mechanisms. Therefore, there is an urgent need to identify additional anti-angiogenic molecules which have the capacity to sustain long-term therapeutic effects. In this study, a potent anti-angiogenic activity of recombinant nANGPTL4 was observed. Recombinant nANGPTL4 reduces EC proliferation and sprouting angiogenesis in both sprouting and cornea pocket assays. Although the role of nANGPTL4 in sprouting angiogenesis was not previously assessed in the literature, some studies have reported anti-angiogenic functions of flANGPTL4. For instance, flANGPTL4 reduced angiogenesis in gastric cancer primary tumors and in *in vivo* Matrigel plug assays (*136*). In addition, it was shown that flANGPTL4 inhibits angiogenesis in developmental angiogenesis (*185*), in models of myocardial infarction (*133*) and stroke (*186*). The results of this study suggest that the n-terminal fragment of ANGPTL4 may be responsible for the anti-angiogenic effects of ANGPTL4 observed in the literature.

A previous study by Kirsch *et al*. suggested that nANGPTL4 binds to SDC4 in Xenopus development. Upon receptor binding, SDC4 was shown to form a complex with LRP6. Subsequently, this protein complex is internalized via clathrin-mediated endocytosis and degraded in lysosomes, resulting in the

downregulation of Wnt signaling (*115*). Wnt signaling is reported to affect sprouting angiogenesis in physiological and pathological conditions and plays a vital role in actively growing vessels (*53*).This study revealed that nANGPTL4 acts similarly on lung ECs to reduce Wnt signaling and sprouting angiogenesis.

As compared to the effect in the lungs, this study showed that nANGPTL4 has no effect on Wnt signaling and vascularity in the primary tumor. The results suggest that this might be due to the reduced expression of SDC4 in the primary tumor vasculature compared to the lung vasculature. This observation would explain the central paradox of CTR: How can a primary tumor-secreted cytokine inhibit angiogenesis at the metastatic site while allowing progressive growth of the primary tumor (*104, 187*)? Differential expression of signaling receptors in different vascular beds could potentially mediate the selective anti-angiogenic effect at the metastatic site.

Despite its effect on ECs, ANGPTL4 was previously described to regulate inflammation and affect immune cells. Specifically, ANGPTL4 can affect macrophage activation (*126*) towards the proinflammatory phenotype (*127*). In addition, ANGPTL4 was characterized as an acute phase protein, whose expression is stimulated during the acute phase response (*128*). As immune cells are an additional mediator of CTR, further studies have to be performed to analyze whether ANGPTL4 affects immune cells, which might contribute to its anti-metastatic effect.

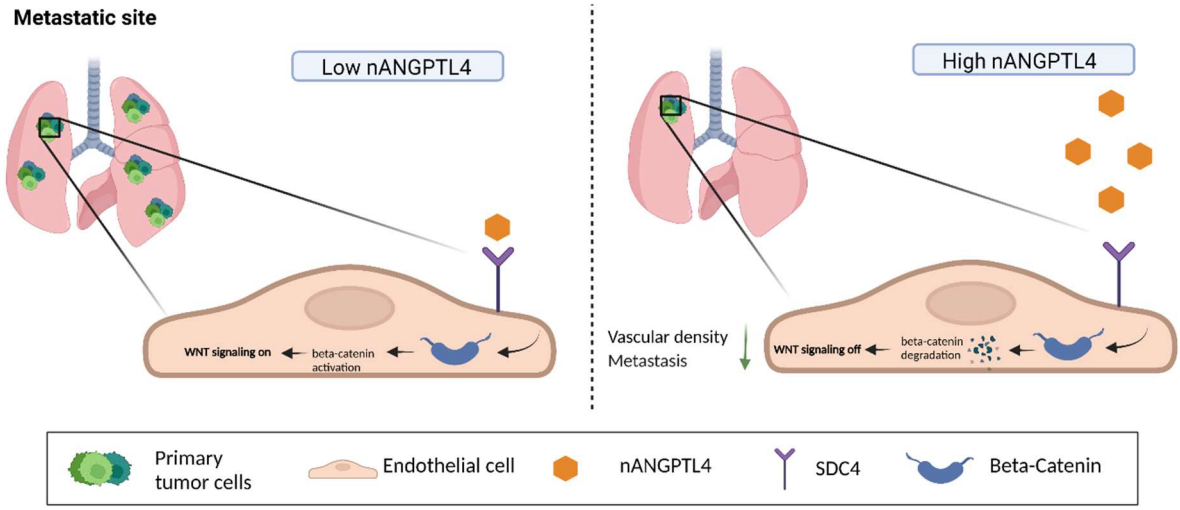

Figure 28: Molecular mechanism of nANGPTL4 at the metastatic site.
In physiological conditions, Wnt signaling is active in ECs. However, upon therapeutic administration of nANGPTL4, binding of nANGPTL4 to SDC4 leads to a downregulation of Wnt signaling in metastatic lung ECs. Subsequently, vascular density and metastasis are reduced. This illustration was created with BioRencer.com. Adapted with permission from (*174*).

4.1.2. Therapeutic administration of nANGPTL4 decreases metastasis

As most melanoma patients die due to metastasis (*188*), it is essential to identify molecules involved in the different steps of the metastatic cascade, thereby providing better treatment regimens to target metastasis. For ANGPTL4, both pro-metastatic (*118, 137-139*) and anti-metastatic activities (*135, 136*) have been reported in the literature. However, only a few studies differentiate between the cleavage fragments. Previous reports have shown that cANGPTL4 enhances metastasis by increasing vascular leakiness and angiogenesis (*118, 174*). On the contrary, this study identified a metastasis-reducing effect of systemic nANGPTL4. In several pre-clinical mouse models, nANGPTL4 reduced metastasis and enhanced overall survival when administered as a recombinant protein or AAV. The opposing functions of the ANGPTL4 cleavage fragments might explain the conflicting literature on ANGPTL4 function in metastasis. As such, a metastasis-promoting effect of ANGPTL4 was observed in reports upregulating ANGPTL4 locally in the primary tumor (*118, 131, 137, 139, 141, 149, 189, 190*). On the other hand, a metastasis-reducing effect of ANGPTL4 was instead observed in studies in which ANGPTL4 was upregulated systemically. For instance, Galaup *et al.* observed a reduction of metastasis upon systemic overexpression of ANGPTL4 via electro transfer (*135*). Concordantly, systemic administration of ANGPTL4 via overexpressing adenovirus reduces metastasis in a model of hepatocellular carcinoma (*151*) and transgenic overexpression of ANGPTL4 reduces tumorigenesis (*191*). This study suggests that the anti-angiogenic effect of ANGPTL4 results from proteolytic liberation of systemically acting nANGPTL4.

Clinical data on cancer patients suggest that metastasis occurs mainly after the primary tumor has been removed (*106, 107*). According to the hypothesis of CTR, primary tumor-derived molecules contribute to delaying metastatic progression in cancer patients (*104*). This notion highlights the need to identify other primary tumor-derived proteins that contribute towards delaying metastatic tumor progression in cancer patients. The current study has identified ANGPTL4 as a critical determinant of CTR and identified nANGPTL4 as a primary tumor-derived inhibitor of metastasis. The data suggest that, upon primary tumor resection, therapeutic administration of nANGPTL4 could aid in reducing metastasis in cancer patients. Nevertheless, this study highlights that nANGPTL4 has to be administered constantly and the therapy has to be started before metastasis occurs or when the primary tumor is small. Additional studies are needed to further optimize the treatment scheme and to analyze potential side effects of nANGPTL4 therapy.

Clinical trials showed that anti-angiogenic therapy alone often fails to produce an enduring response in cancer patients as tumors adapt to anti-angiogenic therapies by functionally evading angiogenesis blockade (*64*). However, several clinical trials showed the benefits of combining anti-angiogenic therapy with chemotherapy (*36*). In addition, the IMbrave trial showed that combining anti-angiogenic

therapy with immunotherapy significantly improved progression-free and overall survival of patients with advanced hepatocellular carcinoma (*192*). This highlights the importance of anti-angiogenic therapies in modulating the vascular network, thereby improving the therapeutic response of chemotherapy and immune checkpoint inhibitors. According to this notion, further experiments have to be performed in order to assess whether the combination with immunotherapy or chemotherapy improves the response of nANGPTL4 treatment in pre-clinical mouse experiments.

4.1.3. Serum nANGPTL4 correlates with disease progression and survival in melanoma patients

Several biomarker studies revealed that ANGPTL4 expression correlates with primary tumor growth and metastasis in multiple cell types (*145, 193, 194*). Previous results from our laboratory could show that ANGPTL4 levels increase with malignancy in colon cancer and melanoma patients (*174*). Given the differential effects of the ANGPTL4 cleavage fragments, this study further analyzed the distribution of the cleavage fragments in cancer patients and correlated its expression with disease progression. In melanoma and lung cancer patients, it was shown that nANGPTL4 and cANGPTL4 are differentially distributed in primary tumor and serum samples. While cANGPTL4 stays local in the primary tumor, nANGPTL4 is highly expressed in the systemic circulation. Given that cANGPTL4 was previously detected to promote angiogenesis (*174*) and this study identified an angiogenesis-reducing effect of nANGPTL4, the differential distribution of the cleavage fragments goes in hand with Folkman's description of contextual angiogenic factors. According to this notion, pro-angiogenic molecules are believed to be short-lived and locally acting, whereas anti-angiogenic molecules are proposed to be long-lived and systemically acting (*195*).

As the incidence of melanoma is steadily increasing, there is an urgent need to identify biomarkers of melanoma that will allow reliable monitoring of disease progression and metastasis. As the patient serum is easily accessible, current research has shifted towards identifying biomarkers within the serum rather than studying markers in the tissue themselves. Among the currently available biomarkers, lactate dehydrogenase (LDH) is the most widely known serum biomarker in melanoma. Besides, S100B correlates with the clinical stage of melanoma patients and is often used as a biomarker for disease progression. However, it is especially suitable for evaluation in patients with an advanced disease rather than patients in the early stages of melanoma (*196*). By performing a longitudinal study of melanoma patient sera, this study revealed that the expression of nANGPTL4 negatively correlates with disease progression. In addition, survival analysis of a larger patient cohort revealed that increasing nANGPTL4 levels in the serum correlate with better overall survival in melanoma patients. These results validate the pre-clinical findings that circulating nANGPTL4 might contribute to delaying

metastatic tumor progression. In order to further validate the potential of nANGPTL4 as a biomarker for disease progression, studies in larger patient cohorts have to be performed. In addition, further studies are needed to identify whether nANGPTL4 has better sensitivity and specificity than the currently used biomarkers LDH and S100B.

4.2. E40K mutated nANGPTL4 does not affect tumor development and metastasis

nANGPTL4 binds to LPL and inhibits LPL activity. Therefore, high levels of nANGPTL4 were previously shown to upregulate plasma TG levels and thereby increase the risk of developing cardiovascular disease (*182*). A genome-wide association study identified that carriers of the E40K mutation in nANGPTL4 display lower levels of TGs in the blood and carry a lower risk of developing cardiovascular diseases (*163*). The adverse effects on lipid metabolism and cardiovascular disease would be a major side effect of nANGPTL4 treatment. In order to minimize these side effects, the E40K mutated nANGPTL4 could be administered, which can not inhibit LPL. However, the effect of E40K mutated nANGPTL4 on the metastatic program has not been previously studied. Therefore, the second part of this study aimed to identify whether E40K mutated nANGPTL4 affects tumor development and metastasis. Primary tumor experiments revealed that overexpression of E40K mutated nANGPTL4 has no effect on the primary tumor growth and vasculature. In contrast to nANGPTL4, E40K mutated nANGPTL4 had no effect on lipid metabolism. Overexpression of E40K mutated nANGPTL4 in the primary tumor and systemic administration of E40K mutated nANGPTL4 has no effect on metastasis and survival in pre-clinical mouse models. Overall, the E40K mutation causes the loss of the anti-metastatic function of nANGPTL4. Therefore, the administration of E40K mutated nANGPTL4 might not be of therapeutic value in metastatic cancer patients.

The reason for the loss of nANGPTL4 anti-metastatic action remains to be studied. Published *in vitro* experiments have shown that the E40K mutation prevents oligomerization of ANGPTL4, destabilizing the protein and thereby preventing extracellular accumulation of ANGPTL4. In addition to Glu-40, amino acids Cys-76 and Cys-80 were shown to be required for the oligomerization of ANGPTL4. Mutation of any of these residues significantly reduces the stability of ANGPTL4 in the cell culture medium (*114*). To identify mutations that inhibit the binding of ANGPTL4 to LPL and, at the same time, maintain the ability to form oligomers, a screen of different mutations should be performed. For example, an analysis of the results of the DiscovEHR human genetics study identified 13 other mutations in ANGPTL4 besides E40K, which prohibit the binding of ANGPTL4 to LPL (*163*). Analyzing the effect of any of these ANGPTL4 variants on metastasis could aid in optimizing ANGPTL4 anti-metastatic therapy for fewer side effects.

Despite destabilizing the protein, Glu-40 might be essential for the binding of nANGPTL4 to SDC4. Kirsch *et al.* previously performed immunoprecipitation and proximity ligation assays to show that nANGPTL4 binds to SDC4 (*115*). However, they did not identify the essential amino acid residues for its binding. Further characterization of the binding mechanism will provide further insight and identify the sites required for nANGPTL4 anti-metastatic action.

Overall, the present study has revealed ground-breaking insights into the mechanism of CTR and identified nANGPTL4 as a potent inhibitor of angiogenesis and metastasis in several pre-clinical mouse models. In addition, the study highlighted the potential of nANGPTL4 as a biomarker for disease progression and survival in cancer patients. Nonetheless, the introduction of the E40K mutation was shown to abolish the anti-metastatic function of nANGPTL4. Consequently, E40K mutated nANGPTL4 can not be therapeutically used in cancer patients.

5. Materials and Methods

5.1. Materials

5.1.1. Chemicals

Chemicals were purchased from the following companies:

Table 1 Chemical suppliers

Company
AppliChem (www.appliedchem.com)
Carl Roth (www.carl-roth.de)
Gerbu (www.gerbu.de)
Merck (www.merck.de)
Roche (www.roche-applied-science.com)
Serva (www.serva.de)
Sigma-Aldrich (www.sigmaaldrich.com)
Thermo Fisher Scientific (www.thermofisher.com)

5.1.2. Growth factors, proteins and enzymes

Table 2 Growth factors, proteins and enzymes

Protein	Company
Liberase	Roche
Proteinase K	Gerbu
Recombinant human nANGPTL4	R&D Systems
Recombinant human Wnt3a	R&D Systems
Recombinant human VEGF	R&D Systems
RNase free DNAse	R&D Systems

5.1.3. Cells

Table 3 Human cell lines

Cells	Description	Company	Medium
HEK293T	Human embryonic kidney cells	ATCC	IMDM + 10% FCS + 1% P/S
HUVEC	Human umbilical vein endothelial cells (pooled from several donors)	Promo Cell	Endopan + suppl + 3% FCS

Table 4 Mouse cell lines

Cells	Description	Company	Medium
B16F10	Melanoma cells	ATCC	DMEM + 10% FCS + 1% P/S
LLC	Lewis Lung Carcinoma	ATCC	DMEM + 10% FCS + 1% P/S
MLEC	Mouse lung endothelial cells	Cell Biologics	Complete mouse EC medium + suppl + 5% FCS
MT-RET	Melanoma cells	ATCC	DMEM + 10% FCS + 1% P/S

Table 5 Insect cells

Cells	Description	Company	Medium
Hi5	Insect ovarian cells	EMBL	Sf-900 III SFM medium

5.1.4. Cell culture reagents

Table 6 Cell culture reagents

Reagent	Company
Blasticidin S	Merck
Complete mouse EC medium + Supplements	Cell Biologics
Collagen from rat tails	Self-produced
Dimethylsulfoxide (DMSO)	AppliChem
Dulbecco's Modified Eagle medium – Glutamax	Thermo Fisher Scientific
Dulbecco´s phosphate buffered saline (PBS)	PAA
Endopan 3 + FCS + Supplements	PAN Biotech
Fetal Calf Serum (FCS, heat inactivated)	PAA
Gelatin	Sigma-Aldrich
HEPES buffer	Sigma-Aldrich
Iscove's Modified Dulbecco's Medium	Sigma-Aldrich
Medium199	Sigma-Aldrich
Methylcellulose	Sigma-Aldrich
Opti-MEM I (1x) + GlutaMAX™-I Gibco	Gibco
PEI solution	Sigma-Aldrich
Penicillin/streptomycin (100x 10^4U/10mg/ml)	PAA
Puromycin	Gibco
Sf-900 III SFM medium	Thermo Fisher Scientific
Trypan blue	Gibco
Trypsin-EDTA (10x)	Sigma-Aldrich

5.1.5. Bacterial and virus strains

Table 7 Bacterial and virus strains

Description	Company
AAV9 from pAAV-CMV>EGFP:WPRE	Vector Builder
AAV9 from pAAV-CMV>nANGPTL4/V5/P2A/EGFP:WPRE	Vector Builder
AAV9 from pAAV-CMV>nANGPTL4 E40K/V5/P2A/EGFP:WPRE	Vector Builder
E. coli DH10EMBacY cells	EMBL
E. coli One Shot Top 10F	Invitrogen
pAceBac-EGT mANGPTL4-NT virus	EMBL Proteomics Core Facility

5.1.6. Primers and Oligonucleotides

All primers were purchased from Eurofins.

Table 8 Genotyping, mycoplasma and mutagenesis primers

Genotype	Primer name	Sequence (5'-3')
ANGPTL4^{KO}	ANGPTL4 for	ACG CCA CAC ACA CAC ACT
	ANGPTL4 WT rev	CTC AAA AGC CCC GCA GTA
	ANGPTL4 KO rev	GCC TAC CCG CTT CCA TTG CT
Mycoplasma	MGSO	TGCACCATCTGTCACTCTGTTAACCTC
	GPO	GGGAGCAAACAGGATTAGATACCCT
nANGPTL4 E40K mutagenesis	E40K for	ATC CTG GGA CAA GAT GAA CTT GCT GG
	E40K rev	GCA AAG CGC GGT GGC TCT

5.1.7. TaqMan™ assays

All TaqMan™ assays were purchased from Applied Biosystems.

Table 9 Human TaqMan™ assays

Gene	Ordering number
AXIN2	Hs00610344_m1
GAPDH	Hs02758991_g1
RN18S	Hs03928985_g1
SDC4	Hs01120908_m1

Table 10 Mouse TaqMan™ assays

Gene	Ordering number
ANGPTL4 (n-terminal)	Mm00480428_g1
Axin2	Mm00443610_m1
Gapdh	Mm99999915_g1
Rn18S	Mm03928990_g1
Sdc4	Mm00488527_m1

5.1.8. Vectors

Table 11 Vectors

shRNA	Target Gene	shRNA – Vector no.	Company
non-targeting	Non-silencing control	RHS4346	Horizon Discovery
human shRNA-1	*SDC4*	V3LHS_411904	Horizon Discovery
human shRNA-2	*SDC4*	V2LHS_30982	Horizon Discovery
mouse shRNA	*Sdc4*	V2LMM_1292	Horizon Discovery
Control GFP	Non-silencing control Turbo GFP	RHS4346	Horizon Discovery

Table 12 Expression Vectors

Backbone	Target Gene	Ordering number	Company
pLenti6/V5-Dest	-	V49610	Invitrogen
pLenti6/V5-nANGPTL4	*ANGPTL4*	This study	-
pLenti6/V5-nANGPTL4 E40K	*ANGPTL4*	This study	-

5.1.9. PCR/RT-qPCR reagents

Table 13 PCR and RT-qPCR reagents

Reagent	Company
Direct PCR Lysis Reagent	PeqLab
DNase/Rnase free H_2O	Gibco
RedTaq® ReadyMix™ PCR Reaction Mix	Sigma-Aldrich
TaqMan® Fast Advanced PCR Master Mix	Applied Biosystems

5.1.10. Western blot reagents

Table 14 Western blot reagents

Reagent	Company
Bovine Serum Albumin (BSA)	PAA
Nitrocellulose membrane	GE Healthcare
Orthovanadate	Merck
PageRuler Prestained Protein Ladder	Thermo Fisher Scientific
Pierce ECL Western Blotting Substrate	Thermo Fisher Scientific
Re-Blot Plus Strong Solution	Merck
Rotiphorese Gel 30	Carl-Roth
SuperSignal West Dura Extended Duration Substrate	Thermo Fisher Scientific

5.1.11. Antibodies

Table 15 Primary antibodies

Antigen	Reactivity	Species	Dilution	Conjugate	Source	Ordering number
Actin	human	rabbit	1:1000	-	Santa Cruz	Sc-1616-R
ANGPTL4 (C-specific)	human	rabbit	1:1000	-	Abcam	ab115798
ANGPTL4 (n-specific)	human	rabbit	1:1000	-	Mandard et al., 2004	N/A
β-catenin	mouse	rabbit	1:100	-	Cell Signaling	#8814
CD16/32 (Fc-block)	mouse	rat	1:100	-	eBioscience	14-0161-86
CD31	mouse	rat	1:200	APC	BD Biosciences	551262
CD31	mouse	rat	1:100	.	BD Biosciences	550300
CD45	mouse	mouse	1:400	FITC	BD Biosciences	553775
Desmin	mouse	rabbit	1:200	-	Abcam	Ab15200-1
Integrin $\alpha_5\beta_1$	human	mouse	-	-	Millipore	mab1969
Integrin $\alpha_v\beta_3$	human	mouse	-	-	Millipore	mab1976
Integrin $\alpha_v\beta_5$	human	mouse	-	-	Millipore	mab1961
LYVE1	mouse	rat	1:250	Alexa 488	eBiosciences	53-0443-82
PDPN	mouse	hamster	1:100	Alexa 488	eBioscience	53-5381-82
TER-199	mouse	rat	1:200	FITC	BD Biosciences	561032
Transferrin	human, mouse	rabbit	1:1000	-	ThermoFisher Scientific	PA3-913
V5	all species	rabbit	1:1000	-	Cell signaling	13202

Table 16 Secondary antibodies

Reactivity	Species	Dilution	Conjugate	Company	Ordering number
mouse IgG	rabbit	1:5000	HRP	DAKO	P0260
rabbit IgG	goat	1:500	Alexa 546	Life technologies	A11071
rabbit IgG	goat	1:5000	HRP	DAKO	P0448
rat IgG	goat	1:200	Alexa 488	Life technologies	A21049

5.1.12. Staining reagents

Table 17 Staining reagents

Reagent	Company
BODIPY™ 493/503	Thermo Fisher Scientific
CD31 MicroBeads, mouse	Miltenyi Biotech
Fluorescent mounting medium	DAKO
FxCycle – violet	Invitrogen
Hoechst Dye 33258, 1mg/ml	Sigma-Aldrich

Normal goat serum ready-to-use	Zymed
Roti-Histofix 4% (pH 7)	Carl Roth
Tissue-Tek® O.C.T.™ Compound	Scigen

5.1.13. Kits

Table 18 Kits

Reagent	Company
Arcturus™ PicoPure™ RNA Isolation Kit	Applied Biosystems
Click-iT™ EdU Alexa Fluor Flow Cytometry Kit	Thermo Fisher Scientific
GenElute™ Mammalian Total RNA Purification Kit	Sigma-Aldrich
LR-clonase II enzyme mix	Invitrogen
Pierce BCA Assay Kit	Thermo Fisher Scientific
Q5® Site-Directed Mutagenesis Kit	New England Biolabs
QuantiTect® Reverse Transcription Kit for cDNA Synthesis	Qiagen

5.1.14. Reagents for animal experimentation

Table 19 Reagents for animal experimentation

Reagent	Company
Bepanthen® eye cream	Roche
Betaisodona	Mundipharma
Ethicon suture silk 4-0	Johnson & Johnson MEDICAL
Ethicon suture silk 5-0	Johnson & Johnson MEDICAL
Ketavet	Pfizer
NaCl solution	Braun
Rompun	Bayer
Surgical tools and equipment	Fine Science Tools

5.1.15. Consumables

Table 20 Consumables

Consumable	Company
96 well plates	Steinbrenner Laborsysteme
384 well plates	4titute
Cannula (20G, 27G, 29G, 30G)	BD Biosciences
Cell culture dishes (10cm)	TPP
Cell scraper	Corning
Cell strainer (40 μm, 100 μm)	BD Biosciences
Cotton swab	Edeka elcos face
Countess™ cell counting chamber slides	Thermo Fisher Scientific
Cryotubes	Carl-Roth

FACS tubes	BD Biosciences
Filter containing pipette tips	Sarstedt
Microscope cover glasses	VWR international
Microscope glass slides	Menzel-Gläser
Octenisept®	Schülke
Peel-A-Way™ Embedding Molds	Merck
Pipette tips	Nerbe
Reaction tubes (0.5ml, 1.5ml, 2ml)	Eppendorf
Reaction tubes (15ml, 50 ml)	Greiner
Sealing foil	Applied Biosystems
Square dishes	Greiner
Sterile pipettes	Corning
Syringes	Dispomed
Terumo® Syringe (1 ml, 5ml, 10 ml)	Terumo
Tissue culture 6 well	Sarstedt
Tissue culture 24 well plate, ultra-low attachment	Sigma-Aldrich

5.1.16. Equipments

Table 21 Equipments

Equipment	Company
Aria cell sorting platform	BD Biosciences
Agarose gel documentation system	Peqlab
Amersham™ Imager 600	GE Healthcare
Axio ScanZ7.1 slide scanner	Zeiss
BioRad gel casting system	BioRad
BioRad gel running system	BioRad
BioRad Western blotting equipment	BioRad
Canto II	BD Biosciences
Cell culture hood	Thermo Fisher Scientific
Cell culture incubator	Thermo Fisher Scientific
Centrifuge	Thermo Fisher Scientific
Countess™ automated cell counter	Thermo Fisher Scientific
Developing cassette Western blot	Amersham Bioscience
Digital Electronic Caliper	Fine Science Tools
Freezing box	Thermo Fisher Scientific
Heating block	Eppendorf
HM355S microtome	Thermo Fisher Scientific
iMark™ Microplate Reader	BioRad
Magnetic stand	Thermo Fisher Scientific
Microtome Hyrax C50	Zeiss

Mixer mill MM200	Retsch
Multistep pipette	Eppendorf
Mr. Frosty Freezing Container	Thermo Fisher Scientific
Nanophotometer® N60	INTAS
Olympus IX 71	Olympus
Pipettes	ErgoOne
QIAxcel Advanced System	Qiagen
QuadroMACS Separator	Miltenyi Biotech
Scale	Ohaus
Special accuracy weighing device	Mettler Toledo
StepOnePlus Real-Time PCR System	Thermo Fisher Scientific
Shaver	Moser
Stereomicroscope	Leica
Table centrifuge (5417R)	Eppendorf
Thermocycler	Thermo Fisher Scientific
UV transluminator	Intas
Vortex	Neolab
Water bath	Julabo

5.1.17. Softwares

Table 22 Softwares

Software	Company
Cell P® software	Olympus
FACSDiva™	BD Biosciences
Fiji	ImageJ platform
FlowJo	BD Biosciences
Gene Set Enrichment Analysis	Broad Institute
Graph Pad Prism (v6.0)	Graph Pad
Ingenuity Pathway Analysis	Qiagen
Light Cycler 480 software	Roche
Molecular Signature Database	Broad Institute
StepOne™ Software v2.1	Thermo Fisher Scientific
ZEN black	Zeiss
ZEN blue	Zeiss

5.1.18. Solutions and buffers

Table 23 Recipe for preparing solutions and buffers

Buffer		Composition
Ammonium chloride potassium buffer (ACK)	150 mM	NH_4Cl
	10 M	$KHCO_3$

	100 mM	Na_2EDTA
		adjust pH 7.2-7.4BD
Blotting buffer (1x)	192mM	Glycine
	25mM	Trizma Base
Dialysis Buffer	50 mM	Na phosphate pH 7.2
	150 mM	NaCl
FACS buffer	3% (v/v)	Fetal calf serum in PBS
Phosphate buffered saline (PBS)	1.34 M	NaCl
	27 mM	KCl
	200 mM	Na_2HPO_4
	4.7 mM	KH_2HPO_4
		adjust pH 7.4
Permeabilization buffer	0.3 %	Triton in PBS
5x Protein sample buffer	250 mM	Tris-HCl (pH 6.8)
	10 %	SDS
	0.5 %	Bromophenol blue solution
	50 %	Glycerol
		add 10% β-mercaptoethanol before use
RIPA lysis buffer (modified)	50 mM	Tris-HCl (pH 7.5)
	150 mM	NaCl
	1 mM	EDTA
	1 %	NP-40
	0.25 %	Na-deoxycholate
	2 mM	Na-orthovanadate
	1 x	Protease inhibitor Mix G
Running buffer (1x)	192 mM	Glycine
	25 mM	Trizma Base
	0.1%	SDS
Separating gel (12%) (1Gel)	3.3 ml	H2O
	2.5 ml	1.5M Tris-HCl pH 8.8
	100 µl	10% SDS
	4 ml	30% Acrylamide
	100 µl	APS
	4 µl	TEMED
Separating gel (5%) (1Gel)	2.7 ml	H2O
	0.5 ml	1M Tris-HCl (pH 6.8)
	40 µl	10%SDS
	0.67 ml	30% Acrylamide
	40 µl	APS
	4 µl	TEMED
StrepTactin Running Buffer	100 mM	Tris pH 8.0
	150 mM	NaCl
	1 mM	EDTA
Tris-Buffered Saline Tween-20 (TBS-T)	10 mM	Tris/HCl, pH 7.5
	100 mM	NaCl
	0.1%	Tween-20

5.2. Methods

5.2.1. Cell culture

5.2.1.1. Cell maintenance

LLC, B16F10, MT-RET and HEK293T were obtained from ATCC. All cancer cell lines were cultured in DMEM high glucose (Gibco) supplemented with 10% FCS and 1% penicillin/streptomycin (Sigma). Human umbilical endothelial cells (HUVEC, Promocell) were cultured in Endopan-3 medium supplemented with growth factors (PAN Biotech GmbH) and mouse lung endothelial cells (mLEC, Cell Biologics) were cultured in EC medium supplemented with growth factors (Cell Biologics). HUVECs and mLECs were cultured between passages one and six. For passaging, 80-90% confluent cells were washed with PBS and subsequently detached with Trypsin-EDTA at 37°C for 2 min. Culture medium was added to neutralize Trypsin-EDTA and the cells were pelleted by centrifugation for 5 min at 200 g. After the supernatant was discarded, the pellet was resuspended in culture medium and desired cell dilutions were prepared. HUVECs and mLECs were splitted in a 1:3 ratio, while tumor cells were diluted in a 1:10 ratio. Prior to seeding, cell culture plates were coated with 0.1% gelatine (mLEC) or 0.2% gelatine (HUVEC) for 30 min at 37°C.

5.2.1.2. Cryopreservation of cells

Cultured cells were detached from cell culture plates as described above and centrifuged at 200 g for 5 min. Subsequently, the supernatant was discarded and the cell pellet was resuspended in 1 ml of the cell-type specific medium containing 10% DMSO and an additional 10% of FCS. Upon resuspension, the cell suspension was transferred to cryotubes and slowly frozen to -80°C in an isopropanol containing freezing box (Mr. Frosty Freezing Container, Thermo Fisher Scientific). On the next day, cells were transferred to the liquid nitrogen tank for long-term storage. For thawing cells, cryotubes were placed at 37°C for 2 min. Cells were mixed with a pre-warmed culture medium and centrifuged at 200 g for 5 min to remove DMSO. The supernatant was removed and the cell pellet was resuspended in a 10 ml cell-type specific medium and seeded into a cell culture dish.

5.2.1.3. Counting of cells

Detached cells were mixed with trypan blue in a 1:1 dilution and the cell concentration was determined with an automated cell counting machine (Countess, Thermo Scientific) according to the manufacturer's instructions. Subsequently, appropriate cell numbers were seeded in cell culture plates or used for *in vivo* injection.

5.2.1.4. Lentiviral production and transduction

Lentivirus was produced in HEK293T cells by transfecting cells with the lentiviral construct of interest (21 µg), envelope plasmid pMD2.G (14µg) and packaging plasmid psPAX2 (21µg) by using PEI solution (Sigma). After transfection, lentiviral supernatant was harvested twice: 48h and 72h post-transfection. The supernatant was filtered through a 0.45 µm filter and centrifuged at 800'000 g for 2 h at 4°C. Subsequently, the lentiviral pellet was diluted in PBS and stored at -80°C. LLC, B16F10 and HUVEC cell lines were transfected with lentiviral particles expressing the shRNA constructs (Horizon discovery): non-targeting (RHS4346), shRNA construct containing Turbo GFP (RHS4346), sh-1 human *SDC4* (V3LHS_411904), sh-2 human *SDC4* (V2LHS_30982) and shRNA mouse *Sdc4* (V2LMM_1292). After transfection, the cells were selected with blasticidin (10 µg/ml). In addition, LLC and B16F10 cell lines were transduced with lentiviral particles expressing the pLenti6/V5-nANGPTL4, pLenti6/V5-nANGPTL4 E40K or pLenti6/V5 empty vector. After transfection, the cells were selected with puromycin (1 µg/ml). Control or nANGPTL4-overexpressing LLC cells were transduced with shCtrl or sh*Sdc4*. Stable cell lines were generated by selecting both blasticidin (10 µg/ml) and puromycin (1 µg/ml) resistant cells.

5.2.1.5. Cloning, expression and purification of ANGPTL4 proteins

The mouse nANGPTL4 sequence (amino acids 24-164 of ANGPTL4) was cloned into the pACEBac1-EGT vector (EMBL). After the nANGPTL4 sequence the vector included a HRV 3C protease cleavage site and a c-terminal StrepIItag. This construct was used for transposition in E. coli DH10EMBacY cells and the extracted bacmid DNA was then used to generate recombinant baculovirus. 5ml of baculovirus was added to 0.5 liter of Hi5 cells at a density of $1x10^6$ cells/ml to produce recombinant nANGPTL4 protein. The infected Hi5 cells were grown for 48h in Sf-900 III SFM medium (Thermo Fischer Scientific) at 27ºC.and cells were harvested by centrifugation. The cell pellet was discarded and the cell culture medium was mixed carefully with 50ml of a buffer containing 1 M Tris pH 8.0, 1.5M NaCl, 10mM EDTA and 1.2ml BioLock solution (IBA). The solution was gently stirred on ice for 15min and filtered over a sterile 22 µm Steritop bottle top filter (Merck Millipore). The resulting supernatant was loaded onto a 1ml StrepTactinXT Superflow high capacity column (IBA) which was pre-equilibrated with running buffer (100mM Tris pH 8.0, 150mM NaCl, 1mM EDTA). After loading, washing of the column was performed with running buffer and running buffer supplemented with 50mM biotin was used for elution. The elution fractions containing mouse nANGPTL4 were pooled and dialyzed overnight at 4ºC against storage buffer (50mM Na phosphate pH 7.2, 150mM NaCl).

5.2.2. Cellular assays

5.2.2.1. Cell adhesion assay

mLECs ($1.5x10^5$) were seeded in a 6-well plate to form a monolayer after 24h. GFP-labeled B16F10 cells ($5x10^5$) in Opti-MEM media (Life Technologies) were seeded on top of the mLEC monolayer. After allowing the tumor cells to adhere for 40 min, non-adherent tumor cells were washed with PBS and the count of adhering tumor cells was determined using BD CantoII.

5.2.2.2. EdU cell proliferation assay

Proliferation assays of B16F10, HUVECs and mLECs were performed using the Click-iT® EdU Alexa Fluor® 647 Flow Cytometry Assay Kit (Life Technologies). For each cell line, 150.000 cells were seeded per 6-well and allowed to adhere for 24h. B16F10 and mLECs were treated with 400 ng mouse recombinant nANGPTL4 or the respective buffer for 16h in starvation medium. HUVECs were treated with 400 ng human recombinant protein or PBS for 16h in starvation medium. After 13h of recombinant protein treatment, EdU was added for the remaining 3h (10 µM). Next, cells were harvested and fixed for 15 min with Click-iT® fixative solution. Permeabilization was performed in saponin based permeabilization buffer for 15 min. EdU+ cells were detected by incubating cells with Click iT® detection cocktail for 30 min followed by analysis with a BD FACSCanto II flow cytometer. The percentage of EdU positive cells was determined with the FlowJoTM software.

For the mLEC and B16F10 co-culture assay, 300.000 mLECs were seeded per 6-well and allowed to adhere for 24h. mLECs were treated with 400 ng of mouse recombinant protein or buffer for 16h in starvation medium. Afterwards, 500.000 GFP labeled B16F10 tumor cells in Opti-MEM were seeded on top of the mLEC monolayer and allowed to adhere for 2h. Subsequently, EdU was added for 3h (10 µM). Next, cells were harvested, fixed, permeabilized and stained for EdU as described above. The percentage of proliferating GFP+ tumor cells was determined with the FlowJoTM software.

5.2.2.3. Sprouting assay

HUVEC (20.000) were diluted in 20% Methocel / 80% EGM solution and plated in 25µl droplets on a squared petri dish. Subsequently, they were incubated upside down at 37°C to form spheroids. On the next day, spheroids were collected in PBS + 10% FCS and the spheroids were resuspended in a solution of 80% Methocel and 20% FCS. 500µl of a collagen mix was added to the spheroids (62.5µl Medium199, 0.5ml Collagen, 6µl 2M NaOH, 50µl HEPES buffer). Subsequently, 1 mL of the collagen-spheroid mix were added in a 24-well plate and the gels were polymerized for 30min at 37°C. The spheroids were treated with the following recombinant proteins: 10ng of VEGF-A (VEGF-A high, R&D, 293-VE), 1ng of VEGF-A (VEGF-A low) and 400ng of nANGPTL4 (R&D, 8249-AN) for 24h. For sprouting assays with integrin-blocking antibodies, collagen gels were incubated with 2µg of each integrin-blocking antibody

or mouse IgG for 1h followed by the addition of the respective recombinant proteins. After stimulation, gels were fixed by adding 1ml Histofix. Images were acquired using Olympus IX-81 microscope and cumulative sprout length was measured using Cell P® software. Ten spheroids were analyzed for each experimental condition.

5.2.3. Cloning

5.2.3.1. Amplification and plasmid purification

Transformed bacteria culture or bacterial glycerol stock containing the required plasmid were grown in 5 ml (Miniprep) or 300 ml (Maxiprep) of LB media with the appropriate antibiotics. The culture was grown in the bacterial shaker overnight at 37°C and 250 rpm. On the next day, the bacterial cells were pelleted by centrifuging at maximum speed for 10 min (Mini prep) or 30 min (Maxiprep). At 4°C. The supernatant was discarded and plasmid purification was performed with the PureLink™ Quick Plasmid MiniPrep-Kit or NucleoBond-Xtra Maxi kit according to the manufacturer's instructions.

5.2.3.2. LR reaction

The LR cloning reaction was performed according to the manufacturer's instructions. 50 ng of *nANGPTL4* or *nANGPTL4 E40K* entry clone was mixed with 100 ng of the destination plasmid pLenti6.2/V5-DEST. Rnase-free water was added to achieve a reaction volume of 7 µl. To start the recombination reaction, 2 µl of LR clonase II was added to the reaction mixture and incubated for 1h at RT. Afterwards, 1 µl of Proteinase K solution was added and incubated at 37°C for 10 min to stop the recombination reaction. The LR reaction mixture was used for bacterial transfection.

5.2.3.3. Transformation

The LR reaction mixture or 100 ng of the desired plasmid was added to 50 µl One Shot™ Stbl3™ competent *E.coli*. The mixture was incubated on ice for 20 min and subsequently heat shocked at 42°C for 45 s. In the next step, the reaction mixture was incubated on ice for 2 min. 500 µl of S.O.C. media was added to the reaction and was further shaken at 250 rpm and 37°C for 1h. 100 µl of the transformed bacteria were plated on LB agar plates containing the appropriate antibiotics and incubated overnight at 37°C. On the next day, 2-3 colonies were picked and amplified. Then, the DNA was isolated with the PureLink™ Quick Plasmid Miniprep-Kit. The sequence of the clones was verified using the standard Sanger sequencing.

5.2.4. Human patient samples

5.2.4.1. Patient samples and ethical approval

Fresh frozen melanoma and lung tumor and serum samples were provided by the University Medical Centre Mannheim. The study was approved by the Ethical Committee of Heidelberg University (2010-318N-MA). Informed written consent was obtained from all participants. They agreed to use their samples for research and to publish the acquired data in accordance with the Helsinki principles for the enrolment in research protocols.

5.2.4.2. Patient classification and serum collection

A certified, interdisciplinary tumor board (dermatologist, ENT, general surgery, radiology, nuclear medicine, neurosurgery) classified the patients based on serum parameters (S100A) and radiological examination (using the internationally accepted RECIST 1.1 criteria). A patient was characterized with a stable disease when there was no sufficient increase and no decrease in their tumor burden (growth of pre-existing metastasis or occurrence of new metastasis) compared to the previous measurements. In contrast, a patient with an increase in tumor burden compared to the last measurement was considered to have a progressive disease. The serum levels of nANGPTL4 were determined from samples collected one week before the tumor board meeting.

5.2.5. Mice

Male C57BL/6J (WT) were purchased from Charles River. ANGPTL4-/- mice were kindly provided by S. Kersten. All mice were housed in a 12h light/dark cycle with free access to food and drinking water in specific pathogen-free animal facilities. All animal experiments were approved by the governmental Animal Care and Use Committees (permits: G23/16, G286/18, G101/20, DKFZ 305 and DKFZ370 from Regierungspräsidium Karlsruhe, Germany).

5.2.5.1. Tumor models

All mice were regularly monitored for humane endpoint criteria. Tumor volumes were measured with a digital caliper and tumor volumes were calculated using the following formula (volume = ½ length x width x height).

5.2.5.1.1. Experimental metastasis models

B16F10 or MT-RET cells ($2.5x10^5$) were injected in the tail vein of 8-10 weeks old male WT mice. Mice were sacrificed 2 weeks after tumor cell injection. Lungs were harvested, the number of metastases was counted and images of metastasized lungs were taken with a stereomicroscope.

For the LLC experimental metastasis model, $1.5x10^5$ LLC with control and nANGPTL4 overexpression and control or *SDC4*-silencing were injected in the tail vein of WT mice. 2 weeks after tumor cell injection, mice were sacrificed and images of metastasized lungs were taken with a stereomicroscope. The metastatic area in the lung was determined using Fiji.

5.2.5.1.2. LLC spontaneous metastasis model

LLC ($1x10^6$) were subcutaneously injected in C57BL/6J mice. Primary tumor size was regularly measured and tumors were surgically resected at an average size of 150 mm^3. For tumor resections, mice were anesthetized by interperitoneally injecting a solution of Ketamin (100 mg/kg) and Xylazin (10 mg/kg) diluted in 0.9% NaCl. During the operation, anesthetized mice were put on a heat mat and eyes were creamed with bepanthen to prevent drying. The surgical area was sterilized using 70% ethanol and incisions were made around the tumor. The blood vessels feeding the tumor were carefully cauterized and the primary tumor was completely removed. Number 5 suture silk was used to suture the peritoneum and number 4 suture silk was used for the skin. Post resection, mice were routinely checked for the endpoint criteria and mice were sacrificed as soon as the defined endpoint criteria were reached.

5.2.5.1.3. Primary tumor models

For primary tumor experiments, $1x10^6$ WT B16F10 or B16F10 overexpressing a control, *nANGPTL4*, *nANGPTL4 E40K* plasmid were subcutaneously injected. At a tumor size of 500 mm^3, mice were sacrificed and the primary tumor was sampled. For the primary tumor experiment with B16F10 overexpressing a control, *nANGPTL4*, *nANGPTL4 E40K* plasmid, mice were subjected to 12h food withdrawal before the end of the experiment.

5.2.5.2. Cornea pocket assay

A partial incision was made in the middle of the cornea using a 30-degree micro knife on anesthetized male C57BL/6J mice. Subsequently, a von Graefe knife was inserted under the edge of the inferior lip of the partial incision to create the pocket and to lengthen it towards the inferior limbus. Equal size slow-release pellets were prepared by mixing appropriate amounts of growth-factor with 5µl Hydron (12% poly (2-hydroxyethyl methacrylate/ 99.5% ethanol) and 1µl 10 % sucralfate solution (in PBS). Pellets (0.4mm x 0.4mm) were implanted into the pocket at 1.0±0.2mm distance from the corneal limbus, as previously described (*197*). The pellets were prepared with 200ng nANGPTL4 and/or 160ng VEGF-A (R&D). The mice were sacrificed after 7 days and the corneas were isolated. Corneas were fixed

in cold methanol for 10min, washed with PBS+0,3% Triton for permeabilization and stained with anti CD31 antibody (BD Bioscience). Images were taken with Zeiss Axio Scan and analyzed with Fiji.

5.2.5.3. Therapeutic administration of nANGPTL4

C57BL/6J mice were pre-treated with one shot of either nANGPTL4 protein or PBS intravenously. Two days later, $2,5x10^5$ B16F10 or MT-RET cells were intravenously injected. Mice were administered thereafter with nANGPTL4 protein or PBS intravenously twice a week. Two weeks later, lungs were collected, and melanoma metastatic foci were counted. For injection of denatured nANGPTL4, recombinant nANGPTL4 was denatured at 95°C for 30 min prior to its administration.

5.2.5.4. Administration of nANGPTL4-overexpressing AAV

10^{11} viral particles of Ctrl or nANGPTL4 AAV were intravenously injected in C57BL/6J mice. Ten days after AAV injection, $2,5x10^5$ B16F10 cells were intravenously injected. Two weeks later, lungs were collected and metastatic foci were counted. In the LLC resection model, 10^6 LLCs were injected subcutaneously in C57BL/6J mice. 9 days after tumor cell injection 10^{11} viral particles of Ctrl or nANGPTL4 AAVs were intravenously injected. Primary tumors were resected at an average size of 250-450mm^3. The mice were regularly checked for the experimental endpoint criteria after resection.

5.2.5.5. Blood withdrawal

For terminal blood withdrawal, mice were anesthetized by interperitoneally injecting a solution of Ketamin (120 mg/kg) and Xylazin (20 mg/kg) diluted in 0.9% NaCl. Afterwards, blood was withdrawn by cardiac puncture. After collection of the whole blood, the blood was allowed to clot by leaving it undisturbed at room temperature for 15 – 30 min. The clot was removed by centrifuging at 1,000-2,000 x g for 10 minutes in a refrigerated centrifuge. Subsequently, the serum was loaded on a western blot or send for serum analysis.

5.2.6. Immunofluorescence staining

5.2.6.1. Preparation of cryoblocks and cryosections

Excised lungs and tumors were embedded in TissueTek O.C.T. compound (Sakura) on dry ice. Subsequently, samples were stored at -80°C. The cryomicrotome Hyrax C50 (Zeiss) was used to cut 7 µm cryosections. Sections were dried for 10 min at RT and subsequently stored at -80°C.

5.2.6.2. IF staining and analysis

Cryosections were fixed in ice-cold methanol (-20°C) for 10 min. Afterwards, sections were washed and blocked in 10% ready-to-use normal goat serum (Life Technologies) for 1h. The primary antibody was incubated overnight at 4°C [rat anti-CD31 (BD Bioscience, #550300), rabbit anti-β-catenin (Cell Signaling, #8814), rabbit anti-desmin (Abcam, #Ab15200-1)]. After primary antibody incubations, the sections were washed three times in TBS-T for 5 min each and incubated with the secondary antibodies[anti-rat Alexa488, anti-rabbit Alexa546 (LifeTechnologies)] for 1h at RT. For lipid staining, the BODIPY™ 493/503 dye was added to the secondary antibody mixture and incubated for 1h. Next, sections were washed three times with TBS-T for 5 min. Afterwards, Hoechst staining (1:5000, Merck) was performed and sections were mounted with DAKO mounting medium (Agilent). Images were acquired with Zeiss Axio Scan and Fiji was used for image analysis.

5.2.7. Flow cytometry: Isolation of endothelial cells

Enzymatic digestion of mouse lung ECs and mouse tumor ECs was performed with 5 ml DMEM high glucose medium containing 4 mg/ml liberase and 10 µg/ml Dnase1 at 37°C for 30 min. For dissociation, tissue lysates were first passed through 19 G syringes and filtered through 100 µM filters. In the next step, erythrocytes were lysed by incubating tissue lysate with ammonium chloride potassium (ACK) lysis buffer.

5.2.8. Protein biochemistry

5.2.8.1. Preparation of protein lysates

Snap-frozen human tumor tissues were lysed by grinding in a mixer mill (Retsch) in modified RIPA lysis buffer supplemented with the phosphatase inhibitor orthovanadate (4 mM). 4 µl lysis buffer was used per µg of frozen tissue. After grinding, samples were incubated on ice for 20 min. Whole cell lysates were centrifuged at 14,000 rpm at 4°C for 5 min. Subsequently, the supernatant was removed and transferred to new tubes. For long-term storage, lysates were stored at -80°C. The Pierce™ BCA Assay kit was used according to the manufacturer's protocol to determine protein concentrations.

5.2.8.2. SDS-Polyacrylamide gel electrophoresis (PAGE) and Western blot

For human tissue lysates, 50 µg of total protein was boiled in 5x laemmli buffer at 95°C for 5 min. For serum samples, 0.4 µl of serum (human) or 5 µl serum (mouse) were directly boiled in 5x laemmli buffer without prior lysis. Proteins were separated on 12% SDS-PAGE gels with the BioRad gel casting and running system in 1x running buffer. To determine the size of the protein, 5 µl of Page Ruler

Prestained Protein ladder was loaded. The gels were run at 80 V for 30 min to enter the stacking gel. Afterwards, the voltage of gel electrophoresis was increased to 120 V for 1 h. After the gel was run, the proteins were transferred onto a nitrocellulose membrane for 90 min at 400 mA in 1x blotting buffer. Blocking of the membranes was performed with 5% milk in TBS-T for 1 h at RT. After blocking, the membranes were incubated overnight at 4°C with the following primary antibodies: cANGPTL4 (Abcam, ab115798), nANGPTL4 (Mandard *et al.,* 2004), Transferrin (ThermoFisher, PA3-913), Actin (Santa Cruz, Sc-1616-R), V5 (Cell Signaling, 13202), diluted 1:1000 in PBS-T containing 5% milk powder at 4°C overnight. Following primary antibody incubation, the membranes were washed 3x for 5 min with TBS-T and incubated with specific secondary horseradish peroxidase-conjugated antibodies (anti-rabbit HRP, DakoCytomation, P0448) for 1h at RT. Next, the membranes were washed 3x for 5 min with TBS-T and proteins were visualized with Enhanced Chemiluminescence Western blotting Substrate (ECL, Pierce). For weaker signals, *SuperSignal* West Dura Extended Duration Substrate (Thermo Fisher Scientific) was used for visualization. Proteins were viewed using Amersham imager 600 (GE). Densiometric analysis was performed using Fiji.

5.2.9. Molecular biology

5.2.9.1. Genotyping PCR

100 µl Direct PCR Lysis Reagent with 10 µg Proteinase K was added to tail tips and samples were incubated at 55 °C over night. Subsequently, tails were heated to 95°C for 20 min to inactivate the enzyme. The lysate was centrifuged and 3 µl of extracted DNA was used for the genotyping PCR. Lysates were stored at -20 °C for later re-genotyping. Genotyping was performed using the Taq polymerase kit (Qiagen). The PCR reaction was run with an Applied Biosystems thermocycler and analyzed with the QIAxcel Advanced system according to the manufacturer's instructions.

Table 24 $ANGPTL4^{KO}$ genotyping

PCR mix (Qiagen kit)			**PCR program**		
dd H2O	12.6 µl		**Step**	**Temperature**	**Time**
Q solution	5.2 µl		1	94 °C	4 min
Buffer 10x	2.6 µl		2	94 °C	30 sec
MgCl2	1 µl		3	64 °C	20 sec
dNTPs (2.5 mM)	0.6 µl		4	72 °C	40 sec
primer ANGPTL4 for	0.6 µl		go to step 2: 32x		
primer ANGPTL4 WT rev	0.6 µl		5	72 °C	2 min
primer ANGPTL4 KO rev	0.6 µl		6	4 °C	forever
Taq (5 U/µl)	0.2 µl				
DNA	1 µl				
WT band: 350 bp, KO band: 550 bp					

5.2.9.2. Mycoplasma PCR

For mycoplasma detection, 1 ml of cell culture medium was removed from cultured cells and centrifuged to remove cell debris. 2 µl of supernatant was directly used for detection PCR. Mycoplasma PCR was performed using the Taq polymerase kit (Qiagen). The PCR reaction was run with an Applied Biosystems thermocycler and analyzed with the QIAxcel Advanced system according to the manufacturer's instructions.

Table 25 Mycoplasma detection

PCR mix (Qiagen kit)			**PCR program**		
dd H2O	6.8 µl		**Step**	**Temperature**	**Time**
Q solution	2.6 µl		1	95 °C	5 min
Buffer 10x	1.25 µl		2	95 °C	30 sec
MgCl2	0.5 µl		3	58 °C	30 sec
dNTPs (2.5 mM)	0.25 µl		4	72 °C	1 min
MGSO (10 µM)	0.25 µl		go to step 2: 40x		
GPO (10 µM)	0.25 µl		5	72 °C	10 min
Taq (5 U/µl)	0.1 µl		6	4 °C	forever
DNA	2.0 µl				
Mycoplasma contamination: 270 bp					

5.2.9.3. Mutagenesis PCR

Mutagenesis of mouse *nANGPTL4* gateway entry clones was performed with the Q5® Site-Directed Mutagenesis Kit (NEB) according to the manufacturer's protocol. Mutagenesis PCR was performed with the Q5® Hot Start High-Fidelity 2x Master Mix with the appropriate primers. The Applied Biosystems thermocycler was used to run the PCR reaction. In the next step, an enzyme mix containing a kinase, ligase and Dpnl was added to the PCR product and incubated at RT for 5 min to allow circularization of the DNA and removal of the template DNA. Afterwards, transformation into chemically competent cells was performed to amplify the *nANGPTL4 E40K* mutated entry clone.

Table 26 E40K mutagenesis PCR

PCR mix (Q5 Mutagenesis Kit)			**PCR program**		
Q5 Hot Start High-Fidelity 2x Master Mix	12.5 µl		**Step**	**Temperature**	**Time**
Forward Primer (10 µM)	1.25 µl		1	98 °C	30 sec
Reverse Primer (10 µM)	1.25 µl		2	98 °C	10 sec
Template DNA (20 ng/µl)	1 µl		3	68 °C	30 sec
dd H2O	9 µl		4	72 °C	1 min 45 sec
			go to step 2: 25x		
			5	72 °C	2 min
			6	4 °C	forever

5.2.9.4. RNA extraction

RNA from cell culture was isolated with the GenElute Mammalian Total RNA Purification Kit (Sigma) according to the manufacturer's protocol. RNA of sorted lung and tumor ECs was isolated with the Arcturus™ PicoPure™ RNA Isolation Kit according to the manufacturer's instructions. After purification, RNA concentration was determined using the NanoPhotometer N60 and the RNA was stored at -80°C.

5.2.9.5. cDNA synthesis

cDNA synthesis from previously isolated RNA (1 µg) was performed with the QuantiTect Reverse Transcription Kit (Qiagen) according to the manufacturer's protocol. Afterwards, cDNA was diluted 1:20 in H_2O for qPCR and was stored at -20 °C.

5.2.9.6. Quantitative PCR

RT-qPCR was performed by using the synthesized cDNA with TaqMan Fast Advanced Mastermix (Life Technologies) and TaqMan probes (Applied Biosciences) on a StepOnePlus Real-Time PCR System (Thermo Fisher Scientific). Each reaction was performed in triplicates. Gene expression was calculated by ΔCT quantification method, normalized to *Gapdh* or *Rn18S*.

Table 27 TaqMan quantitative PCR

qPCR reaction mix	
	1 reaction
cDNA	2 µl
TaqMan Fast Advanced Master Mix	5 µl
TaqMan gene expression assay	0.2 µl
dd H2O	2.8 µl

qPCR program		
Step	**Temperature**	**Time**
1. Pre-denaturation	95 °C	30 sec
2. Denaturation	95 °C	2 sec
3. Amplification	60 °C	20 sec
go to step 2: 45x		

5.2.10. RNA sequencing and data analysis

Lung ECs from control and nANGPTL4 AAV treated mice were FACS-sorted and total RNA was isolated using an Arcturus PicoPure RNA isolation kit (Thermo Fisher Scientific) according to the manufacturer's protocol. The sequencing libraries were prepared using SMARTer Ultra Low RNA v4 Kit (Clontech) with 10 ng of base material and sequenced on Novaseq 6000 S1 (50-bp paired-end). The RNA sequencing data was processed and aligned using the DKFZ OTP RNAseq workflow (Reisinger *et al.,* 2017). Differential gene expression analysis was performed using DESeq2 and the downstream gene set enrichment analysis was conducted employing clusterProlifer 4.0 (Love *et al.,* 2014; Wu *et al.,* 2021).

5.2.11. Statistical analysis

All data are represented as mean with error bars depicted as SD or SEM (indicated in the figure legends). n represents the number of independent experiments for *in vitro* experiments and the number of mice for *in vivo* experiments. The GraphPad Prism 6 software was used for statistical analyses. Non-parametric Mann Whitney U-test, two-tailed unpaired Student's t-test or paired t-test were performed. A p-value of less than 0.05 was considered significant. Significance was marked by asterisks (*p<0.05, **p<0.01, ***p<0.001, ****p<0.0001).

5.2.12. Data availability

The raw RNAseq data has been deposited under the GEO accession no. GSE210291.

6. Abbreviations

AAV	Adeno-associated virus
ACK	Ammonium chloride potassium
ACTN4	α-actinin-4
AMPK	AMP-activated protein kinase
Ang1	Angiopoietin 1
ANGPTL4	Angiopoietin-like 4
APS	Ammonium persulfate
BMP7	Bone morphogenetic protein 7
BRAF	v-raf murine sarcoma viral oncogene homolog B1
Ca2+	Calcium
cANGPTL4	c-terminal fragment of Angiopoietin-like 4
CDKDN2	Cyclin-dependent kinase inhibitor 2A
CEP	Circulating endothelial precursor cell
CK1	Casein kinase1
CTC	Circulating tumor cell
CTLA4	Cytotoxic T-lymphocyte-associated protein 4
CTR	Concomitant tumor resistance
Ctrl	Control
DAG	Diacylglycerol
DAPI	4’,6-diamidino-2-phenylindole
Dll4	Delta like canonical Notch ligand 4
DNA	Deoxyribonucleic acid
DTC	Disseminated tumor cell
Dvl	Dishevelled
EC	Endothelial cell
ECM	Extracellular matrix
EdU	5-ethynyl-2'-deoxyuridine
EGF	Epidermal growth factor
EMT	Epithelial-mesenchymal transition
eNOS	Endothelial nitric oxide synthase

ERK	Extracellular signal-regulated kinase
FACS	fluorescence-activated cell sorting
FAK	Focal adhesion kinase
FCS	Fetal calf serum
FGF	Fibroblast growth factor
Fiaf	Fasting-induced adipose factor
FL	Full-length Angiopoietin-like 4
flANGPTL4	Full-length Angiopoietin-like 4
Fz	Frizzled
GDR15	Growth differentiation factor 15
GFP	Green fluorescent protein
GM-CSF	Granulocyte-macrophage colony-stimulating factor
GPIHBP1	Glycosylphosphatidylinositol anchored high density lipoprotein binding protein 1
GSK3β	Glycogen synthase kinase-3β
H20	Water
HEK	Human embryonic kidney cells
HIF	Hypoxia-inducible factor
HSV-1	Herpes simples virus, type 1
HUVEC	Human umbilical endothelial cell
i.v.	Intravenous
IF	Immunofluorescence
IP3	1,4,5-trisphosphate
Ko	Knockout
LD	Lipid droplet
LLC	Lewis lung carcinoma
LPL	Lipoprotein lipase
LRP5/6	lipoprotein receptor-related proteins 5 or 6
MAPK	Mitogen-activated protein kinases
MC1R	Melanocortin receptor 1
MDSC	Myeloid-derived suppressor cell
MEK	Mitogen-activated protein kinase
min	Minutes

mLEC	Mouse lung endothelial cell
mm	Millimeter
MMP	Matrix metalloproteinase
MSH	Melanocyte stimulating hormone
mTOR	Mammalian target of rapamycin
mTORC2	Mammalian target of rapamycin complex 2
NaCl	Socium chloride
nANGPTL4	n-terminal fragment of Angiopoietin-like 4
NF1	Neurofibromin 1
NO	Nitric oxide
NRP	Neuropilin
ns	Non-significant
NT	n-terminal fragment of Angiopoietin-like 4
P/S	Penicillin/streptomycin
PBS	Phosphate buffered saline
PBS-T	Phosphate-buffered saline Tween
PC5/6	Proprotein convertase 5/6
PCR	Polymerase chain reaction
PCSK3	Proprotein convertase subtilisin/kexin type3
PD	Progressive disease
PD-1	Programmed death 1
PDGF-B	Platelet-derived growth factor B
PDGFR	Platelet-derived growth factor receptor
PD-L1	Programmed death ligand 1
PEI	Polyethyleneimine
PLc	Phospholipase C
PlGF	Placental growth factor
PPAR	Peroxisom-proliferator-aktivierte rezeptoren
PPP6C	Phosphoprotein phosphatase 6
RAC1	Rac family small GTPase 1
Rho	Ras homolog family member
RIPA	Radioimmunoprecipitation assay

RNA	Ribonucleic acid
RT	Room temperature
s.c.	Subcutaneous
SD	Stable disease
SD	Standard deviation
SDC-4	Syndecan-4
SDS	Sodium dodecyl sulfate
SDS-PAGE	Sodium dodecyl sulfate polyacrylamide gel electrophoresis
sec	Seconds
SEM	Standard error of the mean
shRNA	Short hairpin ribonucleic acid
SRC	SRC proto-oncogene, non-receptor tyrosine kinase
Taq	Thermus aquaticus
TBS-T	Tris-buffered saline Tween
TEMED	Tetramethylethylenediamine
TG	Triglyceride
TGF-β	Transforming growth factor-β
Tie	Tyrosine kinase with immunoglobulin-like and EGF-like domain
TME	Tumor microenvironment
Treg	Regulatory T-cells
T-VEC	Talimogene laherparepvec
UV	Ultraviolet
V	Volt
v/v	Volume/volume
VEGF	Vascular endothelial growth factor
VEGFR	Vascular endothelial growth factor receptor
WT	Wildtype

7. Publications

Corresponding manuscript to thesis:

Hübers C*, Abdul Pari AA*, Grieshober D*, Petkov M, Schmidt A, Messmer T, Heyer CM, Schölch S, Kapel SS, Gengenbacher N, Singhal M, Schieb B, Fricke C, Will R, Remans K, Utikal JS, Reissfelder C, Schlesner M, Hodivala-Dilke KM, Kersten S, Goerdt S, Augustin HG#, Felcht M#. Primary tumor-derived systemic nANGPTL4 inhibits metastasis. J Exp Med. 2023 Jan 2;220(1):e20202595.

Additional published work:

Preuss SF*, Grieshober D*, Augustin HG. Systemic reprogramming of EC signaling in metastasis and cachexia. Physiology, *accepted manuscript*

* equally contributing first authors

# equally contributing last authors

8. References

1. D. Hanahan, Hallmarks of cancer: new dimensions. *Cancer Discov* **12**, 31-46 (2022).
2. SEER Training Modules. U. S. National Institutes of Health, National Cancer Institute (2023).
3. G. R. Dagenais *et al.*, Variations in common diseases, hospital admissions, and deaths in middle-aged adults in 21 countries from five continents (PURE): a prospective cohort study. *Lancet* **395**, 785-794 (2020).
4. H. Sung *et al.*, Global cancer statistics 2020: GLOBOCAN estimates of incidence and mortality worldwide for 36 cancers in 185 countries. *CA Cancer J Clin* **71**, 209-249 (2021).
5. A. A. Abdul Pari, M. Singhal, H. G. Augustin, Emerging paradigms in metastasis research. *J Exp Med* **218**, e20190218 (2020).
6. S. N. Pavri, J. Clune, S. Ariyan, D. Narayan, Malignant melanoma: beyond the basics. *Plast* **138**, 330e-340e (2016).
7. Malignant melanoma of the skin. *Zentrum für Krebsregisterdaten*, (2023).
8. G. L. Manney *et al.*, Unprecedented arctic ozone loss in 2011. *Nature* **478**, 469-475 (2011).
9. G. C. Leonardi *et al.*, Cutaneous melanoma: From pathogenesis to therapy (Review). *Int J Oncol* **52**, 1071-1080 (2018).
10. A. Blum, C. Garbe, J. Bauer, Epidemiology and risk factors for malignant melanoma. *Der Onkologe* **10**, 688-700 (2004).
11. J. Y. Lin, D. E. Fisher, Melanocyte biology and skin pigmentation. *Nature* **445**, 843-850 (2007).
12. R. Rabbie, P. Ferguson, C. Molina-Aguilar, D. J. Adams, C. D. Robles-Espinoza, Melanoma subtypes: genomic profiles, prognostic molecular markers and therapeutic possibilities. *J Pathol* **247**, 539-551 (2019).
13. L. B. Alexandrov *et al.*, Signatures of mutational processes in human cancer. *Nature* **500**, 415-421 (2013).
14. D. E. Brash, UV signature mutations. *Photochem Photobiol* **91**, 15-26 (2015).
15. T. Budden, N. A. Bowden, The role of altered nucleotide excision repair and UVB-induced DNA damage in melanomagenesis. *Int J Mol Sci* **14**, 1132-1151 (2013).
16. Genomic classification of cutaneous celanoma. *Cell* **161**, 1681-1696 (2015).
17. Leitlinienprogramm Onkologie (Deutsche Krebsgesellschaft, Deutsche Krebshilfe, AWMF): Diagnostik, Therapie und Nachsorge des Melanomshsorge des Melanoms. **Kurzversion 3.3**, (2020).
18. P. K. Dhanyamraju, T. N. Patel, Melanoma therapeutics: a literature review. *J. Biomed* **36**, 77-97 (2022).
19. B. Switzer, I. Puzanov, J. J. Skitzki, L. Hamad, M. S. Ernstoff, Managing metastatic melanoma in 2022: a clinical review. *J Oncol Pract* **18**, 335-351 (2022).
20. R. H. I. Andtbacka *et al.*, Talimogene laherparepvec improves durable response rate in patients with advanced melanoma. *J Clin Oncol* **33**, 2780-2788 (2015).
21. C. A. Larocca, N. R. LeBoeuf, A. W. Silk, H. L. Kaufman, An update on the role of talimogene laherparepvec (T-VEC) in the treatment of melanoma: best practices and future directions. *Am J Clin Dermatol* **21**, 821-832 (2020).
22. Y. Yuan, Y.-C. Jiang, C.-K. Sun, Q.-M. Chen, Role of the tumor microenvironment in tumor progression and the clinical applications (Review). *Oncol Rep* **35**, 2499-2515 (2016).

23. X. Jiang *et al.*, The role of microenvironment in tumor angiogenesis. *J Exp Clin Cancer Res* **39**, 204 (2020).

24. S. Rafii, J. M. Butler, B.-S. Ding, Angiocrine functions of organ-specific endothelial cells. *Nature* **529**, 316-325 (2016).

25. M. K. Pugsley, R. Tabrizchi, The vascular system: An overview of structure and function. *J Pharmacol Toxicol Methods* **44**, 333-340 (2000).

26. E. Kang, J. W. Shin, Pericyte-targeting drug delivery and tissue engineering. *Int J Nanomedicine* **11**, 2397-2406 (2016).

27. H. G. Augustin, G. Y. Koh, Organotypic vasculature: From descriptive heterogeneity to functional pathophysiology. *Science* **357**, (2017).

28. G. Eelen, L. Treps, X. Li, P. Carmeliet, Basic and therapeutic aspects of angiogenesis updated. *Circ Res* **127**, 310-329 (2020).

29. R. Demir, A. Yaba, B. Huppertz, Vasculogenesis and angiogenesis in the endometrium during menstrual cycle and implantation. *Acta Histochem* **112**, 203-214 (2010).

30. A. G. Arroyo, M. L. Iruela-Arispe, Extracellular matrix, inflammation, and the angiogenic response. *Cardiovasc Res* **86**, 226-235 (2010).

31. F. H. Al-Ostoot, S. Salah, H. A. Khamees, S. A. Khanum, Tumor angiogenesis: current challenges and therapeutic opportunities. *Cancer Treat* **28**, 100422 (2021).

32. M. Singhal, H. G. Augustin, Beyond angiogenesis: exploiting angiocrine factors to restrict tumor progression and metastasis. *Cancer Res* **80**, 659-662 (2020).

33. R. H. Adams, K. Alitalo, Molecular regulation of angiogenesis and lymphangiogenesis. *Nat Rev Mol Cell Biol* **8**, 464-478 (2007).

34. C. S. Melincovici *et al.*, Vascular endothelial growth factor (VEGF) - key factor in normal and pathological angiogenesis. *Rom J Morphol Embryol* **59**, 455-467 (2018).

35. K. Alitalo, T. Tammela, T. V. Petrova, Lymphangiogenesis in development and human disease. *Nature* **438**, 946-953 (2005).

36. R. S. Apte, D. S. Chen, N. Ferrara, VEGF in signaling and disease: beyond discovery and development. *Cell* **176**, 1248-1264 (2019).

37. H. Gerhardt *et al.*, VEGF guides angiogenic sprouting utilizing endothelial tip cell filopodia. *J Cell Biol* **161**, 1163-1177 (2003).

38. N. Ferrara *et al.*, Heterozygous embryonic lethality induced by targeted inactivation of the VEGF gene. *Nature* **380**, 439-442 (1996).

39. M. Simons, E. Gordon, L. Claesson-Welsh, Mechanisms and regulation of endothelial VEGF receptor signalling. *Nat Rev Mol Cell Biol* **17**, 611-625 (2016).

40. W. Zhou *et al.*, Targeting VEGF-A/VEGFR2 Y949 Signaling-Mediated Vascular Permeability Alleviates Hypoxic Pulmonary Hypertension. *Circulation* **146**, 1855-1881 (2022).

41. I. Shiojima, K. Walsh, Role of Akt signaling in vascular homeostasis and angiogenesis. *Circ Res* **90**, 1243-1250 (2002).

42. F. Kuhnert, J. R. Kirshner, G. Thurston, Dll4-Notch signaling as a therapeutic target in tumor angiogenesis. *Vascular Cell* **3**, 20 (2011).

43. R. Riahi *et al.*, Notch1–Dll4 signalling and mechanical force regulate leader cell formation during collective cell migration. *Nature Commun* **6**, 6556 (2015).

44. H. G. Augustin, G. Y. Koh, G. Thurston, K. Alitalo, Control of vascular morphogenesis and homeostasis through the angiopoietin-Tie system. *Nat Rev Mol Cell Biol* **10**, 165-177 (2009).

45. M. Thomas, H. G. Augustin, The role of the Angiopoietins in vascular morphogenesis. *Angiogenesis* **12**, 125-137 (2009).

46. J. R. Miller, The Wnts. *Genome Biol* **3**, (2002).

47. J. J. Olsen *et al.*, The role of Wnt signalling in angiogenesis. *Clin Biochem Rev* **38**, 131-142 (2017).

48. L. Qian, J. P. Mahaffey, H. L. Alcorn, K. V. Anderson, Tissue-specific roles of Axin2 in the inhibition and activation of Wnt signaling in the mouse embryo. *Proc Natl Acad Sci USA* **108**, 8692-8697 (2011).

49. V. Easwaran *et al.*, beta-Catenin regulates vascular endothelial growth factor expression in colon cancer. *Cancer Res* **63**, 3145-3153 (2003).

50. W. Shu, Y. Q. Jiang, M. M. Lu, E. E. Morrisey, Wnt7b regulates mesenchymal proliferation and vascular development in the lung. *Development* **129**, 4831-4842 (2002).

51. T. Ishikawa *et al.*, Mouse Wnt receptor gene Fzd5 is essential for yolk sac and placental angiogenesis. *Development* **128**, 25-33 (2001).

52. M. Wright, M. Aikawa, W. Szeto, J. Papkoff, Identification of a Wnt-responsive signal transduction pathway in primary endothelial cells. *Biochem* **263**, 384-388 (1999).

53. H.-J. Choi, H. Park, H.-W. Lee, Y.-G. Kwon, The Wnt pathway and the roles for its antagonists, DKKS, in angiogenesis. *IUBMB Life* **64**, 724-731 (2012).

54. P. H. Burri, R. Hlushchuk, V. Djonov, Intussusceptive angiogenesis: Its emergence, its characteristics, and its significance. *Dev Dyn* **231**, 474-488 (2004).

55. S. E. Abdullah, R. Perez-Soler, Mechanisms of resistance to vascular endothelial growth factor blockade. *Cancer* **118**, 3455-3467 (2012).

56. C. Du Cheyne, M. Smeets, W. De Spiegelaere, Techniques used to assess intussusceptive angiogenesis: A systematic review. *Dev Dyn* **250**, 1704-1716 (2021).

57. E. A. Kuczynski, A. R. Reynolds, Vessel co-option and resistance to anti-angiogenic therapy. *Angiogenesis* **23**, 55-74 (2020).

58. A. Cuypers, A.-C. K. Truong, L. M. Becker, P. Saavedra-García, P. Carmeliet, Tumor vessel co-option: The past & the future. *Front* **12**, (2022).

59. S. L. Wechman, L. Emdad, D. Sarkar, S. K. Das, P. B. Fisher, Chapter two - vascular mimicry: triggers, molecular interactions and in vivo models. *Adv Cancer Res* **148**, 27-67 (2020).

60. T. Asahara *et al.*, Isolation of putative progenitor endothelial cells for angiogenesis. *Science* **275**, 964-967 (1997).

61. M. Singhal *et al.*, Endothelial cell fitness dictates the source of regenerating liver vasculature. *J Exp Med* **215**, 2497-2508 (2018).

62. S. Gkountela *et al.*, Circulating tumor cell clustering shapes DNA methylation to enable metastasis seeding. *Cell* **176**, 98-112.e114 (2019).

63. J. Folkman, Tumor angiogenesis: therapeutic implications. *N Engl J Med* **285**, 1182-1186 (1971).

64. G. Bergers, D. Hanahan, Modes of resistance to anti-angiogenic therapy. *Nat Rev Cancer* **8**, 592-603 (2008).

65. O. Casanovas, D. J. Hicklin, G. Bergers, D. Hanahan, Drug resistance by evasion of antiangiogenic targeting of VEGF signaling in late-stage pancreatic islet tumors. *Cancer Cell* **8**, 299-309 (2005).

66. T. T. Batchelor *et al.*, AZD2171, a pan-VEGF receptor tyrosine kinase inhibitor, normalizes tumor vasculature and alleviates edema in glioblastoma patients. *Cancer Cell* **11**, 83-95 (2007).

67. Y. Shaked *et al.*, Therapy-induced acute recruitment of circulating endothelial progenitor cells to tumors. *Science* **313**, 1785-1787 (2006).

68. G. Bergers, S. Song, N. Meyer-Morse, E. Bergsland, D. Hanahan, Benefits of targeting both pericytes and endothelial cells in the tumor vasculature with kinase inhibitors. *J Clin Investig* **111**, 1287-1295 (2003).

69. S. Ren, X. Xiong, H. You, J. Shen, P. Zhou, The combination of immune checkpoint blockade and angiogenesis inhibitors in the treatment of advanced non-small cell lung cancer. *Front Immunol* **12**, 237-247 (2021).

70. Y. Huang *et al.*, Vascular normalizing doses of antiangiogenic treatment reprogram the immunosuppressive tumor microenvironment and enhance immunotherapy. *Proc Natl Acad Sci USA* **109**, 17561-17566 (2012).

71. R. S. Finn *et al.*, Atezolizumab plus bevacizumab in unresectable hepatocellular carcinoma. *N Engl J Med* **382**, 1894-1905 (2020).

72. J. Fares, M. Y. Fares, H. H. Khachfe, H. A. Salhab, Y. Fares, Molecular principles of metastasis: a hallmark of cancer revisited. *Signal Transduct Target Ther* **5**, 28 (2020).

73. A. W. Lambert, D. R. Pattabiraman, R. A. Weinberg, Emerging biological principles of metastasis. *Cell* **168**, 670-691 (2017).

74. K. J. Luzzi *et al.*, Multistep nature of metastatic inefficiency: dormancy of solitary cells after successful extravasation and limited survival of early micrometastases. *Am J Pathol* **153**, 865-873 (1998).

75. Surveillance, epidemiology, and end results (SEER) 17 registries. National Cancer Institute, (2022).

76. D. R. Welch, D. R. Hurst, Defining the hallmarks of metastasis. *Cancer Res* **79**, 3011-3027 (2019).

77. C. L. Chaffer, B. P. San Juan, E. Lim, R. A. Weinberg, EMT, cell plasticity and metastasis. *Cancer Metastasis Rev* **35**, 645-654 (2016).

78. M. Egeblad, Z. Werb, New functions for the matrix metalloproteinases in cancer progression. *Nature reviews. Cancer* **2**, 161-174 (2002).

79. S. P. H. Chiang, R. M. Cabrera, J. E. Segall, Tumor cell intravasation. *Am J Physiol, Cell Physiol* **311**, C1-C14 (2016).

80. J. Majidpoor, K. Mortezaee, Steps in metastasis: an updated review. *Med Oncol* **38**, 3 (2021).

81. M. Najafi, A. Ahmadi, K. Mortezaee, Extracellular-signal-regulated kinase/mitogen-activated protein kinase signaling as a target for cancer therapy: an updated review. *Cell Biol Int* **43**, 1206-1222 (2019).

82. K. De Bock, M. Mazzone, P. Carmeliet, Antiangiogenic therapy, hypoxia, and metastasis: risky liaisons, or not? *Nat Rev Clin Oncol* **8**, 393-404 (2011).

83. L. Erpenbeck, M. P. Schön, Deadly allies: the fatal interplay between platelets and metastasizing cancer cells. *Blood* **115**, 3427-3436 (2010).

84. A. B. Al-Mehdi *et al.*, Intravascular origin of metastasis from the proliferation of endothelium-attached tumor cells: a new model for metastasis. *Nat Med* **6**, 100-102 (2000).

85. B. Strilic, S. Offermanns, Intravascular survival and extravasation of tumor cells. *Cancer Cell* **32**, 282-293 (2017).

86. G. P. Gupta *et al.*, Mediators of vascular remodelling co-opted for sequential steps in lung metastasis. *Nature* **446**, 765-770 (2007).

87. H. Wang *et al.*, The osteogenic niche Is a calcium reservoir of bone micrometastases and confers unexpected therapeutic vulnerability. *Cancer Cell* **34**, 823-839.e827 (2018).

88. I. J. Fidler, G. L. Nicolson, Fate of recirculating B16 melanoma metastatic variant cells in parabiotic syngeneic recipients. *J Natl Cancer Inst* **58**, 1867-1872 (1977).

89. A. Descot, T. Oskarsson, The molecular composition of the metastatic niche. *Exp Cell Res* **319**, 1679-1686 (2013).

90. T. Celià-Terrassa, Y. Kang, Metastatic niche functions and therapeutic opportunities. *Nat Cell Biol* **20**, 868-877 (2018).

91. V. Baeriswyl, G. Christofori, The angiogenic switch in carcinogenesis. *Semin Cancer Biol* **19**, 329-337 (2009).

92. Y. Liu, X. Cao, Characteristics and significance of the pre-metastatic niche. *Cancer Cell* **30**, 668-681 (2016).

93. H. S. Kuznetsov *et al.*, Identification of luminal breast cancers that establish a tumor-supportive macroenvironment defined by proangiogenic platelets and bone marrow–derived cells. *Cancer Discov* **2**, 1150-1165 (2012).

94. F. Bruzzese *et al.*, Local and systemic protumorigenic effects of cancer-associated fibroblast-derived GDF15. *Cancer Res* **74**, 3408-3417 (2014).

95. P. Ehrlich, H. Apolant, Experimentelle Carcinomstudien an Mäusen. (1906).

96. H. Kubo, S. Mensurado, N. Goncalves-Sousa, K. Serre, B. Silva-Santos, Primary tumors limit metastasis formation through induction of IL15-mediated cross-talk between patrolling monocytes and NK cells. *Cancer Immunol Res* **5**, 812-820 (2017).

97. J. M. Kirstein, M. N. Hague, P. M. McGowan, A. B. Tuck, A. F. Chambers, Primary melanoma tumor inhibits metastasis through alterations in systemic hemostasis. *J Mol Med* **94**, 899-910 (2016).

98. R. Piranlioglu *et al.*, Primary tumor-induced immunity eradicates disseminated tumor cells in syngeneic mouse model. *Nat Commun* **10**, 1430 (2019).

99. A. M. Hamilton, K. M. Parkins, D. H. Murrell, J. A. Ronald, P. J. Foster, Investigating the impact of a primary tumor on metastasis and dormancy using MRI: new insights into the mechanism of concomitant tumor resistance. *Tomography* **2**, 79-84 (2016).

100. M. S. O'Reilly *et al.*, Angiostatin: a novel angiogenesis inhibitor that mediates the suppression of metastases by a Lewis lung carcinoma. *Cell* **79**, 315-328 (1994).

101. K. Camphausen *et al.*, Radiation therapy to a primary tumor accelerates metastatic growth in mice. *Cancer Res* **61**, 2207-2211 (2001).

102. O. V. Volpert, J. Lawler, N. P. Bouck, A human fibrosarcoma inhibits systemic angiogenesis and the growth of experimental metastases via thrombospondin-1. *Proc Natl Acad Sci USA* **95**, 6343-6348 (1998).

103. M. Franco *et al.*, A serum-mediated mechanism for concomitant resistance shared by immunogenic and non-immunogenic murine tumours. *Br J Cancer* **74**, 178-186 (1996).

104. R. A. Ruggiero *et al.*, Concomitant tumor resistance: the role of tyrosine isomers in the mechanisms of metastases control. *Cancer Res* **72**, 1043-1050 (2012).

105. A. V. Digtyar, N. V. Pozdnyakova, N. B. Feldman, S. V. Lutsenko, S. E. Severin, Endostatin: current concepts about its biological role and mechanisms of action. *Biochemistry* **72**, 235-246 (2007).

106. W. D. Beecken, T. Engl, D. Jonas, R. A. Blaheta, Expression of angiogenesis inhibitors in human bladder cancer may explain rapid metastatic progression after radical cystectomy. *Int. J Mol Med* **23**, 261-266 (2009).

107. C. F. Peeters, R. M. de Waal, T. Wobbes, J. R. Westphal, T. J. Ruers, Outgrowth of human liver metastases after resection of the primary colorectal tumor: a shift in the balance between apoptosis and proliferation. *Int J Cancer* **119**, 1249-1253 (2006).

108. G. Santulli, Angiopoietin-like proteins: a comprehensive look. *Front Endocrinol* **5**, 4 (2014).

109. I. Kim *et al.*, Hepatic expression, synthesis and secretion of a novel fibrinogen/angiopoietin-related protein that prevents endothelial-cell apoptosis. *Biochem J* **346**, 603-610 (2000).

110. S. Kersten *et al.*, Characterization of the fasting-induced adipose factor FIAF, a novel peroxisome proliferator-activated receptor target gene. *J Biol Chem* **275**, 28488-28493 (2000).

111. J. C. Yoon *et al.*, Peroxisome proliferator-activated receptor gamma target gene encoding a novel Angiopoietin-related protein associated with adipose differentiation. *Mol Cell Biol* **20**, 5343-5349 (2000).

112. L. La Paglia *et al.*, Potential role of ANGPTL4 in the cross talk between metabolism and cancer through PPAR signaling pathway. *PPAR Res* **2017**, 8187235 (2017).

113. P. Zhu, Y. Y. Goh, H. F. Chin, S. Kersten, N. S. Tan, Angiopoietin-like 4: a decade of research. *Biosci* **32**, 211-219 (2012).

114. W. Yin *et al.*, Genetic variation in ANGPTL4 provides insights into protein processing and function. *J Biol Chem* **284**, 13213-13222 (2009).

115. N. Kirsch *et al.*, Angiopoietin-like 4 is a Wnt signaling antagonist that promotes LRP6 turnover. *Dev Cell* **43**, 71-82.e76 (2017).

116. Y. Y. Goh *et al.*, Angiopoietin-like 4 interacts with integrins beta1 and beta5 to modulate keratinocyte migration. *Am J Pathol* **177**, 2791-2803 (2010).

117. Y. Y. Goh *et al.*, Angiopoietin-like 4 interacts with matrix proteins to modulate wound healing.*J Biol Chem* **285**, 32999-33009 (2010).

118. R. L. Huang *et al.*, ANGPTL4 modulates vascular junction integrity by integrin signaling and disruption of intercellular VE-cadherin and claudin-5 clusters. *Blood* **118**, 3990-4002 (2011).

119. A. Sodhi *et al.*, Angiopoietin-like 4 binds neuropilins and cooperates with VEGF to induce diabetic macular edema. *J Clin Invest* **129**, 4593-4608 (2019).

120. H. K. Kim *et al.*, Hypothalamic Angptl4/Fiaf is a novel regulator of food intake and body weight. *Diabetes* **59**, 2772-2780 (2010).

121. L. Aronsson *et al.*, Decreased fat storage by Lactobacillus paracasei is associated with increased levels of angiopoietin-like 4 protein (ANGPTL4). *PloS one* **5**, (2010).

122. S. Kersten, Role and mechanism of the action of angiopoietin-like protein ANGPTL4 in plasma lipid metabolism. *J Lipid Res* **62**, 100150 (2021).

123. A. Xu *et al.*, Angiopoietin-like protein 4 decreases blood glucose and improves glucose tolerance but induces hyperlipidemia and hepatic steatosis in mice. *Proc Natl Acad Sci USA* **102**, 6086-6091 (2005).

124. A. W. F. Janssen *et al.*, Loss of angiopoietin-like 4 (ANGPTL4) in mice with diet-induced obesity uncouples visceral obesity from glucose intolerance partly via the gut microbiota. *Diabetologia* **61**, 1447-1458 (2018).

125. L. Lichtenstein *et al.*, Angptl4 upregulates cholesterol synthesis in liver via inhibition of LPL- and HL-dependent hepatic cholesterol uptake. *Arterioscler* **27**, 2420-2427 (2007).

126. L. Lichtenstein *et al.*, Angptl4 protects against severe proinflammatory effects of saturated fat by inhibiting fatty acid uptake into mesenteric lymph node macrophages. *Cell Metab* **12**, 580-592 (2010).

127. D. I. Cho *et al.*, Antiinflammatory activity of ANGPTL4 facilitates macrophage polarization to induce cardiac repair. *JCI Insight* **4**, (2019).

128. B. Lu, A. Moser, J. K. Shigenaga, C. Grunfeld, K. R. Feingold, The acute phase response stimulates the expression of angiopoietin like protein 4. *Biochem Biophys Res Commun* **391**, 1737-1741 (2010).

129. Y. Li *et al.*, Angiopoietin-like protein 4 promotes hyperlipidemia-induced renal injury by down-regulating the expression of ACTN4. *Biochem Biophys Res Commun* **595**, 69-75 (2022).

130. S. S. Chugh, C. Macé, L. C. Clement, M. Del Nogal Avila, C. B. Marshall, Angiopoietin-like 4 based therapeutics for proteinuria and kidney disease. *Front* **5**, 23 (2014).

131. P. Zhu *et al.*, Angiopoietin-like 4 protein elevates the prosurvival intracellular O2−:H2O2 ratio and confers anoikis resistance to tumors. *Cancer Cell* **19**, 401-415 (2011).

132. A. Cazes *et al.*, Extracellular matrix-bound angiopoietin-like 4 inhibits endothelial cell adhesion, migration, and sprouting and alters actin cytoskeleton. *Circ Res* **99**, 1207-1215 (2006).

133. A. Galaup *et al.*, Protection against myocardial infarction and no-reflow through preservation of vascular integrity by angiopoietin-like 4. *Circulation* **125**, 140-149 (2012).

134. E. Gomez Perdiguero *et al.*, ANGPTL4–αvβ3 interaction counteracts hypoxia-induced vascular permeability by modulating Src signalling downstream of vascular endothelial growth factor receptor 2. *J Pathol* **240**, 461-471 (2016).

135. A. Galaup *et al.*, Angiopoietin-like 4 prevents metastasis through inhibition of vascular permeability and tumor cell motility and invasiveness. *Proc Natl Acad Sci USA* **103**, 18721-18726 (2006).

136. E. Okochi-Takada *et al.*, ANGPTL4 is a secreted tumor suppressor that inhibits angiogenesis. *Oncogene* **33**, 2273-2278 (2014).

137. K. Hu *et al.*, Hypoxia-inducible factor 1 upregulation of both VEGF and ANGPTL4 is required to promote the angiogenic phenotype in uveal melanoma. *Oncotarget* **7**, 7816-7828 (2016).

138. T. Zhang, A. Kastrenopoulou, Q. Larrouture, N. A. Athanasou, H. J. Knowles, Angiopoietin-like 4 promotes osteosarcoma cell proliferation and migration and stimulates osteoclastogenesis. *BMC Cancer* **18**, 536 (2018).

139. K. Baba *et al.*, Hypoxia-induced ANGPTL4 sustains tumour growth and anoikis resistance through different mechanisms in scirrhous gastric cancer cell lines. *Sci Rep* **7**, 11127 (2017).

140. S. Le Jan *et al.*, Angiopoietin-Like 4 is a proangiogenic factor produced during ischemia and in conventional renal cell carcinoma. *Am J Pathol* **162**, 1521-1528 (2003).

141. R. Kolb *et al.*, Obesity-associated inflammation promotes angiogenesis and breast cancer via angiopoietin-like 4. *Oncogene* **38**, 2351-2363 (2019).

142. L. Tian *et al.*, Activating peroxisome proliferator-activated receptor gamma mutant promotes tumor growth in vivo by enhancing angiogenesis. *Cancer Res* **69**, 9236-9244 (2009).

143. T. Ma *et al.*, Viral G protein-coupled receptor up-regulates Angiopoietin-like 4 promoting angiogenesis and vascular permeability in Kaposi's sarcoma. *Proc Natl Acad Sci USA* **107**, 14363-14368 (2010).

144. Y. Qin *et al.*, ANGPTL4 influences the therapeutic response of patients with neovascular age-related macular degeneration by promoting choroidal neovascularization. *JCI Insight* **7**, (2022).

145. K. Shibata, T. Nakayama, H. Hirakawa, S. Hidaka, T. Nagayasu, Clinicopathological significance of angiopoietin-like protein 4 expression in oesophageal squamous cell carcinoma. *J Clin Pathol* **63**, 1054-1058 (2010).

146. X. Li *et al.*, Angiopoietin-like 4 enhances metastasis and inhibits apoptosis via inducing bone morphogenetic protein 7 in colorectal cancer cells. *Biochem* **467**, 128-134 (2015).

147. J.-W. Chen, Y.-J. Luo, Z.-F. Yang, L.-Q. Wen, L. Huang, Knockdown of angiopoietin-like 4 inhibits the development of human gastric cancer. *Oncol Rep* **39**, 1739-1746 (2018).

148. D. Padua *et al.*, TGFbeta primes breast tumors for lung metastasis seeding through angiopoietin-like 4. *Cell* **133**, 66-77 (2008).

149. D. Padua *et al.*, TGFβ primes breast tumors for lung metastasis seeding through Angiopoietin-like 4. *Cell* **133**, 66-77 (2008).

150. E. Gomez, M. Durand, A. Galaup, S. Germain, D016 Angptl4 modulates in vivo developmental and pathological angiogenesis. *Arch Cardiovasc* **102**, S41-S42 (2009).

151. K. T.-P. Ng *et al.*, Clinical relevance and therapeutic potential of angiopoietin-like protein 4 in hepatocellular carcinoma. *Mol Cancer* **13**, 196 (2014).

152. W. Dijk, S. Kersten, Regulation of lipoprotein lipase by Angptl4. *Trends Endocrinol Metab* **25**, 146-155 (2014).

153. V. Sukonina, A. Lookene, T. Olivecrona, G. Olivecrona, Angiopoietin-like protein 4 converts lipoprotein lipase to inactive monomers and modulates lipase activity in adipose tissue. *Proc Natl Acad Sci USA* **103**, 17450-17455 (2006).

154. S. Mysling *et al.*, The angiopoietin-like protein ANGPTL4 catalyzes unfolding of the hydrolase domain in lipoprotein lipase and the endothelial membrane protein GPIHBP1 counteracts this unfolding. *eLife* **5**, e20958 (2016).

155. A. R. Gutgsell, S. V. Ghodge, A. A. Bowers, S. B. Neher, Mapping the sites of the lipoprotein lipase (LPL)-angiopoietin-like protein 4 (ANGPTL4) interaction provides mechanistic insight into LPL inhibition. *J Biol Chem* **294**, 2678-2689 (2019).

156. W. Dijk *et al.*, Angiopoietin-like 4 promotes intracellular degradation of lipoprotein lipase in adipocytes. *J Lipid Res* **57**, 1670-1683 (2016).

157. A. Köster *et al.*, Transgenic angiopoietin-like (angptl)4 overexpression and targeted disruption of angptl4 and angptl3: regulation of triglyceride metabolism. *Endocrinology* **146**, 4943-4950 (2005).

158. U. Desai *et al.*, Lipid-lowering effects of anti-angiopoietin-like 4 antibody recapitulate the lipid phenotype found in angiopoietin-like 4 knockout mice. *Proc Natl Acad Sci USA* **104**, 11766-11771 (2007).

159. N. Mehta *et al.*, Differential association of plasma angiopoietin-like proteins 3 and 4 with lipid and metabolic traits. *Arterioscler* **34**, 1057-1063 (2014).

160. A. Muendlein *et al.*, Angiopoietin-like protein 4 significantly predicts future cardiovascular events in coronary patients. *Atherosclerosis* **237**, 632-638 (2014).

161. H. Adachi *et al.*, Angptl 4 deficiency improves lipid metabolism, suppresses foam cell formation and protects against atherosclerosis. *Biochem* **379**, 806-811 (2009).

162. S. Romeo *et al.*, Population-based resequencing of ANGPTL4 uncovers variations that reduce triglycerides and increase HDL. *Nat Genet* **39**, 513-516 (2007).

163. F. E. Dewey *et al.*, Inactivating variants in ANGPTL4 and risk of coronary artery disease. *N Engl J Med* **374**, 1123-1133 (2016).

164. D. Bailetti *et al.*, ANGPTL4 gene E40K variation protects against obesity-associated dyslipidemia in participants with obesity. *Obes Sci Pract* **5**, 83-90 (2019).

165. V. Gusarova *et al.*, Genetic inactivation of ANGPTL4 improves glucose homeostasis and is associated with reduced risk of diabetes. *Nat Commun* **9**, 2252 (2018).

166. A. Elfenbein, M. Simons, Syndecan-4 signaling at a glance. *J Cell Sci* **126**, 3799-3804 (2013).

167. E. Tkachenko, J. M. Rhodes, M. Simons, Syndecans. *Circ Res* **96**, 488-500 (2005).

168. F. Echtermeyer *et al.*, Delayed wound repair and impaired angiogenesis in mice lacking syndecan-4. *J Clin Investig* **107**, R9-R14 (2001).

169. S. Das *et al.*, Syndecan-4 enhances therapeutic angiogenesis after hind limb ischemia in mice with type 2 diabetes. *Adv Healthc Mater* **5**, 1008-1013 (2016).

170. J. Xie *et al.*, Syndecan-4 over-expression preserves cardiac function in a rat model of myocardial infarction. *J Mol Cell Cardiol* **53**, 250-258 (2012).

171. G. D. Rossi *et al.*, Pathological angiogenesis requires syndecan-4 for efficient VEGFA-induced VE-cadherin internalization. *Arterioscler* **41**, 1374-1389 (2021).

172. A. C. Chiang, J. Massagué, Molecular basis of metastasis. *N Engl J Med* **359**, 2814-2823 (2008).

173. M. J. Tan, Z. Teo, M. K. Sng, P. Zhu, N. S. Tan, Emerging roles of Angiopoietin-like 4 in human cancer. *Mol Cancer Res* **10**, 677-688 (2012).

174. C. Hübers *et al.*, Primary tumor-derived systemic nANGPTL4 inhibits metastasis. *J Exp Med* **220**, (2023).

175. N. Maishi, K. Hida, Tumor endothelial cells accelerate tumor metastasis. *Cancer Sci* **108**, 1921-1926 (2017).

176. A. F. Chambers, A. C. Groom, I. C. MacDonald, Dissemination and growth of cancer cells in metastatic sites. *Nat Rev Cancer* **2**, 563-572 (2002).

177. F. Hillen, A. W. Griffioen, Tumour vascularization: sprouting angiogenesis and beyond. *Cancer Metastasis Rev* **26**, 489-502 (2007).

178. G. De Rossi *et al.*, Pathological angiogenesis requires syndecan-4 for efficient VEGFA-induced VE-cadherin internalization. *Arterioscler* **41**, 1374-1389 (2021).

179. E. Dejana, The role of wnt signaling in physiological and pathological angiogenesis. *Circ Res* **107**, 943-952 (2010).

180. N. Gengenbacher, M. Singhal, H. G. Augustin, Preclinical mouse solid tumour models: status quo, challenges and perspectives. *Nat Rev Cancer***17**, 751-765 (2017).

181. S. Mandard *et al.*, The direct peroxisome proliferator-activated receptor target fasting-induced adipose factor (FIAF/PGAR/ANGPTL4) is present in blood plasma as a truncated protein that is increased by fenofibrate treatment. *J Biol Chem* **279**, 34411-34420 (2004).

182. B. Aryal, N. L. Price, Y. Suarez, C. Fernández-Hernando, ANGPTL4 in metabolic and cardiovascular disease. *Trends Mol Med* **25**, 723-734 (2019).

183. B. Rong, S. Yang, W. Li, W. Zhang, Z. Ming, Systematic review and meta-analysis of Endostar (rh-endostatin) combined with chemotherapy versus chemotherapy alone for treating advanced non-small cell lung cancer. *World J Surg Oncol* **10**, 170 (2012).

184. J. R. Westphal, Technology evaluation: ABT-510, Abbott. *Curr Opin Mol Ther* **6**, 451-457 (2004).

185. E. G. Perdiguero *et al.*, Alteration of developmental and pathological retinal angiogenesis in angptl4-deficient mice. *J Biol Chem* **286**, 36841-36851 (2011).

186. C. Bouleti *et al.*, Protective effects of angiopoietin-like 4 on cerebrovascular and functional damages in ischaemic stroke. *Eur Heart J* **34**, 3657-3668 (2013).

187. R. T. Prehn, Two competing influences that may explain concomitant tumor resistance. *Cancer Res* **53**, 3266-3269 (1993).

188. S. Sundararajan, A. M. Thida, S. Yadlapati, S. Koya, Metastatic melanoma. *StatPearls*, (2022).

189. Y. H. Liao *et al.*, Epidermal growth factor-induced ANGPTL4 enhances anoikis resistance and tumour metastasis in head and neck squamous cell carcinoma. *Oncogene* **36**, 2228-2242 (2017).

190. S. Izraely *et al.*, ANGPTL4 promotes the progression of cutaneous melanoma to brain metastasis. *Oncotarget* **8**, 75778-75796 (2017).

191. Y. Ito *et al.*, Inhibition of angiogenesis and vascular leakiness by angiopoietin-related protein 4. *Cancer Res* **63**, 6651-6657 (2003).

192. S. P. Hack *et al.*, IMbrave 050: a Phase III trial of atezolizumab plus bevacizumab in high-risk hepatocellular carcinoma after curative resection or ablation. *Future Oncol* **16**, 975-989 (2020).

193. T. Nakayama *et al.*, Expression of angiopoietin-like 4 in human gastric cancer: ANGPTL4 promotes venous invasion. *Oncol Rep* **24**, 599-606 (2010).

194. T. Nakayama *et al.*, Expression of angiopoietin-like 4 (ANGPTL4) in human colorectal cancer: ANGPTL4 promotes venous invasion and distant metastasis. *Oncol Rep* **25**, 929-935 (2011).

195. D. Hanahan, J. Folkman, Patterns and emerging mechanisms of the angiogenic switch during tumorigenesis. *Cell* **86**, 353-364 (1996).

196. M. Hessler *et al.*, Melanoma biomarkers and their potential application for in vivo diagnostic imaging modalities. Int J Mol Sci **21**, (2020).

197. Z. Tang *et al.*, A mouse model of the cornea pocket assay for angiogenesis study. *J Vis Exp*, (2011).